Fall 2019

Companion to the Introduction to Modern Dynamics

David D Nolte, *Purdue University*

A Companion to IMD2: Introduction to Modern Dynamics (2nd Edition)

These online Companion Notes are supplements to the textbook (2nd edition) *Introduction to Modern Dynamics: Chaos, Networks, Space and Time* (Oxford University Press, 2019). This is a Junior/Senior textbook for undergraduate mechanics/dynamics taking an updated approach to teaching mechanics.

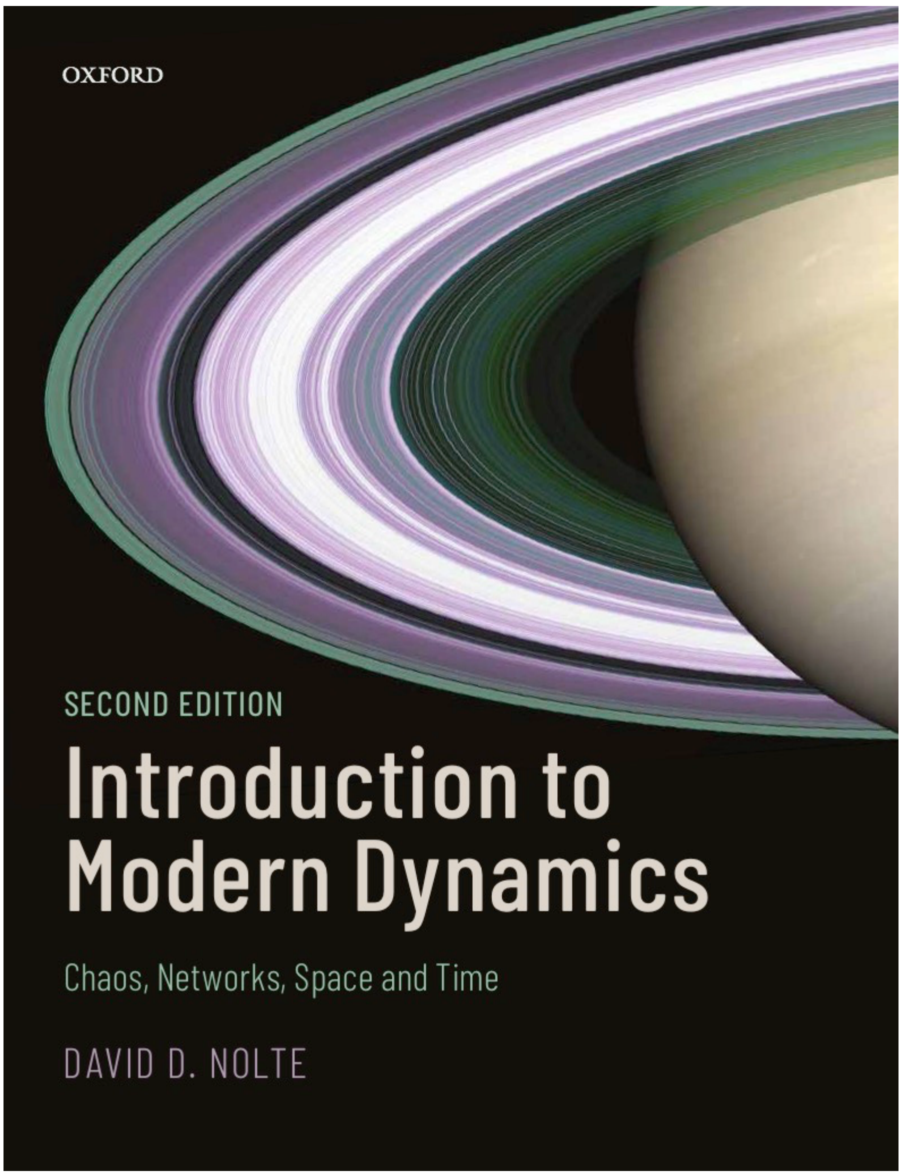

Cover of IMD2

1. Numerical Algorithms:

For the modern physics student, numerical simulation is just as important a tool as analytical skill with mathematics. Coding and running numerical experiments are important for building physical intuition about how complex systems behave. In my opinion ALL practicing physicists need to be fluent in at least one computer language and must be able to work with numerical simulations and able to develop new algorithms.

Supporting Matlab and Python codes for IMD2 can be found at

https://works.bepress.com/ddnolte/

Some Python codes and examples can be found in posts at

https://galileo-unbound.blog/tag/python-code/

Additional Matlab and Python codes related to HW can be downloaded at

https://github.itap.purdue.edu/nolte/Python-Programs-for-Nonlinear-Dynamics

https://github.itap.purdue.edu/nolte/Matlab-Programs-for-Nonlinear-Dynamics

These codes are "bare bones" and are meant as starting points for students to modify and perform their own "numerical experiments".

2. Related Physics Blogs:

Regular blog posts can be found at http://galileo-unbound.blog on topics in nonlinear dynamics and relativity. Many of these have a direct connection to sections of the textbook Introduction to Modern Dynamics.

Nonlinear Dynamics

Stability of the Earth's Rotation

http://galileo-unbound.blog/2021/10/10/physics-of-the-flipping-iphone-and-the-fate-of-the-earth/

Spontaneous Symmetry Breaking: A Mechanical Model

http://galileo-unbound.blog/2021/09/22/spontaneous-symmetry-breaking-a-mechanical-model/

Minkowski Spacetime

http://galileo-unbound.blog/2021/04/24/hermann-minkowskis-spacetime-the-theory-that-einstein-overlooked/

The Physics of Stein's Gate

http://galileo-unbound.blog/2021/03/14/the-butterfly-effect-versus-the-divergence-meter-the-physics-of-steins-gate/

The Lorenz Chaotic Butterfly

http://galileo-unbound.blog/2020/11/16/edward-lorenz-chaotic-butterfly/

The Compound Double Pendulum

http://galileo-unbound.blog/2020/10/18/the-ups-and-downs-of-the-compound-double-pendulum/

Dynamic Equilibria

http://galileo-unbound.blog/2020/09/14/up-side-down-physics-dynamic-equilibrium-and-the-inverted-pendulum/

Homoclinic Tangles

http://galileo-unbound.blog/2020/08/24/henri-poincare-and-his-homoclinic-tangle/

KAM theory

http://galileo-unbound.blog/2019/10/14/how-number-theory-protects-you-from-the-chaos-of-the-cosmos/

Limit-cycle Oscillators

http://galileo-unbound.blog/2019/08/26/the-fast-and-the-slow-of-grandfather-clocks/

Biased Double-Well Potential

http://galileo-unbound.blog/2019/04/24/biased-double-well-potential-bistability-bifurcation-and-hysteresis/

The Duffing Oscillator

http://galileo-unbound.blog/2019/03/20/georg-duffing-and-his-equation/

Hamiltonian Maps

http://galileo-unbound.blog/2018/12/10/the-wonderful-world-of-hamiltonian-maps/

Hamiltonian Chaos and Tapestries

http://galileo-unbound.blog/2018/10/27/how-to-weave-a-tapestry-from-hamiltonian-chaos/

Life in a Solar System with a Super-sized Jupiter

https://galileo-unbound.blog/2022/02/28/life-in-a-solar-system-with-a-super-sized-jupiter/

The Physics of Robinson Crusoe's Economy

https://galileo-unbound.blog/2022/02/10/the-physics-of-robinson-crusoes-economy/

Relativity

The Physics of Starflight: Proxima Centauri b or Bust!

https://galileo-unbound.blog/2022/03/23/the-physics-of-starflight-proxima-centauri-b-or-bust/

Relativistic Harmonic Oscillator

https://galileo-unbound.blog/2022/05/29/the-anharmonic-harmonic-oscillator/

Black Hole Accretion Disk

http://galileo-unbound.blog/2021/08/28/surfing-on-a-black-hole-accretion-disk-death-spiral/

Clock Synchronization in Strong Gravity

http://galileo-unbound.blog/2021/05/16/locking-clocks-in-strong-gravity/

Gravitational Lensing

http://galileo-unbound.blog/2021/04/05/the-lens-of-gravity-einsteins-rings/

Orbiting Photons Around a Black Hole

http://galileo-unbound.blog/2019/07/29/orbiting-photons-around-a-black-hole/

Chapter 1 Physics and Geometry

1. Frenet-Serret Formula

To complete the set of unit vectors associated with a trajectory, there is the binormal unit vector B^a defined by

$$\frac{dN^a}{ds} = -\kappa T^a + \tau B^a \tag{1.1}$$

where τ is called the torsion of the trajectory. The three unit vectors T^a, N^a and B^a are mutually orthogonal. The relationships among these three unit vectors are collectively known as the Serret-Frenet Formulas

Serret-Frenet Formulas	$\frac{dx^a}{ds} = T^a$ $\frac{dT^a}{ds} = \kappa N^a$ $\frac{dN^a}{ds} = -\kappa T^a + \tau B^a$ $\frac{dB^a}{ds} = -\tau N^a$	$\vec{T} \times \vec{N} = \vec{B}$	(1.2)

Serret-Frenet Vectors

$$\frac{d}{ds}\begin{pmatrix} \vec{T} \\ \vec{N} \\ \vec{B} \end{pmatrix} = \begin{pmatrix} 0 & \kappa & 0 \\ -\kappa & 0 & \tau \\ 0 & -\tau & 0 \end{pmatrix}\begin{pmatrix} \vec{T} \\ \vec{N} \\ \vec{B} \end{pmatrix}$$

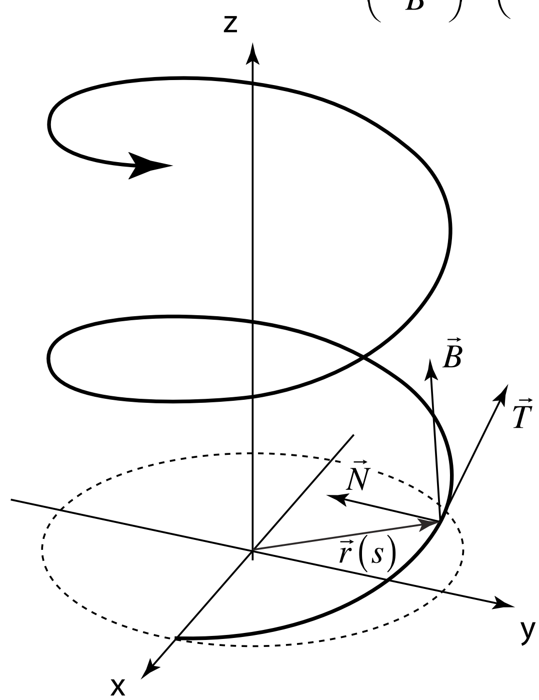

Frenet.ai

Fig. 1.1 A trajectory in 3 dimensions, parameterized by time $\vec{r}(t)$, or equivalently by path length $\vec{r}(s)$, showing the tangent, normal and binormal vectors.

The Frenet-Serret formulas for a simple parabola are:

$$y = ax^2$$

$$\frac{dy}{dx} = 2ax = m$$

$$ds^2 = dx^2 + dy^2 = dx^2\left(1+\left(\frac{dy}{dx}\right)^2\right) = dx^2\left(1+m^2\right)$$

$$T^x = \frac{dx}{ds} = \frac{1}{\sqrt{1+m^2}}$$

$$T^y = \frac{dy}{ds} = \frac{dy}{dx}\frac{dx}{ds} = mT^x$$

$$\kappa N^x = \frac{dT^x}{ds} = \frac{d}{ds}\left(\frac{1}{\sqrt{1+m^2}}\right) = \frac{-2a}{\left(1+m^2\right)^{3/2}} mT^x = \frac{-2a}{\left(1+m^2\right)^{3/2}} T^y$$

$$\kappa N^y = \frac{dT^y}{ds} = \frac{2a}{\left(1+m^2\right)^{3/2}} T^x$$

$$\kappa = \frac{2a}{\left(1+m^2\right)^{3/2}}$$

For a parabolic trajectory of a mass thrown in the x-direction with initial x-speed v_x and falling under gravity g, the constant a is

$$a = -\frac{1}{2}\frac{g}{v_x^2}$$

and the curvature (as a function of time) is

$$\kappa = \frac{-g / v_x^2}{\left(1+\dfrac{g^2 t^2}{v_x^2}\right)^{3/2}}$$

2. Three-Dimensional Rotations

The combination of the three rotation matrices $R(\phi)$, $R(\theta)$ and $R(\psi)$ on pg. 24 of IMD[1] is

$$\begin{aligned} U &= R(\psi)R(\theta)R(\phi) \\ &= \begin{pmatrix} c_\psi c_\phi - c_\theta s_\phi s_\psi & c_\psi s_\phi + c_\theta c_\phi s_\psi & s_\theta s_\psi \\ -s_\psi c_\phi - c_\theta s_\phi c_\psi & -s_\psi s_\phi + c_\theta c_\phi c_\psi & s_\theta c_\psi \\ s_\theta s_\phi & -s_\theta c_\phi & c_\theta \end{pmatrix} \end{aligned}$$

where the shorthand notation is $c_a = \cos a$ and $s_b = \sin a$. The angular velocity in the body frame in terms of these rotation angles is

[1] IMD = *Introduction to Modern Dynamics*

$$\vec{\omega}_{body} = \begin{pmatrix} \dot{\phi} s_\psi s_\theta + \dot{\theta} c_\psi \\ \dot{\phi} c_\psi s_\theta - \dot{\theta} s_\psi \\ \dot{\phi} c_\theta + \dot{\psi} \end{pmatrix}$$

The rotational kinetic energy of a symmetric top is then

$$\begin{aligned} T_{rot} &= \frac{I_1}{2}\left(\omega_1^2 + \omega_1^2\right) + \frac{I_3}{2}\omega_3^2 \\ &= \frac{I_1}{2}\left[\left(\dot{\theta} c_\psi + \dot{\phi} s_\psi s_\theta\right)^2 + \left(-\dot{\theta} s_\psi + \dot{\phi} c_\psi s_\theta\right)^2\right] + \frac{I_3}{2}\left(\dot{\psi} + \dot{\phi} c_\theta\right)^2 \\ &= \frac{I_1}{2}\left(\dot{\theta}^2 + \dot{\phi}^2 \sin^2\theta\right) + \frac{I_3}{2}\left(\dot{\psi} + \dot{\phi}\cos\theta\right)^2 \end{aligned}$$

This expression will be useful when using the Lagrangian formulation of mechanics in Chapter 2.

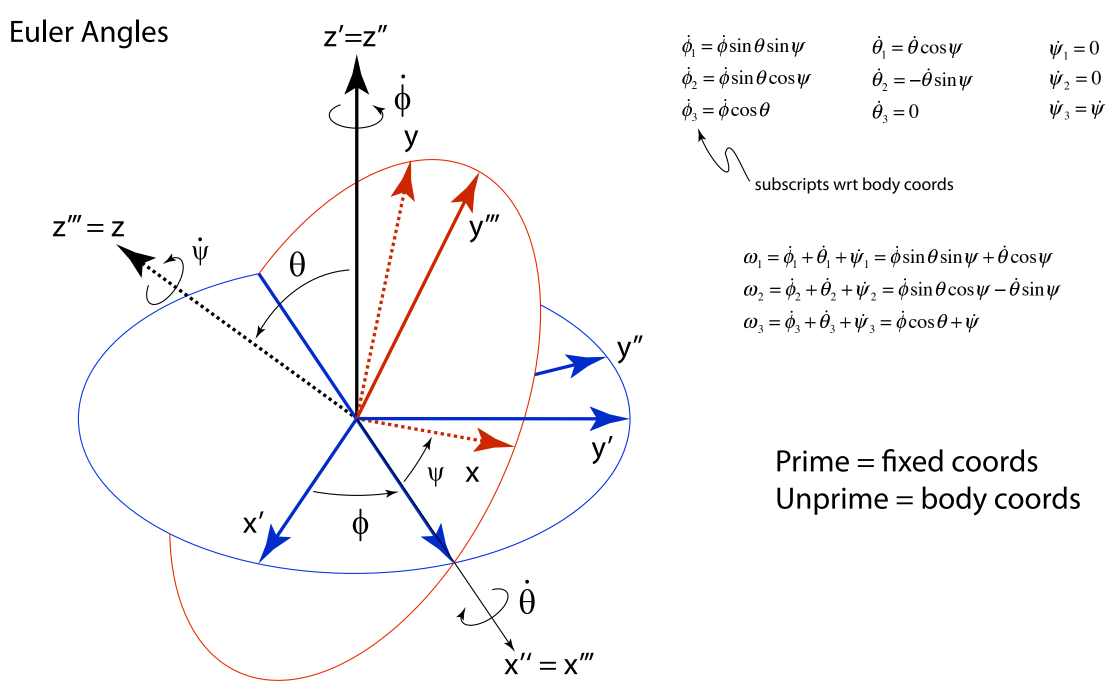

The rotation of basis vectors is a key analytical operation in rotational dynamics. For instance, using the general relation of Eq. (1.95), the derivatives of the basis vectors for rotating frames is

$$\left.\frac{d\vec{e}}{dt}\right|_{fixed} = \left.\frac{d\vec{e}}{dt}\right|_{rot} + \vec{\omega}\times\vec{e}$$
$$= \left.\frac{d\vec{e}}{dt}\right|_{rot} + \begin{pmatrix} 0 & -\omega_3 & \omega_2 \\ \omega_3 & 0 & -\omega_1 \\ -\omega_2 & \omega_1 & 0 \end{pmatrix}\begin{pmatrix} \vec{e}_1 \\ \vec{e}_2 \\ \vec{e}_3 \end{pmatrix}$$

where the cross product can be expressed as a matrix multiplication. The derivatives in the fixed frame vanish, yielding

$$\left.\frac{d\vec{e}}{dt}\right|_{rot} = -\begin{pmatrix} 0 & -\omega_3 & \omega_2 \\ \omega_3 & 0 & -\omega_1 \\ -\omega_2 & \omega_1 & 0 \end{pmatrix}\begin{pmatrix} \vec{e}_1 \\ \vec{e}_2 \\ \vec{e}_3 \end{pmatrix}$$

or

$$\frac{d\vec{e}_x}{dt} = \omega_z\vec{e}_y - \omega_y\vec{e}_z$$
$$\frac{d\vec{e}_y}{dt} = -\omega_z\vec{e}_x + \omega_x\vec{e}_z$$
$$\frac{d\vec{e}_z}{dt} = \omega_y\vec{e}_x - \omega_x\vec{e}_y$$

which is Eq. (1.90).

Translating Frames

Galilean relativity[2] concerns the description of kinematics when the same trajectory is viewed from different inertial frames. An inertial frame is one that moves at constant velocity (no acceleration). The transformation between the two inertial frames is a linear transformation.

[2] The first systematic application of classical relativity was made by Christiaan Huygens (1669) and might more accurately be called Galilean-Huygens relativity.

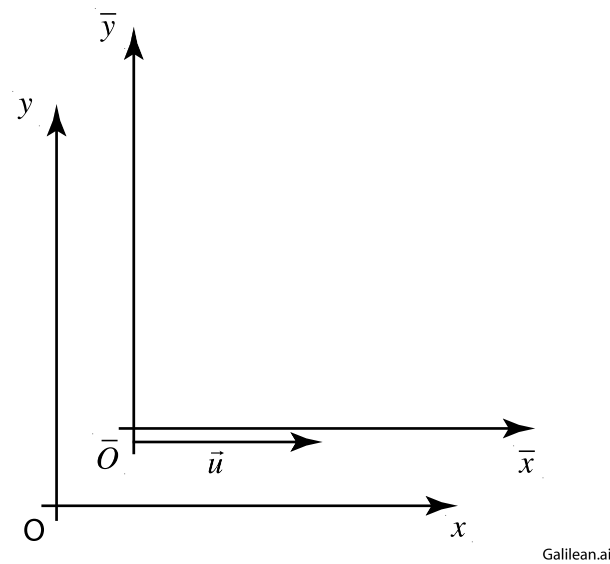

Fig. 1.2 Galilean frames in uniform relative motion. The primed frame is observed from the unprimed frame to move with velocity u.

Consider a general trajectory in frame O defined by $\vec{x}(t) = x^a$ which might be a mass subjected to time-varying forces. A second "primed" frame $\bar{O}$ is moving relative the first with a velocity $\vec{u}(t) = u^a$. The same trajectory seen in the primed frame $\bar{O}$ is given by

$$\begin{aligned} \bar{x}^1 &= x^1 - u^1 t \\ \bar{x}^2 &= x^2 - u^2 t \\ \bar{x}^3 &= x^3 - u^3 t \end{aligned} \tag{1.3}$$

with the inverse transformation given by

$$\begin{aligned} x^1 &= \bar{x}^1 + u^1 t \\ x^2 &= \bar{x}^2 + u^2 t \\ x^3 &= \bar{x}^3 + u^3 t \end{aligned} \tag{1.4}$$

Linear transformations can be expressed in matrix form. In Galilean relativity, the linear transformation is a simple translation. The forward transformation of a vector component is

$$x^{\bar{b}} = \delta_a^{\bar{b}} x^a + u^{\bar{b}} t \tag{1.5}$$

with the inverse transformation

$$x^a = \delta^a_{\bar{b}} x^{\bar{b}} + u^a t \tag{1.6}$$

where $u^{\bar{b}} = -u^a$, and where the Kronecker delta is

$$\delta^{\bar{b}}_a = \begin{cases} 1 & \bar{a} = b \\ 0 & \bar{a} \neq b \end{cases} \tag{1.7}$$

which is also the identity matrix. The primed velocity is the relative velocity observed by the primed observer and is the negative of the un-primed velocity.

For a linear transformation (between inertial frames) straight trajectories in one frame remain straight trajectories in the other. The velocity transformation is expressed as

$$v^{\bar{b}} = \delta^{\bar{b}}_a v^a + u^{\bar{b}} \tag{1.8}$$

which is the classic Galilean relativity equation, and the transformation of accelerations is

$$a^{\bar{b}} = \delta^{\bar{b}}_a a^a \tag{1.9}$$

which guarantees that velocity-independent forces in the one frame are equal to the forces in the other. In other words, “physics” is observed to be the same in both inertial frames.

3. Non-Inertial Transformations

Linear transformations are only a subset of more general transformations that may not be linear. An especially important class of transformations is between non-inertial frames, such as a frame that experiences constant acceleration relative to a fixed frame.

Uniformly Accelerating Frame (non-relativistic)

Accelerating frames are quite different from inertial frames. Observers in the different frames interpret trajectories differently, invoking forces in one frame that are not needed or felt in the other. These forces arise from coordinate transformations and are called fictitious forces.

The simplest non-inertial frame is one that is accelerating with constant acceleration. Consider a primed coordinate frame that is accelerating with acceleration α along the x^3 direction relative to the original unprimed frame. An event at (x^1,x^2,x^3) at time t is observed in the primed frame at

$$
\begin{aligned}
x^{\bar{1}} &= x^1 \\
x^{\bar{2}} &= x^2 \\
x^{\bar{3}} &= x^3 - \frac{1}{2}\alpha t^2
\end{aligned}
\tag{1.10}
$$

or

$$x^{\bar{b}} = \delta_a^{\bar{b}} x^a - \frac{1}{2}\delta_3^{\bar{b}} \alpha t^2 \tag{1.11}$$

(Einstein summation convention assumed), and linear trajectory of a particle in the un-primed frame

$$x^a = x_0^a + v^a t \tag{1.12}$$

becomes a parabolic trajectory in the primed frame

$$x^{\bar{b}} = \delta_a^{\bar{b}} \left(x_0^a + v^a t \right) - \frac{1}{2}\delta_3^{\bar{b}} \alpha t^2 \tag{1.13}$$

Therefore an observer in the primed frame $\bar{O}$ would describe the dynamics of the trajectory in terms of a fictitious force along the –z axis with a magnitude $F_z = -m\alpha$, while the observer in O assumes no force. However, there is an important difference between the observers. While the observer in the unprimed frame O experiences no force on *himself or herself*, the observer in the primed frame $\bar{O}$ *does*. This force could be experienced, for instance, as the force of a space-ship floor on the feet of the observer as it accelerates forwards. If the primed observer does not know that the space-ship is the cause of the force, he or she might assume that the force is a gravitational force, and that the same gravitational force was the cause of the observed parabolic trajectory. This description of the non-inertial force leads to an important principle of physics:

Principle of Equivalence:

> An observer in a uniformly accelerating frame is equivalent to an observer in a uniform gravitational field.

According to this principle, physics in a uniform gravitational field is equivalent to physics in a frame that experiences constant linear acceleration. This principle is an important motivation for General Relativity.

The Deflection of Light by Gravity

The equivalence principle makes it easy to prove that gravity must bend the path of a light ray. Consider the cases of an Earth-bound elevator (elevator stationary in a gravitational field) compared to a constantly accelerating outer-space elevator (no gravitation). Each has a pin-hole at the top through which a photon enters at time $t = 0$, and the photon hits the far wall at a time $t = L/c$. Where does the photon hit the far wall?

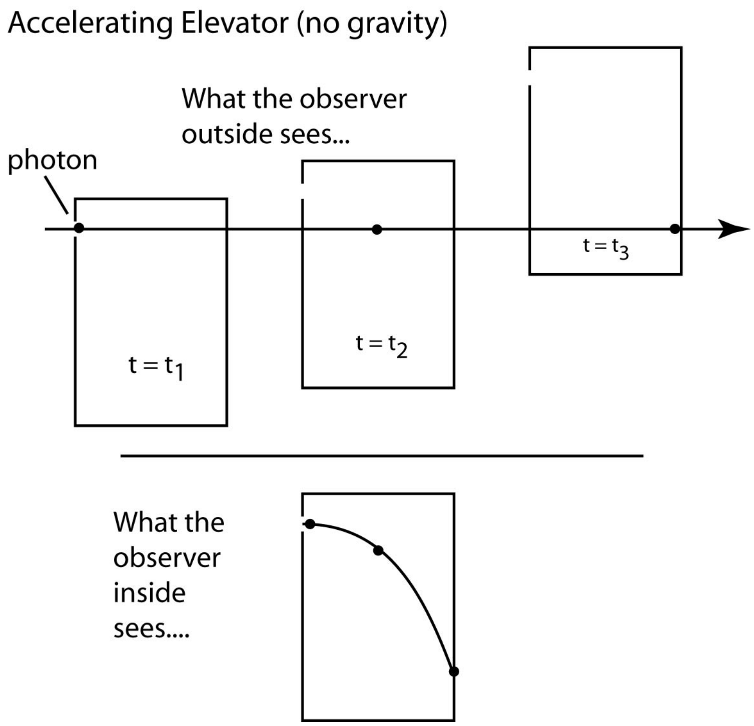

Fig. 1.3 Einstein thought experiment showing that gravity (equivalent to an accelerating elevator) deflects light.

Example 1.6: Light in an Elevator

Consider the case of the constantly accelerating elevator out in space far from any gravitating body. The light path in the fixed frame is

$$\begin{aligned} x^1 &= ct \\ x^3 &= 0 \end{aligned} \tag{1.14}$$

However, the observer in the elevator sees

$$\begin{aligned} x^{\bar{1}} &= ct \\ x^{\bar{3}} &= -\frac{1}{2}gt^2 = -\frac{1}{2}g\left(\frac{L}{c}\right)^2 \end{aligned} \tag{1.15}$$

By the principle of equivalence, an Earth-bound observer in a stationary elevator must see the same thing. The photon enters the pinhole at the top of the elevator and hits the far wall a distance $gL^2/2c^2$ from the ceiling. The inescapable conclusion is that gravity bends light! Admittedly, the effect is small. The gravitational deflection for a 1 m wide elevator accelerating with g is

$$\Delta x^{\bar{3}} = -\frac{1}{2} g \left(\frac{L}{c} \right)^2 = -6x10^{-17}\ m \tag{1.16}$$

which is almost a million times smaller than the radius of a proton. To see the effect of gravity on light, it is usually necessary to make observations over scales of solar systems or larger, and to use large gravitating bodies such as the sun or even whole galaxies. On the other hand, exquisitely sensitive solid state detectors, called Mössbauer resonance detectors, can measure effects of gravity on light over the length of a tall tower. But this is measured as a nuclear absorption effect rather than as a deflection.

The Equivalence Principle is a central motivation for General Relativity, which is the topic of Chapter 11. However, an important caveat must be mentioned when applying the Equivalence Principle. In the elevator thought experiment, the "equivalent" elevator on Earth was assumed to be in a *uniform* gravitational field. By *uniform* is meant that it is constant in both space and time. Such uniform gravitational fields are not realistic, and may only apply as approximations over very local ranges. For instance, the Equivalence Principle was first used by Einstein to calculate the deflection of a light ray by the Sun at a time when he was exploring the consequences of relativity in non-inertial frames, but before he had developed the full tensor theory of general relativity. The equivalence principle, when applied to uniform fields, only modifies the time-component of the space-time metric, but ignores any contribution from the curvature of space-time. In fact, the deflection calculated using the Equivalence Principle alone leads to an answer that is exactly half of the correct deflection obtained using the full theory of General Relativity.

4. Coriolis Physics

The effective force is

$$\vec{F}_{eff} = -2m\vec{\omega} \times \vec{v}_r \tag{1.17}$$

Consider an object moving due east:

$$\vec{v}_r = v_0 \vec{e}_y$$

then

$$\vec{\omega} = \vec{e}_z \omega \cos\theta - \vec{e}_x \omega \sin\theta$$

$$\begin{aligned}
\vec{\omega} \times \vec{v}_r &= \begin{vmatrix} \vec{e}_x & \vec{e}_y & \vec{e}_z \\ -\omega \sin\theta & 0 & \omega \cos\theta \\ 0 & v_0 & 0 \end{vmatrix} \\
&= \vec{e}_x \left(-\omega v_0 \cos\theta \right) + \vec{e}_z \left(-\omega v_0 \sin\theta \right) \\
&= \omega v_0 \left(-\cos\theta \vec{e}_x - \sin\theta \vec{e}_z \right)
\end{aligned}$$

The effective force is

$$\vec{F}_{eff} = 2m\omega v_0 \left(\cos\theta \vec{e}_x + \sin\theta \vec{e}_z \right)$$

which has a southward and upward component.

5. Rigid Body Precession

Consider a spinning rigid body, either force-free (a thrown football) or under torque (a precessing top with a fixed tip). The diagram in Fig. 1.4 is drawn at the instant that $\psi = 0$ so that the x-axis is pointing into the page at this instant and the z-axis is along the principal body axis. Since the axes are the body axes, and the body is spinning, the angle $\psi = \omega_\psi t$ is changing linearly in time. This means that the precession vector (vertical at this instant) is moving as a cone about the body axis.

Precession of a spinning rigid body (in the absence of nutation) is observed in the fixed frame as a "wobble" of the body axis around the fixed axis. The spin gives one contribution to the total angular velocity, and the precession gives another so that the total angular velocity is the vector addition of spin with precession.

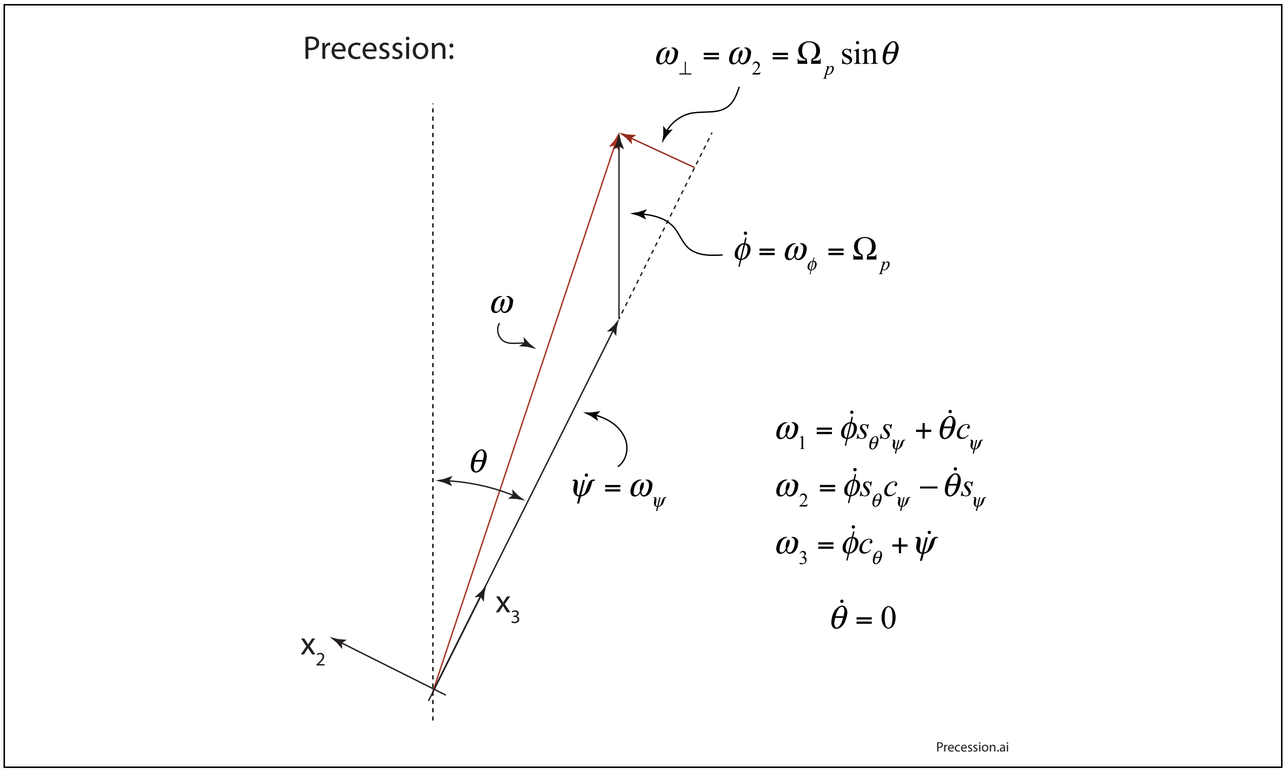

Fig. 1.4 Relationships among spin, precession and angular frequency.

In the case of *force-free motion (thrown wobbling football)*, the angular velocity given by

$$\Omega = \frac{(I_3 - I_1)}{I_1}\omega_3 \tag{1.18}$$

is the rate that the body cone rolls about the fixed cone. However, what we observe is the precession of the body axis around the fixed axis … but this is at the angular frequency $\Omega_p \neq \Omega$. What is this frequency?

The precession angular frequency is

$$\Omega_p = \frac{\omega_2}{\sin\theta} \tag{1.19}$$

Using $L_2 = I_1\omega_2$ and $L_2 = L\sin\theta$ gives

$$\begin{aligned}\Omega_p &= \frac{\omega_2}{\sin\theta}\\ &= \frac{L_2/I_1}{L_2/L} = \frac{L}{I_1}\end{aligned} \tag{1.20}$$

Therefore, the angular precession frequency is the total angular momentum divided by the transverse moment of inertia. The larger the angular momentum (the higher the spin) the faster the precession.

In the case of the tilted top with fixed tip, the precession angular frequency is again

$$\Omega_p = \frac{\omega_2}{\sin\theta} \tag{1.21}$$

but in this case (with torque), the transverse angular frequency was found to be

$$\omega_\perp = \frac{mgb\sin\theta}{I_3\omega_3} \tag{1.22}$$

Therefore, the precession is given by

$$\Omega_p = \frac{mgb}{I_3\omega_3} \tag{1.23}$$

This is interesting, because now the precession is *slower* for high spins, in contrast to the force free case above where the precession was faster for higher spins. Even though Fig. 1.4 applies to both cases, the physics leading to the precession is different.

6. Summary

Degrees of Freedom (DOF):

The number of degrees of freedom of a system is the number of initial conditions needed to uniquely specify a trajectory of the system in state space. If the system is composed of N particles with inertia, and there are K additional equations of constraint among the dynamical variables, then DOF = 6N – K and the trajectories are constrained to lie on a D = 6N – K dimensional manifold in the state space. There can be D generalized coordinates defined that span the manifold.

Serret-Frenet Formulas:

A position on a general 3D trajectory is defined by three mutually orthogonal vectors: Tangent T^i, Normal N^i and Binormal B^i.

$$\begin{aligned}
\frac{dx^a}{ds} &= T^a \\
\frac{dT^a}{ds} &= \kappa N^a \qquad\qquad N^i \times T^i = B^i \\
\frac{dN^a}{ds} &= -\kappa T^a + \tau B^a \\
\frac{dB^a}{ds} &= -\tau N^a
\end{aligned} \tag{1.21}$$

Equations of a Mathematical Flow:

A mathematical flow is an ordinary differential equation (ODE).

$$\frac{dq^a}{dt} = F^a\left(q^a; t\right) \tag{1.43}$$

This is perhaps the most important equation of this textbook. Most of the chapters in this book explore aspects of mathematical flows.

Jacobian matrix of a linear transformation:

The Jacobian matrix plays important roles in coordinate transformations and stability analysis.

row index

$$J_b^a = \frac{\partial x^a}{\partial q^b} \tag{1.48}$$

column index

The upper index (contravariant) is a row index, and the lower index (covariant) is a column index.

Metric Distance:

The arc-length differential ds

$$ds^2 = g_{11}\left(dq^1\right)^2 + g_{22}\left(dq^2\right)^2 + g_{33}\left(dq^3\right)^2 \tag{1.54}$$

plays a central role in the mathematical treatment of trajectories through complex, and possible curved, spaces.

Time-derivatives in a rotating frame:

The relationship between vectors observed in the rotating and fixed frames is given by

$$\left.\frac{d\vec{Q}}{dt}\right|_{fixed} = \left.\frac{d\vec{Q}}{dt}\right|_{rotating} + \vec{\omega}\times\vec{Q} \tag{1.94}$$

where the second term gives rise to fictitious forces.

Effective force in a rotating frame:

The effective force on a mass moving in a rotating frame contains several terms that are called fictitious forces.

$$\vec{F}_{eff} = m\vec{a}_r = F - m\ddot{\vec{R}} - m\dot{\vec{\omega}}\times\vec{r} - m\vec{\omega}\times\left(\vec{\omega}\times\vec{r}\right) - 2m\vec{\omega}\times\vec{v}_r \tag{1.102}$$

The third term relates to the angular acceleration of the rotating frame. The fourth term is the centrifugal term. The fifth term is the Coriolis term.

Moment of Inertia:

The physics of rotating solid bodies uses the concept of moments of inertia. The inertia tensor is

$$I_{ab} = \sum_{\alpha} m_\alpha \left[\delta_{ab}\left(\sum_b \left(x_\alpha^b\right)^2\right) - x_\alpha^a x_\alpha^b\right] \tag{1.131}$$

Euler's Equations:

The equations of motion of a rotating body subject to torques are

$$\begin{aligned} I_1\dot{\omega}_1 - \left(I_2 - I_3\right)\omega_2\omega_3 &= N_1 \\ I_2\dot{\omega}_2 - \left(I_3 - I_1\right)\omega_3\omega_1 &= N_2 \\ I_3\dot{\omega}_3 - \left(I_1 - I_2\right)\omega_1\omega_2 &= N_3 \end{aligned} \tag{1.147}$$

Chapter 2 Lagrangian Mechanics

1. Elastic Collision of Two Masses

The conservation of linear momentum is one of the key tools used to analyze the collisions among particles. A common problem encountered in physics is the case of a mass incident on a stationary target in the lab frame. This problem is solved easily in the center-of-mass (CM) frame, and the final trajectories are obtained by transforming the velocities from the CM frame back to the lab frame. The initial conditions are compared to the final conditions for both the lab and the CM frame in Fig. 2.1. The scattering is solved in the CM frame by considering the scattered energies as functions of the CM scattering angle θ.

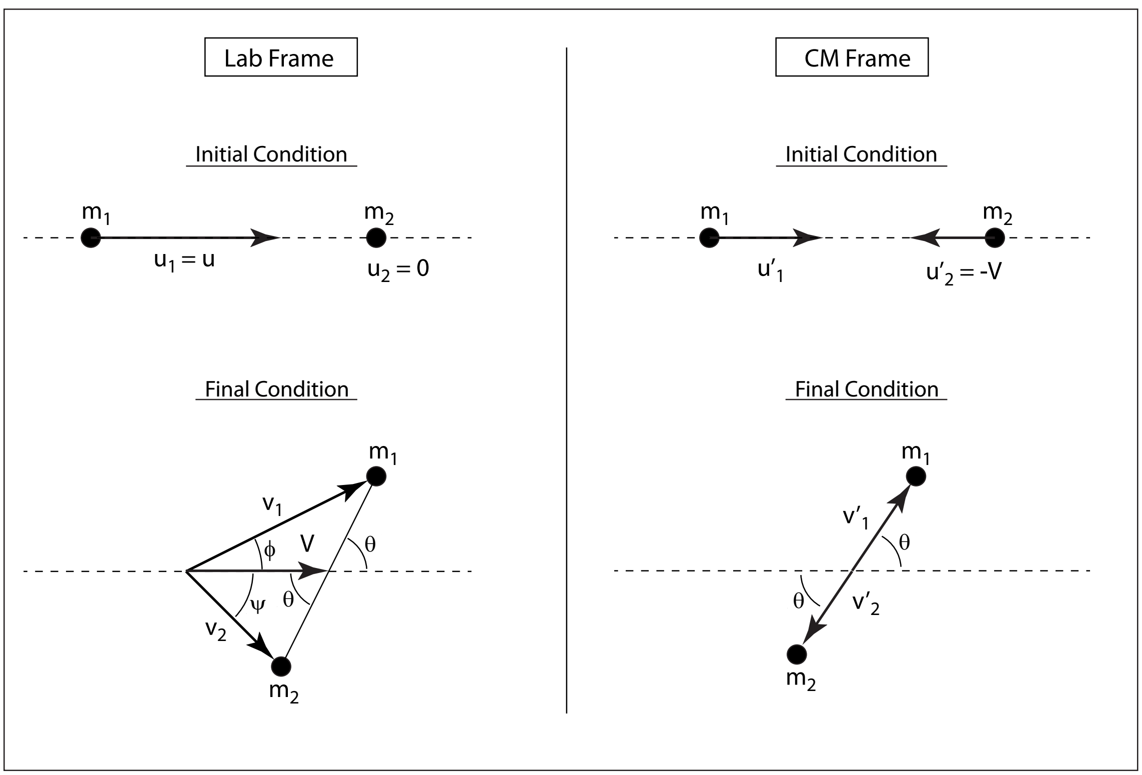

Fig. 2.1 Geometry of the elastic collision of two masses viewed from the Lab frame and from the center-of-mass (CM) frame. The dynamics are analyzed in the CM frame and transformed back into the Lab frame

The center of mass of the two particles is defined by

$$M\vec{R} = m_1\vec{r}_1 + m_2\vec{r}_2 \tag{2.1}$$

and taking the time derivative yields

$$\begin{aligned} M\vec{V} &= m_1\vec{u}_1 + m_2\vec{u}_2 \\ &= m_1\vec{u} \end{aligned} \tag{2.2}$$

which is solved for the center-of-mass velocity as

$$\vec{V} = \frac{m_1\vec{u}}{m_1 + m_2} \tag{2.3}$$

The initial velocities of the particles in the CM frame are

$$\begin{aligned} \vec{u}_1' &= \vec{u} - \vec{V} \\ \vec{u}_2' &= -\vec{V} \end{aligned} \tag{2.4}$$

Conservation of momentum holds throughout the interaction, leading to the simple balance

$$\begin{aligned} m_1\vec{u}_1' &= -m_2\vec{u}_2' \\ m_1\vec{v}_1' &= -m_2\vec{v}_2' \end{aligned} \tag{2.5}$$

Because the masses of the particles remain unchanged by the collision, the final speeds have the same relationship as the initial speeds

$$\begin{aligned} v_1' &= u_1' \\ v_2' &= u_2' \end{aligned} \tag{2.6}$$

Combing this with Eq.**Error! Reference source not found.**) and using Eq.(2.3) for the CM speed, this yields the center-of-mass speeds after the collision

$$\begin{aligned} v_2' &= \frac{m_1 u}{m_1 + m_2} \\ v_1' &= \frac{m_2 u}{m_1 + m_2} \end{aligned} \tag{2.7}$$

in which the final speeds are independent of the scattering angle θ. These are the speeds in the CM frame. To transform back to the lab frame, the components of the final velocity in the CM frame are

$$\begin{aligned} v'_{1x} &= v'_1 \cos\theta \\ v'_{1y} &= v'_1 \sin\theta \end{aligned} \tag{2.8}$$

which transform back into the lab frame as

$$\begin{aligned} v_{1x} &= v'_1 \cos\theta + \frac{m_1 u}{M} \\ v_{1y} &= v'_1 \sin\theta \end{aligned} \tag{2.9}$$

The relationship between θ and ϕ (one of the angles in the lab frame) is obtained by comparing the velocity components in the CM and lab frames

$$\begin{aligned} v_1 \sin\phi &= v'_1 \sin\theta \\ v_1 \cos\phi &= v'_1 \cos\theta + \frac{m_1 u}{M} \end{aligned} \tag{2.10}$$

Dividing these equations yields

$$\begin{aligned} \tan\phi &= \frac{\sin\theta}{\cos\theta + \dfrac{m_1 u}{v'_1 M}} \\ &= \frac{\sin\theta}{\cos\theta + \left(\dfrac{m_1}{m_2}\right)} \end{aligned} \tag{2.11}$$

which always gives a forward boost such that ϕ < θ. The kinetic energy of the first mass in the lab frame is

$$\begin{aligned} K_1 &= \frac{1}{2} m_1 \left[\left(v'_1 \cos\theta + \frac{m_1 u}{M} \right)^2 + \left(v'_1 \sin\theta \right)^2 \right] \\ &= \frac{1}{2} m_1 \left[v_1'^2 + \left(\frac{m_1 u}{M} \right)^2 + 2 \frac{m_1 v'_1 u}{M} \cos\theta \right] \end{aligned} \tag{2.12}$$

and the ratio of the kinetic energy of the first mass to its initial kinetic energy is

$$\begin{aligned} \frac{K_1}{K_0} &= \left[\left(\frac{m_2}{M} \right)^2 + \left(\frac{m_1}{M} \right)^2 + 2 \frac{m_1 m_2}{M^2} \cos\theta \right] \\ &= 1 - 2 \frac{m_1 m_2}{M^2} \left(1 - \cos\theta \right) \end{aligned} \tag{2.13}$$

which is the lab-frame ratio, but it is still expressed in terms of the CM frame scattering angle θ. The ratio equals unity for forward scattering (glancing angle on the target). The relationship Eq.(2.11) between θ and ϕ can be used to express the kinetic energy ratio in terms of the lab-frame angle.

2. The Restricted Three-body Problem

The three-body problem has a long and interesting history, and played a key role in several aspects of modern dynamics. There is no general analytical solution to the three-body problem. To find the behavior of three mutually interacting bodies requires numerical solution. However, there are subsets of the three-body problem that do yield to analytical approaches. One of these is called the restricted three-body problem[3]. It consists of two massive bodies plus a third massless body that all move in a plane. This restricted problem was first tackled by Euler and later by Poincaré, who discovered the existence of chaos in its solutions.

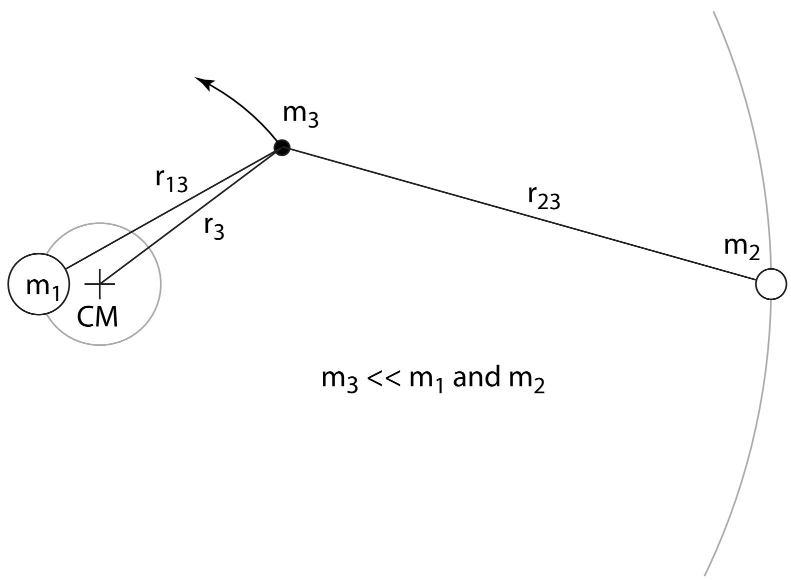

Fig. 2.2 The restricted 3-body problem in the plane. The third mass is negligible relative to the first two masses that obey 2-body dynamics.

The geometry of the restricted three-body problem is shown in Fig. 2.2. The historical interest in the three-body problem is based on considerations of the stability of Earth's orbit around the Sun when considering perturbations by a second planet such as Jupiter. In this problem, take mass $m_1 = m_S$ to be the Sun's mass, $m_2 = m_J$ to be Jupiter's mass, and the third (small) mass is the Earth. The equation of motion for the Earth is

[3] This problem was first studied by Euler in 1760.

$$\ddot{\vec{r}} = -4\pi^2 \left(\frac{\vec{r}-\vec{r}_S}{\left|\vec{r}-\vec{r}_S\right|^3} + \xi \frac{\vec{r}-\vec{r}_J}{\left|\vec{r}-\vec{r}_J\right|^3} \right) \tag{2.14}$$

where

$$\xi = \frac{M_J}{M_\odot} \qquad r_S = \frac{R_{S-J}}{1+\xi} \qquad r_J = \frac{\xi R_{S-J}}{1+\xi}$$

and the parameter ξ characterizes the strength of the perturbation of the Earth's orbit around the Sun. The parameters for the Jupiter-Sun system are

$$r_{S-J} = 5.203 \qquad x_J = r_J \cos\omega_J t \qquad y_J = r_J \sin\omega_J t$$

$$x_S = -r_S \cos\omega_J t \qquad y_S = -r_S \sin\omega_J t$$

with

$$\omega_J = \frac{2\pi}{11.86}$$

for the 11.86 year journey of Jupiter around the Sun. Eq. (2.14) is a four-dimensional non-autonomous flow

$$\begin{aligned}
\dot{v} &= -4\pi^2 \left(\frac{\left(x + r_S \cos\omega_J t\right)}{\left(\left(x + r_S\cos\omega_J t\right)^2 + \left(y + r_S \sin\omega_J t\right)^2\right)^{3/2}} + \xi \frac{\left(x - r_J \cos\omega_J t\right)}{\left|\left(x - r_J\cos\omega_J t\right)^2 + \left(y - r_J \sin\omega_J t\right)^2\right|^{3/2}} \right) \\
\dot{x} &= v \\
\dot{u} &= -4\pi^2 \left(\frac{\left(y + r_S \sin\omega_J t\right)}{\left(\left(x + r_S\cos\omega_J t\right)^2 + \left(y + r_S \sin\omega_J t\right)^2\right)^{3/2}} + \xi \frac{\left(y - r_J \sin\omega_J t\right)}{\left|\left(x - r_J\cos\omega_J t\right)^2 + \left(y - r_J \sin\omega_J t\right)^2\right|^{3/2}} \right) \\
\dot{y} &= u
\end{aligned}$$

The solutions of an Earth orbit are shown in Fig. 2.3. The natural Earth-Sun-Jupiter system has a mass ratio $m_J/m_S = 0.001$. Even in this case, Jupiter causes perturbations of the Earth's orbit by about one percent. If the mass of Jupiter increases, the perturbations would grow larger until around 0.06 when the perturbations become severe and the orbit grows unstable. The Earth gains energy from the momentum of the Sun-Jupiter system and can reach escape velocity. The simulation for a mass ratio of 0.07 shows the Earth ejected from the Solar System.

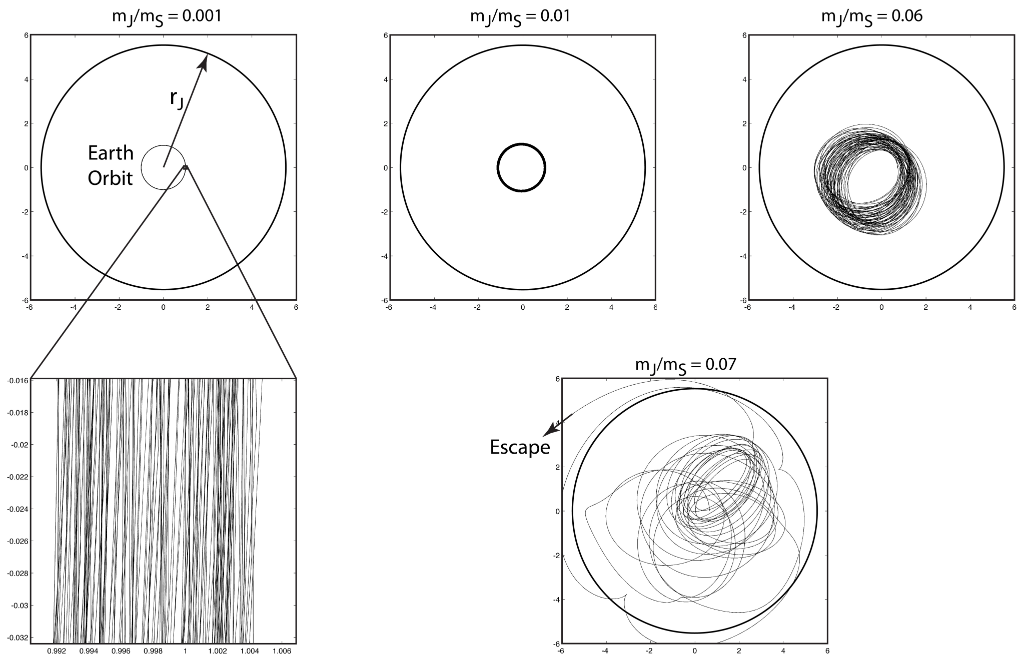

Fig. 2.3 Orbit of Earth as a function of the size of a Jupiter-like planet. The natural system has a Jupiter-Sun mass ratio of 0.001. As the size of Jupiter increases, the Earth orbit becomes unstable and can acquire escape velocity to escape from the Solar System. (From body3.m)

The discovery of chaos in the solar system was a watershed moment in the history of physics. The first hint at the existence of chaos was seen by the French mathematician Henri Poincaré in 1889 as he strove to prove whether the solar system was stable, participating in a mathematics competition sponsored by the king of Sweden. He won the competition by inventing a wide array of new mathematical tools that capture the qualitative behavior of dynamical systems (many of these are introduced in Chap. 3), but during the proof-reading of his winning manuscript, he discovered an error. As he frantically worked to correct his proof in time for printing, he uncovered an infinite nesting of patterns that showed that the restricted 3-body problem was anything but stable, exhibiting complex behavior that was beyond his ability to follow. The published (and corrected) paper contained this first glimpse of chaos, which launched later mathematicians to explore deeper consequences[4]. The history of chaos theory has always been closely entwined with the physics of the solar system, but recent topics in the physics of chaos travel much farther, as will be introduced in Chap. 3 and pursued in many forms (evolutionary theory, nonlinear synchronization, dynamic networks, neural nets, and econophysics) through Chaps. 4-8.

[4] For a history of Poincaré's discovery of chaos, see J. Barrow-Green, *Poincaré and the Three Body Problem* (London Mathematical Society, 1997). Popular books on chaos in the solar system are Ivars Peterson, *Newton's Clockworks* (Macmillan, 1993) and F. Diacu and P. Holmes, *Celestial encounters* (Princeton Univ. Press, 1996).

Chapter 3 Hamiltonian Dynamics and Phase Space

1. Legendre Transforms and the Hamiltonian

Going deeper into the geometric aspects of Legendre transforms, it is important to note a momentum is not in general related linearly to the conjugate generalized velocity. In Cartesian coordinates, one may have $p = m\dot{q}$, but this is not generally true for generalized coordinates. Note, too that momenta p_a are strictly covariant vectors, while generalized coordinates q^a are contravariant vectors. This is seen directly in the definition of the conjugate momenta

$$p_a = \frac{\partial L}{\partial \dot{q}^a}$$

which is a covariant derivative. For non-Cartesian or non-Euclidean geometries, this distinction must be maintained. The Legendre transform guarantees that the transformed function of momenta $H\left(q^a, p_a\right)$ has the correct form in these non-Cartesian and non-Euclidean geometries.

2. Canonical Transformation

There are four types of generating functions M that allow canonical transformations. These are outlined in Table I.

Table 2.1. Four Canonical Transformations

Generating Function	Derivatives	Special Case
$M = F_1\left(q, Q, t\right)$	$p_a = \frac{\partial F_1}{\partial q^a} \qquad P_a = -\frac{\partial F_1}{\partial Q^a}$	$F_1 = q^a Q^a \quad Q^a = p_a \quad P_a = -q^a$
$M = F_2\left(q, P, t\right) - Q^a P_a$	$p_a = \frac{\partial F_2}{\partial q^a} \qquad Q^a = \frac{\partial F_1}{\partial P_a}$	$F_2 = q^a P_a \quad Q^a = q^a \quad P_a = p_a$

$M = F_3(p,Q,t) + q^a p_a$	$q^a = -\dfrac{\partial F_3}{\partial p_a} \qquad P_a = -\dfrac{\partial F_3}{\partial Q^a}$	$F_3 = p_a Q^a \quad Q^a = -q^a \quad P_a = -p_a$
$M = F_4(p,P,t) + q^a p_a - Q^a P_a$	$q^a = -\dfrac{\partial F_4}{\partial p_a} \qquad Q^a = \dfrac{\partial F_4}{\partial P_a}$	$F_4 = p_a P_a \quad Q^a = p_a \quad P_a = -q^a$

As an example, consider the first type of canonical transformation that has

$$q \to q \quad p \to Q \tag{3.1}$$

with

$$M(q,Q,t) = F_1(q,Q,t) \tag{3.2}$$

and

$$\frac{dM}{dt} = \frac{\partial F_1}{\partial t} + \sum_{a=1}^{D}\left[\frac{\partial F_1}{\partial q^a}\dot{q}^a + \frac{\partial F_1}{\partial Q^a}\dot{Q}^a\right] \tag{3.3}$$

This satisfies the condition for a canonical transformation when

$$p_a = \frac{\partial F_1}{\partial q^a} \qquad P_a = -\frac{\partial F_1}{\partial Q^a} \qquad H' = H + \frac{\partial F_1}{\partial t} \tag{3.4}$$

This transformation is a common choice for the simple harmonic oscillator.

3. Conservation of Phase Space Volume (Simple Approach)

(For a detailed history of Phase Space and Liouville's Theorem see the Physics Today article.)

We have for the divergence of a flow (IMD2 Eq. 3.44)

$$\frac{dV}{dt} = \int_V \left(\vec{\nabla} \cdot \vec{f}\right) dV$$

where f is the right-hand-side of the flow in standard form. For small volumes this is

$$\frac{dV}{dt} = \left(\vec{\nabla} \cdot \vec{f}\right) V$$
$$\frac{1}{V}\frac{dV}{dt} = \vec{\nabla} \cdot \vec{f}$$

For a Hamiltonian flow, the vector flow function is

$$\vec{f} = \left(\frac{\partial H}{\partial p_a}, -\frac{\partial H}{\partial q^a} \right)$$

The divergence is thus

$$\begin{aligned} \vec{\nabla} \cdot \vec{f} &= \frac{\partial}{\partial a^a}\left(\frac{\partial H}{\partial p_a}\right) - \frac{\partial}{\partial p_a}\left(\frac{\partial H}{\partial q^a}\right) \\ &= \frac{\partial}{\partial a^a}\frac{\partial H}{\partial p_a} - \frac{\partial}{\partial p_a}\frac{\partial H}{\partial q^a} \\ &= 0 \end{aligned}$$

Therefore, Hamilton's equations guarantee that the divergence of a Hamiltonian flow vanishes—phase-space volume is conserved!

4. Symplectic Geometry of Flows in Phase Space

In Chapter 1, a dynamical *flow* was defined generally as

$$\dot{q}^a = g^a\left(x^1, x^2, \ldots\right) \tag{3.5}$$

where the q^a are the dynamical variables and g^a can be any nonlinear vector function of the dynamical variables. The vector function g^a defines the local flow field, and the solution to the flow equation is $q^a(t)$, which defines a parametric curve (flow line) for each initial condition, with time as the parametric variable. Hamilton's equations clearly define a flow in a 2N-dimensional phase space for N pairs of $\left(q^a, p_a\right)$. However, there is a strong symmetry in Hamilton's equations that impose certain properties on the possible solutions. In other words, Hamilton's equations are not general flows, but are a restricted set of flows. This special symmetry can be used to construct a structure for Hamiltonian trajectories that is called symplectic geometry.

To begin constructing this structure, define a set of 2N coordinates η^a such that

$$\begin{aligned} \eta^a &= q^a \\ \eta^{a+N} &= p_a \end{aligned} \tag{3.6}$$

for a = 1:N. Therefore, the phase flow is described by

$$\left(\dot{\eta}^a, \dot{\eta}^{a+N}\right) = \left(\frac{\partial H}{\partial \eta^{a+N}}, -\frac{\partial H}{\partial \eta^a}\right) \tag{3.7}$$

where we have used Hamilton's equations for the time derivatives. We would like to define a flow on the single set of variables η^a. A compact notation to accomplish this is

$$\dot{\eta}^a = \omega^{ab} \frac{\partial H}{\partial \eta^b} \tag{3.8}$$

where ω^{ab} is a skew-symmetric matrix

$$\omega^{ab} = -\omega^{ba} = \pm 1 \tag{3.9}$$

As an example, for 3 variables and their conjugate momenta, the skew-symmetric matrix is

$$\omega^{ab} = \begin{pmatrix} 0 & 0 & 0 & 1 & 0 & 0 \\ 0 & 0 & 0 & 0 & 1 & 0 \\ 0 & 0 & 0 & 0 & 0 & 1 \\ -1 & 0 & 0 & 0 & 0 & 0 \\ 0 & -1 & 0 & 0 & 0 & 0 \\ 0 & 0 & -1 & 0 & 0 & 0 \end{pmatrix} \tag{3.10}$$

which is block-diagonal. The determinant of this matrix is

$$\left|\omega^{ab}\right| = 1 \tag{3.11}$$

Its product with itself is minus the identity

$$\omega^2 = -I \tag{3.12}$$

and it has following inverse properties

$$\left(\omega^{ab}\right)^{-1} = \left(\omega^{ab}\right)^T = \omega^{ba} = -\omega^{ab} \tag{3.13}$$

The matrix ω^{ab} is of particular utility in evaluating areas in phase space. For instance an area in phase space is expressed as

$$\delta a = \omega^{ab} d\eta^a d\eta^b \tag{3.14}$$

As an example, consider the parallelogram defined by the two vectors in a 6-dimensional phase space

$$d\eta = \left(dq^1, dq^2, dq^3, dp_1, dp_2, dp_3\right) \tag{3.15}$$

and in matrix form Eq. (3.14) is

$$\begin{aligned}
\delta a &= \begin{pmatrix} dq^1(1) \\ dq^2(1) \\ dq^3(1) \\ dp_1(1) \\ dp_2(1) \\ dp_3(1) \end{pmatrix}^T \begin{pmatrix} 0 & 0 & 0 & 1 & 0 & 0 \\ 0 & 0 & 0 & 0 & 1 & 0 \\ 0 & 0 & 0 & 0 & 0 & 1 \\ -1 & 0 & 0 & 0 & 0 & 0 \\ 0 & -1 & 0 & 0 & 0 & 0 \\ 0 & 0 & -1 & 0 & 0 & 0 \end{pmatrix} \begin{pmatrix} dq^1(2) \\ dq^2(2) \\ dq^3(2) \\ dp_1(2) \\ dp_2(2) \\ dp_3(2) \end{pmatrix} \\
&= \left[dq^1(1)dp_1(2) - dp_1(1)dq^1(2)\right] \\
&\quad + \left[dq^2(1)dp_2(2) - dp_2(1)dq^2(2)\right] \\
&\quad + \left[dq^3(1)dp_3(2) - dp_3(1)dq^3(2)\right] \\
&= dq^a(1)dp_a(2) - dp_a(1)dq^a(2)
\end{aligned} \tag{3.16}$$

The relationship on the last line of Eq. (3.16) is more succinctly represented through a so-called "wedge" product, also known as an exterior Grassmann product, represented by

$$\delta a = dq^a \wedge dp_a \tag{3.17}$$

With this definition, there is no need to introduce the matrix ω^{ab}, and we could develop a consistent theory of the geometry of phase space without resorting to any rank-2 tensor, but we will not use the wedge-product notation further.

5. Conservation of Phase Space Volume (Symplectic Approach)

The preceding derivation of Liouville's theorem uses a limiting approximation that is not required for the validity of the theorem. A more powerful proof relies on the special geometry of phase space imposed by the symplectic structure of Hamilton's equations with its associated mathematical tools and proofs. For instance, to show that area in phase space is invariant under time evolution described by Hamilton's equations, consider the time evolution of phase space coordinates from an initial set of coordinates to a new coordinate set

$$\eta^a \to X^a \tag{3.18}$$

The new coordinates are related to the old by the coordinate transformation

$$dX^a = J_b^a d\eta^b \tag{3.19}$$

where J_b^a is the Jacobian of the coordinate transformation determined by the time evolution of the Hamiltonian dynamics. Starting from this equation we have

$$\begin{aligned} dX^a &= J_b^a d\eta^b \\ &= J_b^a \omega^{bc} \frac{\partial H}{\partial \eta^c} dt \end{aligned} \tag{3.20}$$

using Eq. (3.8). Furthermore, by substituting in Eq. (3.19), this yields

$$\begin{aligned} dX^a &= J_b^a \omega^{bc} \frac{\partial H}{\partial \eta^c} dt \\ &= J_b^a \omega^{bc} J_c^d \frac{\partial H}{\partial X^d} dt \end{aligned} \tag{3.21}$$

and by taking the Hamiltonian (symplectic) transformation property of ω^{bc}

$$\omega^{ad} = J_b^a \omega^{bc} J_c^d \tag{3.22}$$

gives

$$dX^a = \omega^{ad} \frac{\partial H}{\partial X^d} dt \tag{3.23}$$

which is just Hamilton's equations (Eq. (3.8)) in the new coordinates. The description of the evolution of an area in phase space is then

$$\begin{aligned}
\delta a &= d\eta^a \omega^{ab} d\eta^b \\
&= -d\eta^a \omega_{ab} d\eta^b \\
&= -d\eta^a J_a^c \omega_{cd} J_b^d d\eta^b \\
&= -\left(d\eta^a J_a^c\right)\omega_{cd}\left(J_b^d d\eta^b\right) \\
&= -dX^c \omega_{cd} dX^d \\
&= dX^c \omega^{cd} dX^d \\
&= \delta A
\end{aligned} \tag{3.24}$$

where δa is the original area, and δA is the evolved area. In other words, the new area after evolution through time is equal to the original area. Therefore, *areas are preserved under time evolution of the Hamiltonian system*.

That volumes in phase space also remain invariant to time evolution can be seen through the relationship between volumes in original coordinates and transformed coordinates

$$dQ^1 \ldots dQ^n dP_1 \ldots dP_n = |J|\, dq^1 \ldots dq^n dp_1 \ldots dp_n \tag{3.25}$$

where |J| is the Jacobian determinant. If $|J| = 1$, then the time evolution keeps the volumes in phase space invariant. Taking the determinant of the symplectic condition of Eq. (3.22) gives

$$|\omega| = |J|^2 |\omega| = \pm 1 \tag{3.26}$$

and hence

$$|J| = \pm 1 \tag{3.27}$$

which is what is needed to show that time evolution keeps volumes of phase space invariant.

In the case of a Hamiltonian system, the flow is defined by

$$\begin{aligned}
\dot{q}^a &= \dot{\eta}^a = f^a\left(\eta^1, \eta^2, \ldots\right) = \frac{\partial H}{\partial \eta^{a+N}} \\
\dot{p}_a &= \dot{\eta}^{a+N} = f^{a+N}\left(\eta^1, \eta^2, \ldots\right) = -\frac{\partial H}{\partial \eta^a}
\end{aligned} \tag{3.28}$$

Therefore, for a small volume of initial conditions

$$\begin{aligned}\frac{1}{V}\frac{dV}{dt} &= \vec{\nabla}\cdot\vec{f} \\ &= \frac{\partial f^a}{\partial \eta^a}\end{aligned} \tag{3.29}$$

The expressions for f^a are given in Eq. (3.28) for the Hamiltonian H, that give

$$\begin{aligned}\frac{1}{V}\frac{dV}{dt} &= \frac{\partial}{\partial \eta^a}\left(\frac{\partial H}{\partial \eta^{a+N}}\right) + \frac{\partial}{\partial \eta^{a+N}}\left(-\frac{\partial H}{\partial \eta^a}\right) \\ &= \frac{\partial^2 H}{\partial \eta^a \partial \eta^{a+N}} - \frac{\partial^2 H}{\partial \eta^a \partial \eta^{a+N}} \\ &= 0\end{aligned} \tag{3.30}$$

and the divergence equals zero identically because of the relationship between the position and momentum partial derivatives of the Hamiltonian [5].

6. Examples of the use of Poisson Brackets

Applying Poisson brackets to position and momentum lead directly back to Hamilton's equations

$$\begin{aligned}\dot{q} &= \frac{\partial q}{\partial q}\frac{\partial H}{\partial p} - \frac{\partial q}{\partial p}\frac{\partial H}{\partial q} = \frac{\partial H}{\partial p} \\ \dot{p} &= \frac{\partial p}{\partial q}\frac{\partial H}{\partial p} - \frac{\partial p}{\partial p}\frac{\partial H}{\partial q} = -\frac{\partial H}{\partial q}\end{aligned}$$

The Poisson bracket between two conjugate variables leads to a non-zero commutator relation

$$\{p,q\} = \frac{\partial p}{\partial q}\frac{\partial q}{\partial p} - \frac{\partial p}{\partial p}\frac{\partial q}{\partial q} = -1$$

[5] The conservation of phase space volume for a Hamiltonian system is called Liouville's theorem. Liouville was one of the leading French mathematicians in the first half of the 1800's, and he published a short paper in 1838 on a relationship among partial derivatives. Jacobi applied this theorem to Hamilton's equations in 1848, which was used by Boltzmann in 1871 to prove that phase space volume was conserved by the thermodynamics of a gas. It is remarkable that Liouville was completely unaware of the relevance of his 1838 theorem to dynamical systems, yet the conservation of phase space today carries his name. The history of phase space and of Liouville's theorem traces an arc through the central topics of 19th-century physics, and made some unexpected turns. A review of the history is given in Nolte (Physics Today, 2010).

This non-zero commutator has a direct analog in the commutation of operators in quantum mechanics, where, for instance

$$\left[\hat{p},\hat{q}\right] = -i\hbar$$

This kind of commutator is a key element in Heisenberg's uncertainty principle, where

$$\sigma_A \sigma_B \geq \frac{1}{2}\left|\left\langle\left[\hat{A},\hat{B}\right]\right\rangle\right|$$

for two quantum operators $\hat{A}$ and $\hat{B}$. If they commute, then a single state (wave function) can be an eigenstate of each. However, if they do not commute, then no state can be found that is simultaneously an eigenstate of each operator.

For general problems, the Poisson bracket can be used to monitor the time change of quantities of interest. For example, in the case of the simple harmonic oscillator with a slowly-varying spring constant, the potential energy varies as

$$\begin{aligned}\frac{d}{dt}V &= \frac{\partial V}{\partial t} + \frac{\partial V}{\partial q}\frac{\partial H}{\partial p} - \frac{\partial V}{\partial p}\frac{\partial H}{\partial q} \\ &= \frac{1}{2}q^2\frac{\partial k}{\partial t} + kq\frac{p}{m} - 0 = \frac{1}{2}q^2\dot{k} + kq\dot{q}\end{aligned}$$

The first term on the right is the change in internal energy of the spring. The last term is recognized as the work per time (power is force times speed) performed on the system by the changing spring constant.

7. Action-Angle Variables

Example 2.6 Action-Angle Variables for the Pendulum

A 1D pendulum provides a simple *nonlinear* example. The Hamiltonian is

$$H = \frac{p_\phi^2}{2mL^2} + mgL\left(1-\cos\phi\right) \tag{3.31}$$

where g is the acceleration due to gravity and p_θ is the angular momentum around the axis of motion. The angular momentum is

$$p_\phi = \pm\sqrt{2mL^2\left[E - mgL\left(1-\cos\phi\right)\right]} \tag{3.32}$$

and the action is

$$J\left(E\right) = \pm\frac{1}{2\pi}\oint\sqrt{2mL^2\left[E - mgL\left(1-\cos\phi\right)\right]}\,d\phi \tag{3.33}$$

This is an elliptic integral which is tabulated numerically.

The action can still be described by

$$\begin{aligned} J &= \frac{H}{\omega} \\ \theta &= \omega t \end{aligned} \tag{3.34}$$

where $\omega = 2\pi / T\left(E\right)$, and *T(E)* is the period of oscillation for a trajectory with energy E. But for the pendulum with arbitrary amplitude, *T(E)* is no longer equal for all trajectories, and the motion is no longer harmonic. The period of oscillation *T(E)* is a function of the energy of the pendulum. Note that the physical angle of the pendulum is $\phi(t)$ and is not a harmonic function, while $\theta(t)$ is the action angle and is a linear function of t.

Action-Angle Canonical Transformation Example: Straight-line Motion

Action-angle variables can be defined even for non-periodic motion. Consider a mass moving in 1-dimension without forces. The linear momentum is a constant of the motion, but the action-angle transformation seeks an action variable with units of angular momentum (angular momentum and action have the same units). The angular momentum is also a constant of this motion, and is

$$\begin{aligned} p_\phi &= m\dot{x}r\cos\phi \\ &= m\dot{x}b \end{aligned}$$

where $r\cos\theta = b$ the impact parameter. Expressing the Hamiltonian in this new variable gives

$$H = \frac{1}{2}m\dot{x}^2 = \frac{p_\phi^2}{2mb^2}$$

The action integral is

$$J = \frac{1}{\pi}\int_{-\pi/2}^{\pi/2} m\dot{x}b\,d\phi = m\dot{x}b = p_\phi$$

and the energy is

$$H = \frac{J^2}{2mb^2}$$

The equations of motion are

$$\dot{\theta} = \frac{\partial H}{\partial J} = \frac{J}{mb^2} = \omega$$
$$\dot{J} = -\frac{\partial H}{\partial \theta} = 0$$

The action angle is

$$\theta = \frac{x}{b} = \tan\phi$$

Note that the action angle θ is not the physical angle ϕ in configuration space. The action angle θ changes uniformly in time, while the rate of change of ϕ does not.

A generating function of Type I can be constructed for this simple problem. Note that

$$m\dot{x} = \frac{\partial F_1}{\partial x} \quad \text{and} \quad J = -\frac{\partial F_1}{\partial \theta}$$

which imply

$$F_1 \sim m\dot{x}x \quad \text{and} \quad F_1 \sim -J\theta$$

which, using $\dot{x} = b\omega$, yields the generating function

$$F_1(x,\theta) = bm\omega x - J\theta$$

for this example.

8. Summary

Euler Equations:

In the calculus of variations, the integral of a function f integrated between two endpoints is minimized when the following condition is satisfied

$$\left(\frac{\partial f}{\partial y}\right)-\frac{d}{dx}\left(\frac{\partial f}{\partial y'}\right)=0 \tag{2.9}$$

These equations determine the condition for stationarity of an integral.

Euler-Lagrange Equations:

The equations of motion are defined by the Lagrangian function $L = T - U$ of generalized coordinates q^a

$$\frac{\partial L}{\partial q^a}-\frac{d}{dt}\left(\frac{\partial L}{\partial \dot{q}^a}\right)=0 \tag{2.20}$$

Conjugate Momenta:

The dynamic momenta p_a that are conjugate to generalized coordinates q^a are

$$p_a=\frac{\partial H}{\partial \dot{q}^a} \tag{2.58}$$

Hamilton's Canonical Equations:

Hamilton's equations of motion for coordinate-momentum pairs are defined by the Hamiltonian function $H = T + U$ as

$$\begin{aligned}\dot{q}^a &= \frac{\partial H}{\partial p_a}\\ \dot{p}_a &= -\frac{\partial H}{\partial q^a}\end{aligned} \tag{2.63}$$

Effective Potential in Central-Force Motion:

Central force motion in a potential $V(r)$ can be reduced to motion in an effective potential

$$\mathcal{V}(r)=V(r)+\frac{\ell^2}{2\mu r^2} \tag{3.91}$$

expressed in terms of the reduced mass μ and the conserved angular momentum ℓ.

Hamilton's Equations in Symplectic Notation:

The symplectic symmetry of the Hamiltonian between conjugate coordinate-momentum pairs allows a simpler expression of Hamilton's equations.

$$\dot{\eta}^a=\omega^{ab}\frac{\partial H}{\partial \eta^b} \tag{3.119}$$

Action-Angle Variables:

Integrable systems can be reduced to action-angle variables with simple equations of motion on a hyperdimensional torus in phase space

$$\begin{aligned}\dot{J}_a &= -\frac{\partial H}{\partial \theta^a} = 0 \\ \dot{\theta}^a &= \frac{\partial H}{\partial J_a} = \omega^a\end{aligned} \tag{3.160}$$

Action:

Action is an integral around a trajectory in phase space

$$J_k = \frac{1}{2\pi}\oint_k p_a\, dq^a \tag{3.166}$$

Chapter 4 Nonlinear Dynamics and Chaos

1. Nullclines and Separatrixes

Nullclines and separatrixes do not in general overlap. Nullclines are the nonlinear functions that define the flow. Separatrixes are the stable and unstable manifolds with directions defined by the eigenvectors at the fixed point. An example of the general case is shown in Fig. 4.1.

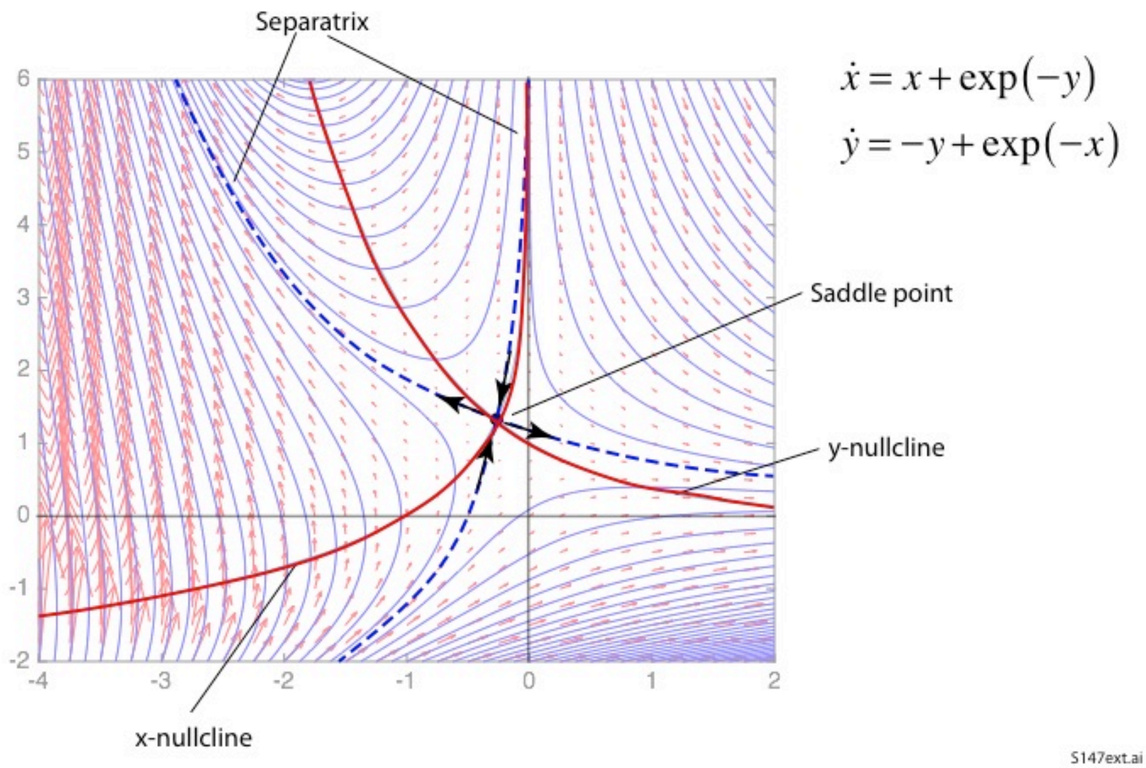

Fig. 4.1 A 2D flow showing nullclines and separatrixes attached to a saddle fixed point. (S147ext.m)

2. Andronov-Hopf Bifurcations

Limit cycles can occur when there is a balance between competing terms in the flow equations. In the case of the van der Pol oscillator, it is the balance between the gain parameter and the nonlinear self-limiting term in the equation. Therefore, one can think of the system as having a *control parameter* that can be used to tune one of the competing terms and hence change the balance. In this situation, there is often a threshold value for the control parameter at which the qualitative behavior of the system changes abruptly. This is called a *bifurcation*.

Consider a flow in (r, θ) where there is a control parameter c that varies continuously from negative values through zero to positive values

$$\begin{aligned}\dot{r} &= r\left(c - r^2\right) \\ \dot{\theta} &= 1\end{aligned} \tag{4.1}$$

The fixed points of the flow are

$$\begin{aligned}r^* &= 0 \\ r^* &= \sqrt{c}\end{aligned} \tag{4.2}$$

where the first is a node at the origin and the second is the radius of a limit cycle. The Lyapunov exponent of the node at $r^* = 0$ is $\lambda = c$, and hence the node is stable if c < 0 and unstable if c > 0. Furthermore, the limit cycle exists only when the argument of the square-root is positive, which also occurs when the control parameter c > 0, and hence the unstable node is bounded by the limit cycle, just as in the case of the Van der Pol oscillator in Eq.(??). Therefore, as the control parameter c increases from negative values and crosses zero, the stable node at the origin converts to an unstable spiral that is bounded by a limit cycle. The radius of the limit cycle increases with increasing magnitude c. Therefore, there is a qualitative and sudden change in behavior of the system at the threshold value c = 0. This constitutes a bifurcation for this flow.

The system dynamics are plotted as a function of time in Fig. 4. as the control parameter slowly increases as a function of time from negative values through the bifurcation threshold to positive values, and then slowly decreases again through the bifurcation threshold. The horizontal axis is the control parameter, parameterized by the time. The amplitude of the limit-cycle oscillations varies as $\sqrt{c}$, shown as the continuous curve in the figure. In the numerical simulation, the system shows a hysteresis with a delayed onset of the oscillations with increasing c, and a delayed extinction with decreasing c. This hysteresis is due to critical slowing down near the threshold and to the finite rate of the sweeping control parameter. The Lyapunov exponent, which is the relaxation rate, approaches zero at the threshold, and there is not enough time for the system to relax as the control parameter is changed through successive values. Once the system is far enough from the threshold, the oscillation amplitude follows the square-root prediction.

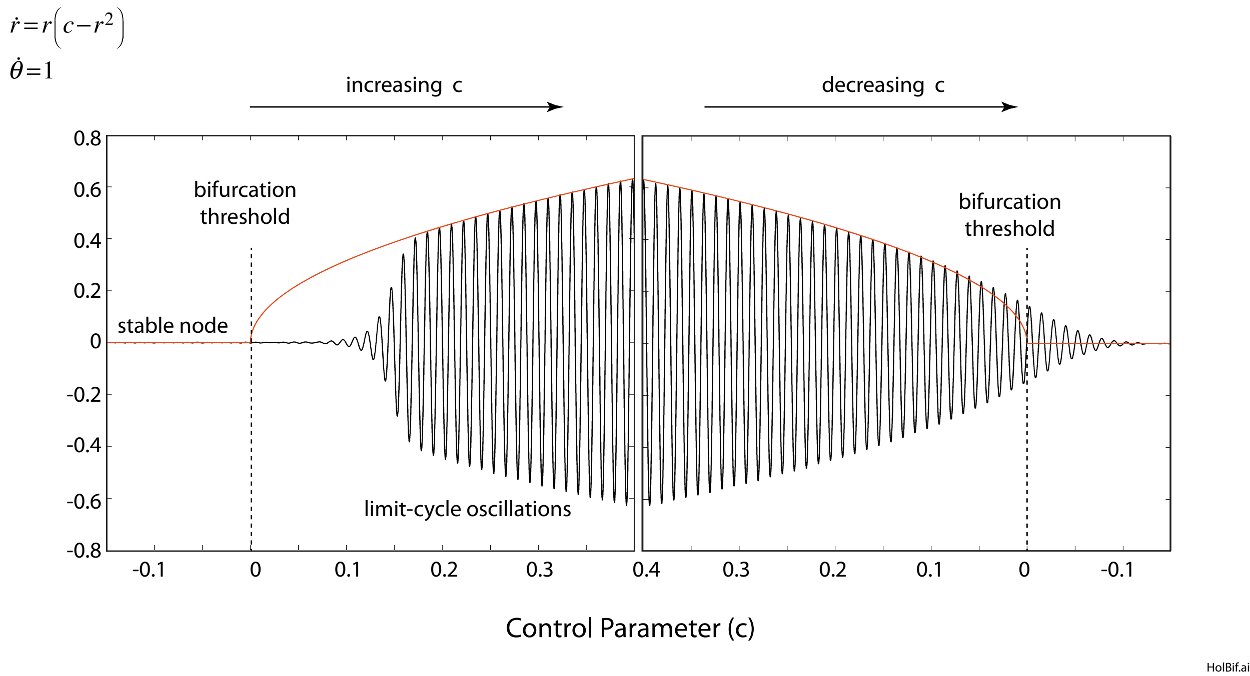

Fig. 4.4 The system dynamics as the control parameter, c, increases slowly from negative (stable node) through the Hopf bifurcation at $c = 0$ to the stable limit cycle. The parameter then decreases slowly through the bifurcation threshold again. The hysteresis between the onset (extinction) of the oscillations is caused by finite-time effects.

An interesting thing happens to the system dynamics when the sign of the r^2 term in Eq. (4.1) is flipped to $(c+r^2)$. The Lyapunov exponent is the same, and the origin is still a stable node for $c < 0$ and unstable for $c > 0$. But in this case, the limit cycle only exists for $c < 0$, and furthermore the stability of the limit cycle changes to an unstable limit cycle. If the control parameter c starts at negative values, the central node is stable, but as $c > 0$, the system catastrophically diverges. In the example with $(c-r^2)$, the system always finds a stable solution regardless of the sign of the control parameter, converging on a stable limit cycle in one case or a stable node in the other. But in the example with $(c+r^2)$, the system only leads to a stable solution in the special case when $c < 0$, and the initial conditions are inside the limit cycle radius. For all other situations, the system diverges. Although each example shows a critical bifurcation threshold, known as an *Andronov-Hopf bifurcation* or sometimes just *Hopf bifurcation*, the system behavior at the bifurcation is qualitatively different. In the first globally stable case, the bifurcation is called *supercritical*, while in the second the bifurcation is called *subcritical*.

There are many types of bifurcations that can occur in nonlinear systems that go beyond the simple Hopf bifurcation examples here. Many of these are classified depending on whether the transitions are continuous or discontinuous, whether or not they lead to system hysteresis, and on their global stability properties[6].

---

[6] Bifurcations tend to have descriptive names, such as pitchfork, flip or saddle-node bifurcations, among others.

3. DLA

The analogy of the scaling of a fractal with fractional dimension is sometimes more easily visualized from the way that the mass enclosed in a surface increases as the surface expands. For instance in systems with Euclidean dimension E, the mass enclosed by a “sphere” of radius r increases as r^E. The mass of a line increases as r, of a plane as r^2 and of a volume as r^3. In these cases the mass dimension is equal to the Euclidean dimension. This idea of a mass dimension is generalized easily to fractal objects, such as the aggregate shown in Fig. 4.5. This aggregate is known as a diffusion-limited aggregate (DLA), and sometimes occurs in colloidal systems. As the radius of the circle increases, the mass within the circle increases as the power $r^{1.7}$. Therefore, this DLA has a mass exponent that behaves as if it were a fractional-dimensional object with fractal dimension D = 1.7.

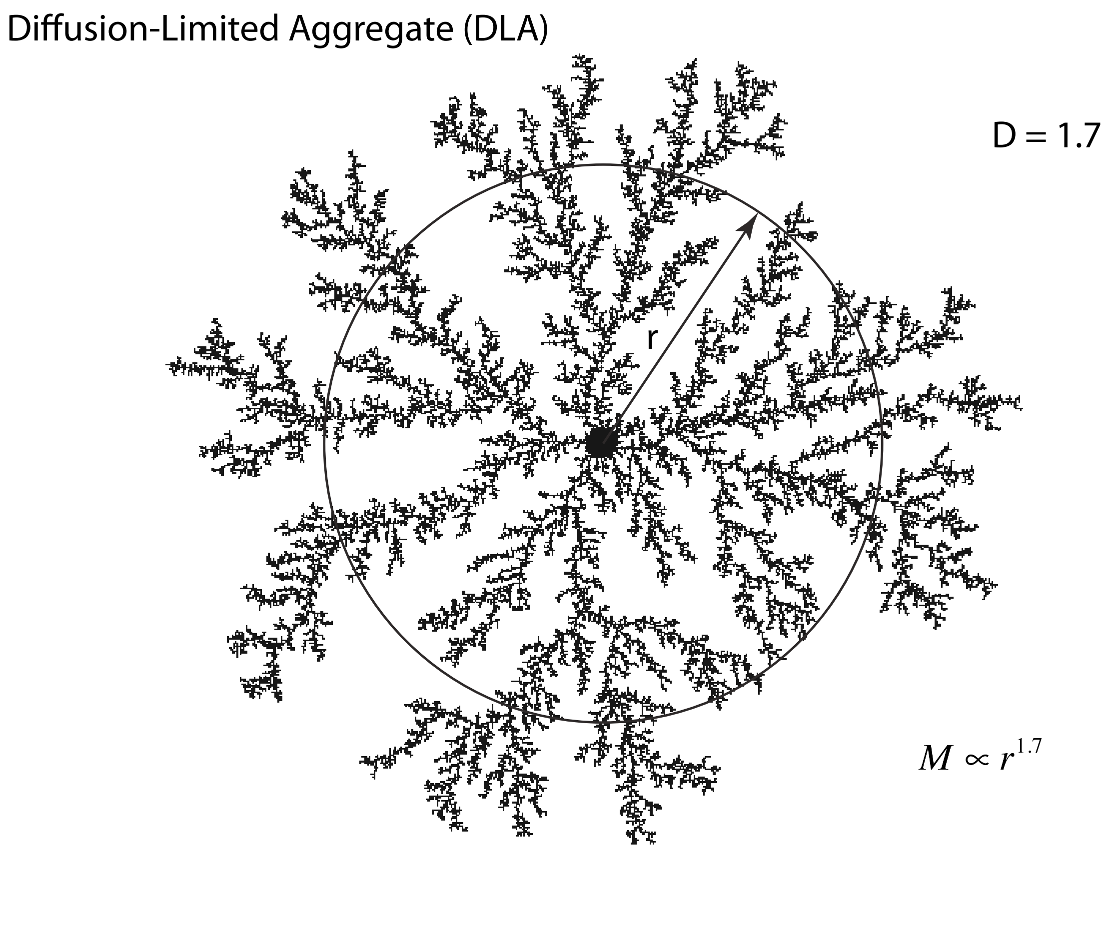

Fig. 4.5 A diffusion-limited aggregate (DLA) is a mass fractal with fractal dimension D = 1.7.

4.4. Fractals and Strange Attractors

One example of a fractal, known as the Koch curve, is shown in Fig. 4.1. The Koch curve begins in generation 1 with $N_0 = 4$ elements. These are shrunk by a factor of b = 1/3 to become the four elements of the next generation, and so on. The number of elements varies with the observation scale according to the equation

$$N(b) = N_0 b^{-D} \tag{4.3}$$

where D is called the fractal dimension. In the example of the Koch curve, the fractal dimension is

$$D = \frac{\ln(N_0)}{\ln(b)} = \frac{\ln(4)}{\ln(3)} = 1.26 \tag{4.4}$$

which is a number less than 2. The fractal is embedded in 2D, but has a fractional dimension that is greater than D = 1 for a line, but less than D = 2 for a plane.

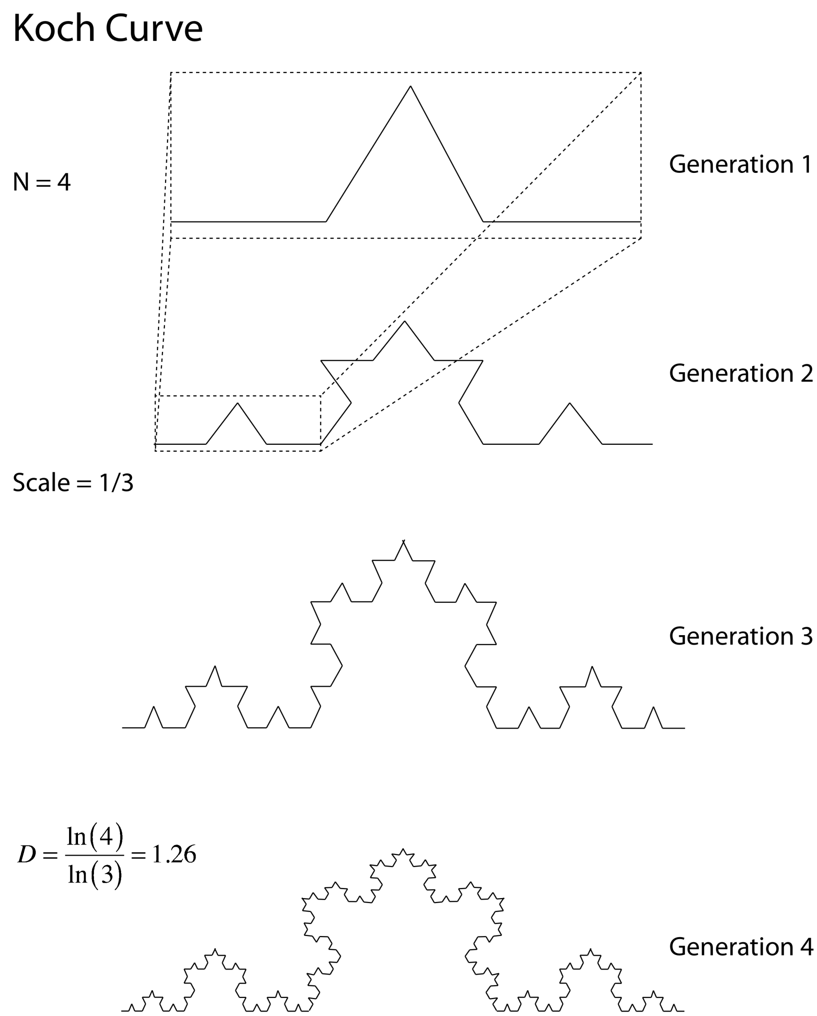

Fig. 4.1 Generation of a Koch curve. The fractal dimension is D = ln(4)/ln(3) = 1.26. At each stage, four elements are reduced in size by a factor of 3. The "length" of the curve approaches infinity as the features get smaller and smaller. But the scaling of the length with size is determined uniquely by the fractal dimension.

From the construction of the Koch curve, it is clear that the number of elements of scale b varies as b^{-D}. However, when confronted by a fractal of unknown structure, one of the simplest methods to find the fractal dimension is through box counting. This method is shown in Fig. 4.2. The fractal set is covered by a set of boxes of size b, and the number of boxes that contain at least one point of the fractal set are counted. As the boxes are reduced in size, the number of covering boxes increases as b^{-D}. To be numerically accurate, this method must be iterated over several orders of magnitude. The number of boxes covering a fractal has this characteristic power law dependence, as shown in Fig. 4.2, and the fractal dimension is obtained as the slope.

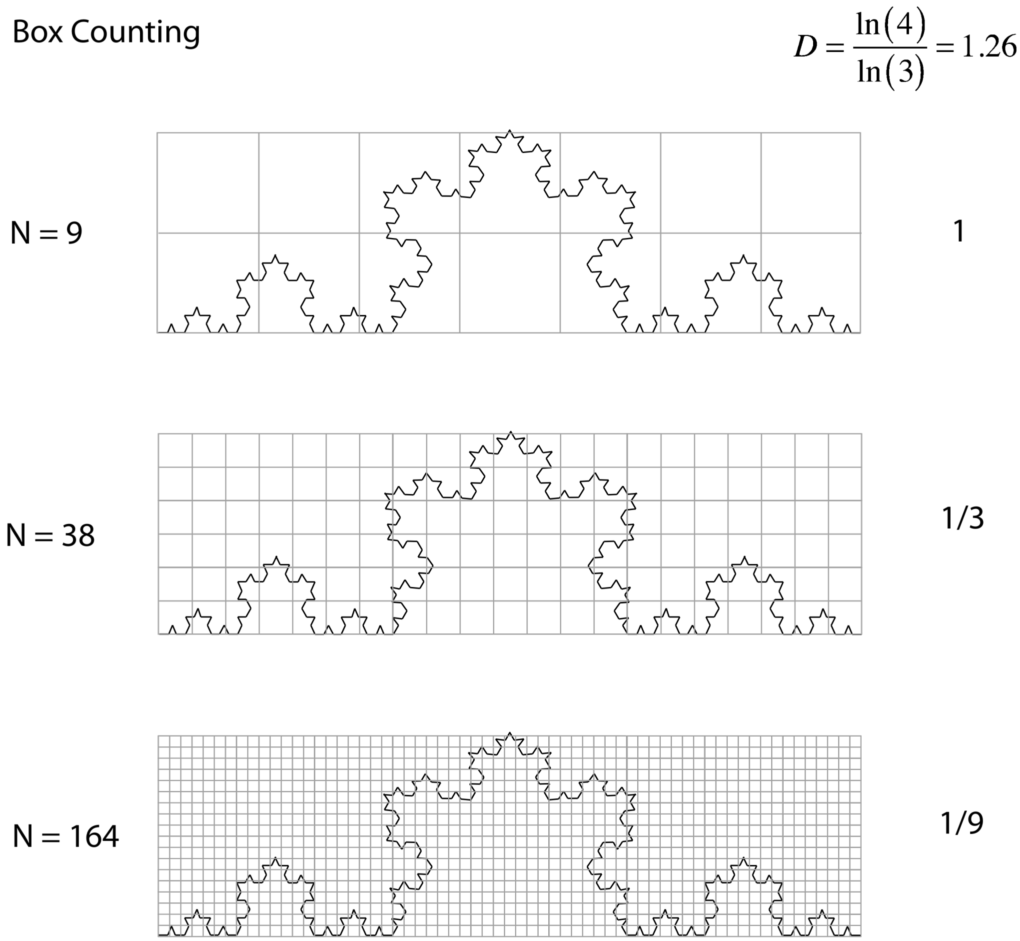

Fig. 4.2 Calculation of the fractal dimension using box counting. At each generation, the size of the grid is reduced by a factor of 3. The number of boxes that contain some part of the fractal curve increases as $N \propto b^{-D}$, where b is the scale

Another type of fractal is known as a *dust*. Fractal dusts are common for chaotic discrete maps that consist of sets of points. An example of a fractal dust is shown in Fig. 4.3. The iterative fractal construction begins with N = 5 sections of a square, each with side length equal to 3 units. At the next iteration, each occupied sub square is converted again to N = 5 smaller sub squares, with a scale ratio of 3. When this process goes to infinity, what remains is a fractal dust. It is a set of points embedded in 2D. The fractal dimension in this example is equal to

$$D = \frac{\ln 5}{\ln 3} = 1.465 \tag{4.5}$$

The fractal dimension of several common chaotic attractors are: Lorenz attractor D = 2.06, Rössler attractor D = 2.01, Logistic map D = 0.538 and Henon map D = 1.26. Each fractal structure has an Euclidean embedding dimension $E \geq D$.

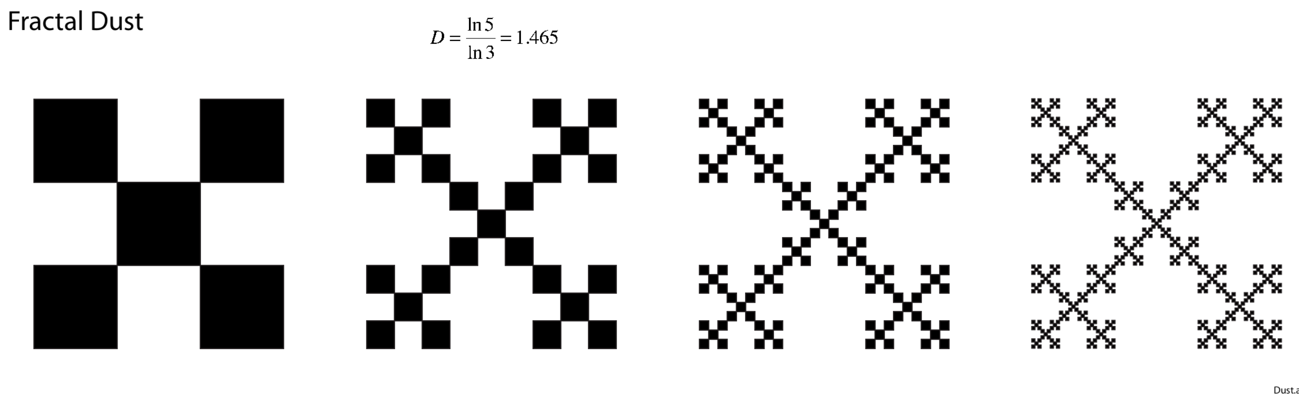

Fig. 4.3 Example of a fractal "dust". The Euclidean dimension is E = 2, but the fractal dimension is 1.465. In the limit of infinite generations, the area of points goes to zero, but the mass dimension approaches the fractal dimension. Strange attractors of a Poincaré section have the character of a dust.

A famous example of a dust as an infinite set is Cantor's ternary set that was published in 1883[7]. This is an infinite set of points composed of all the numbers that are generated by the formula

$$z = \frac{c_1}{3} + \frac{c_2}{3^2} + \ldots + \frac{c_m}{3^m} \qquad \lim m \to \infty \tag{4.6}$$

where the c_m take on all permutations of the two integers [0, 2]. The set generates a function that has derivative zero almost everywhere, yet whose area is equal to unity. This was an example of a function that was not equal to the integral of its derivative. Cantor demonstrated that the size of his set is $\aleph_1$, which is the cardinality of the real numbers, but whereas the real numbers are uniformly distributed, Cantor's set is "clumped". This clumpiness was an essential feature that distinguished it from the one-dimensional number line, and which, thirty five years later, would raise important questions of its dimensionality that would be answered Felix Hausdorff. Cantor's ternary set is a self-similar structure with fractal dimension

$$D = \frac{\ln N}{\ln b} = \frac{\ln 2}{\ln 3} = 0.6309 \tag{4.7}$$

The Cantor set is a dust with *zero measure* (meaning zero total length). An example of the dust is shown in Fig. 4.4 on the left. At each stage in the construction, as the length is scaled by a factor of 3, the middle third is removed. However, there are other related infinite sets that are not self similar known as a *fat-fractal*. For instance, Fig. 4.4 on the right shows a Cantor-like set in which the middle 3rd is removed at the first level, then the middle 9th at the next level, then the middle 27th , etc. The final set has a nonzero total length of 4/7. Cantor sets, and Cantor-like

[7] G. Cantor, "*Grundlagen einer allgemeinen Mannigfaltigkeitslehre*" ("Foundations of a General Theory of Aggregates") Leipzig B. G. Teubner (1883)

sets with finite measure, are both important structures that appear in Hamiltonian chaos. Cantor sets appear in homoclinic tangles, and Cantor-like sets appear in KAM theory (See Chapter 5).

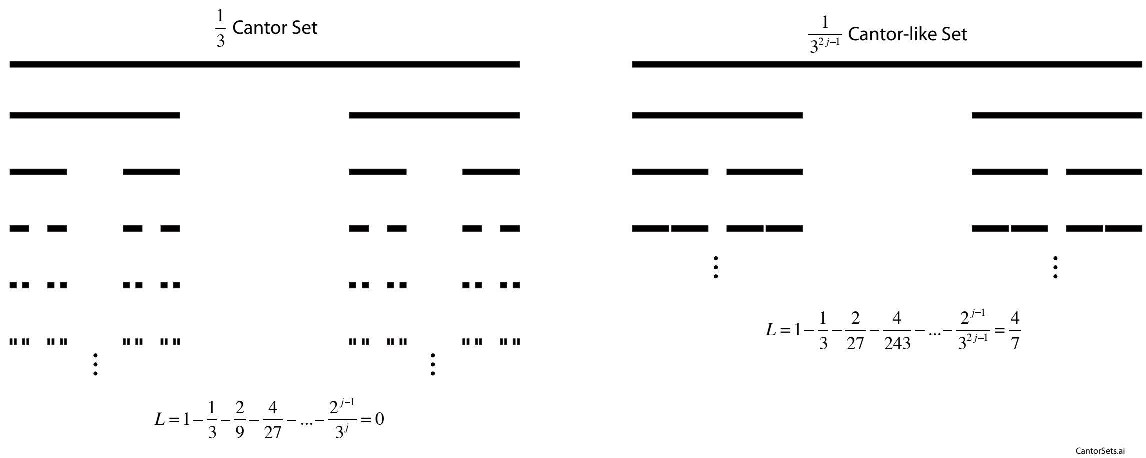

Fig. 4.4 The ternary Cantor set that is a fractal with zero measure. On the right is a Cantor-like set that has non-zero measure.

A table of the fractal dimensions of several well-known strange attractors is shown in Table I, including the embedding Euclidean dimension.

Table I Fractal Dimensions of Selected Strange Attractors

Name	*Embedding Dimension (E)*	*Fractal Dimension (D)*
Logistic map attractor	1	0.538
Ikeda map attractor	2	1.7
Lorenz attractor	3	2.06
Rössler attractor	3	2.01
Duffing attractor	2	1.4
Chua's circuit	2	1.33
Damped-driven pendulum	2	1.6 to 2

Chapter 5 Hamiltonian Chaos

See my Galileo Unbound Blog Posts for:

[Hamiltonian Maps]

[Chaos in the Solar System]

[Arnold's Cat Map]

[Hamiltonian Chaotic Tapestries]

[Compound Double Pendulum]

Chapter 6 Coupled Oscillators and Synchronization

1. Networks of Coupled Linear Oscillators

The general problem of N coupled linear oscillators with heterogeneous couplings has many interesting aspects. These systems are an analog to the thermal and dynamical properties of amorphous materials, like glasses. They can show critical behavior as the density of couplings increases beyond a threshold as a single giant cluster spans the entire network.

For N coupled linear oscillators it is assumed that they are described by N generalized coordinates q^b for b = 1:N and have N normal modes that are stationary solutions to Lagrange's equations. The rectilinear coordinates are functions of the generalized coordinates

$$x^a = x^a\left(q^b\right) \tag{6.1}$$

The kinetic and potential energies in terms of the generalized coordinates are

$$\begin{aligned} T &= \frac{1}{2} m_{ab} \dot{q}^a \dot{q}^b \\ U &= \frac{1}{2} A_{ab} q^a q^b \end{aligned} \tag{6.2}$$

using the Einstein summation convention. The coefficients of the kinetic energy term are

$$m_{ab} = \sum_{\beta} m_{\beta} \frac{\partial x^{\beta}}{\partial q^a} \frac{\partial x^{\beta}}{\partial q^b} \tag{6.3}$$

and the definition of A_{ab} is

$$A_{ab} = \frac{\partial^2 U}{\partial q^a \partial q^b} \tag{6.4}$$

When the expressions for T and U in Eq. (6.2) are inserted into Lagrange's equation

$$\frac{\partial L}{\partial q^a} - \frac{d}{dt} \frac{\partial L}{\partial \dot{q}^a} = 0 \tag{6.5}$$

it becomes

$$\frac{\partial U}{\partial q^a} + \frac{d}{dt}\frac{\partial T}{\partial \dot{q}^a} = 0 \tag{6.6}$$

and the equations of motion are

$$\sum_a \left(A_{ab} q^a + m_{ab} \ddot{q}^a \right) = 0 \tag{6.7}$$

Because we are looking for a stationary solution at a fixed frequency ω, the secular determinant is

$$\left| A_{ab} - \omega^2 m_{ab} \right| = 0 \tag{6.8}$$

leading to the eigenfrequencies and the eigenmodes of the dynamical system.

Example 4.1: Linear Array of Equal Masses and Springs

Consider a linear chain of N identical masses connected in a circle by N identical springs of spring constant k and separated by a lattice constant α. This model is often used to describe lattice vibrations (known as phonons) in solid state crystals. Because of the translational symmetry, it is easiest to work directly with the equations of motion and assume propagating solutions. The equations of motion are

$$m\ddot{q}_n = k\left(q_{n+1} - q_n\right) + k\left(q_{n-1} - q_n\right) \tag{6.9}$$

and the time dependence $e^{-i\omega t}$ converts the equations to

$$-\omega^2 m q_n = k\left(q_{n+1} - q_n\right) + k\left(q_{n-1} - q_n\right) \tag{6.10}$$

The traveling wave solutions have the form

$$q_{n+1} = q e^{ik(n+1)a} \tag{6.11}$$

Putting this assumed solution into the equations of motion gives

$$-\omega^2 m q e^{inka} = kq\left(e^{ik(n+1)a} - e^{inka}\right) + kq\left(e^{ik(n-1)a} - e^{inka}\right) \tag{6.12}$$

Canceling out the term qe^{inka} on each side yields

$$\begin{aligned}-\omega^2 m &= k\left(e^{ika}-1\right)+k\left(e^{-ika}-1\right) \\ &= 2k\left(\cos ka-1\right)\end{aligned} \tag{6.13}$$

The dispersion equation for traveling waves on the periodic chain is

$$\begin{aligned}\omega^2 &= k\left(e^{ika}-1\right)+k\left(e^{-ika}-1\right) \\ &= \frac{2k}{m}\left(1-\cos ka\right)\end{aligned} \tag{6.14}$$

and with a trigonometric identity becomes

$$\omega(k)=\sqrt{\frac{4k}{m}}\left|\sin\frac{1}{2}ka\right| \tag{6.15}$$

This dispersion curve is shown in Fig. 6.1 plotted in k-space, which is the Fourier-transform space of the linear lattice. The k-vector takes values between $k=-\pi/a$ to $k=\pi/a$, which is known as the first Brillouin zone. The dispersion at the center of the zone near k = 0 (long wavelength waves) is linear, with a phase velocity equal to

$$c_s=\sqrt{\frac{k}{m}}a \tag{6.16}$$

which is the speed of sound in this lattice. Near the Brillouin zone boundary, the dispersion flattens and the group velocity goes to zero at the boundary, representing a standing wave.

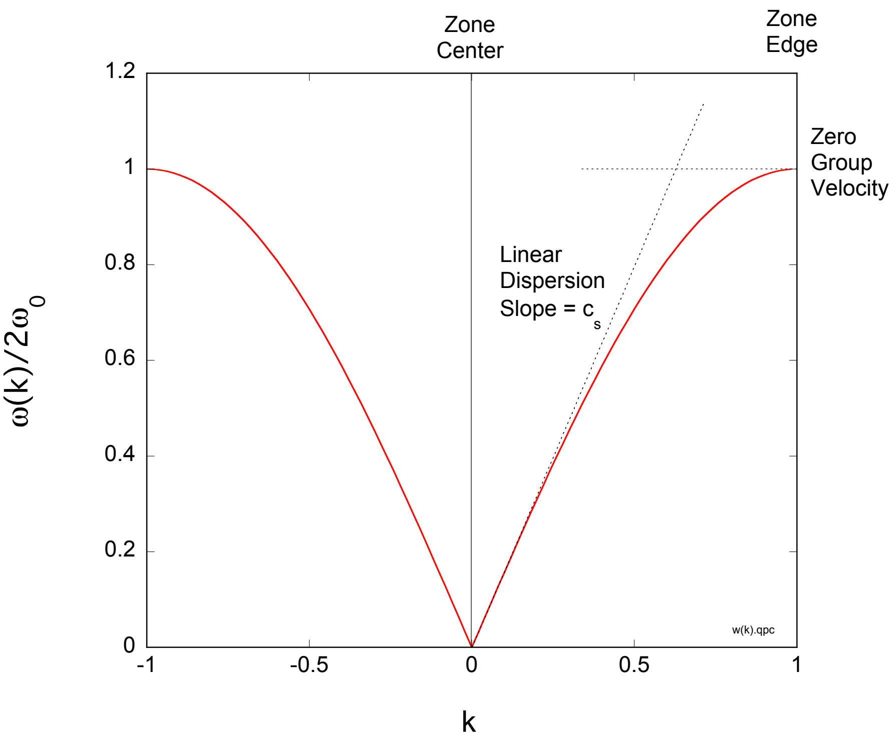

Fig. 6.1 Dispersion curve for a linear chain of N identical masses on springs. The k-vector spans between k = -π/a to π /a.

2. Summary

General Condition for Frequency Locking:

The critical dimensionless coupling strength required to couple two unequal frequencies is

$$g > \frac{\Delta\omega}{\bar{\omega}} \tag{5.22}$$

where $\bar{\omega}$ is the mean frequency, and $\Delta\omega$ is the frequency difference.

Sine-Circle Map:

The discrete sine-circle map is

$$\theta_{n+1} = \mathrm{mod}\left(\left[\theta_n + \Omega - g\sin\left(\theta_n\right)\right], 2\pi\right) \tag{5.32}$$

where the angle is taken mod (2π).

External Synchronization of a Phase Oscillator:

This is one of the simplest models for synchronization

$$\dot{\theta} = \omega_1 + g\sin\left(\omega_d t - \theta\right) \tag{5.38}$$

where θ represents the phase offset between the oscillator and the drive, ω_d is the drive frequency, and ω_1 is the autonomous frequency.

Beat Frequency:

When the coupling between an external drive and a single phase oscillator is not strong enough, the beat frequency is given by

$$\Omega_\psi = \sqrt{\Delta\omega^2 - g^2} \qquad \text{for } \Delta\omega > g \tag{6.17}$$

and is zero when $\Delta\omega < g$.

Chapter 7 Network Dynamics

1. Graph Laplacian Eigenvalue Spectra

The eigenvalues of the graph Laplacian are important properties of networks. For instance, the rapidity of transport processes depends on the eigenvalue spectrum, with the fastest transport rates being proportional to the maximum eigenvalue. As another example, the robustness of network phase-locking of identical oscillators depends on the ratio of the maximum to the minimum eigenvalues λ_{max}/λ_2 of the graph Laplacian. The average eigenvalue spectra are shown in Fig. 5.5 for SF, SW and ER graphs for an average degree <k> = 6 and N = 100 nodes. The SF graph has the broadest spectrum, which implies that phase-locking would not be robust, but transport rates (and rates of infection) would be high. Note that global coupling has all equal eigenvalues $\lambda = N$ providing both greatest ease of phase-locking oscillators across the net and the fastest transport.

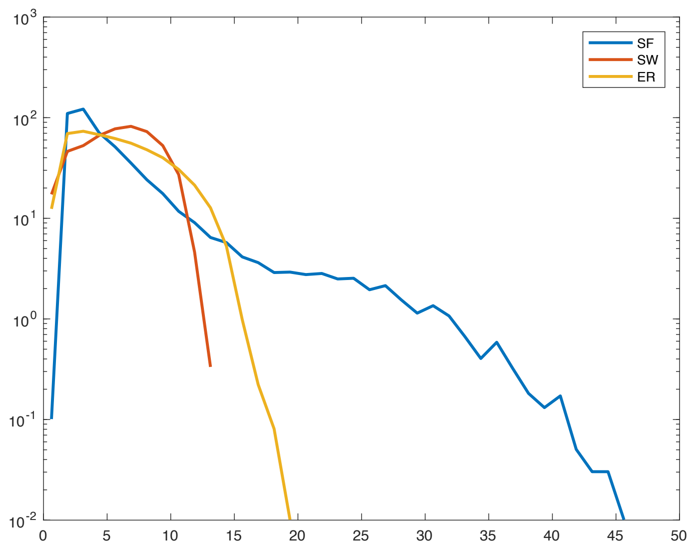

Fig. 5.5 Average eigenvalue spectra of the graph Laplacian for SF, SW and ER graphs with average degree <k> = 6 for graphs with N = 100 nodes.

2. Percolation

A network may have a giant component, but then some nodes (and their links) are removed. A natural question is whether the giant component falls apart (goes through a percolation transition), and how the size of the giant component depends on the fraction of deleted nodes. This question is important for real-world networks like computer networks. The resilience of a network to attack or to partial failure defines the robustness of the network.

Consider a random ER graph with an average degree $\langle k \rangle$ and average squared degree $\langle k^2 \rangle$. The nodes are all originally in place. Then individual nodes are deleted randomly, as well as their associated links. The fraction of nodes of the total that remain is called the occupation probability ϕ. As the occupation probability decreases, the fraction of nodes S that belong to the giant component decreases. Eventually, so many nodes have been removed, that the giant component vanishes at a threshold value of the occupation probability ϕ_c. For a random graph with randomly deleted nodes, this threshold is

$$\phi_c = \frac{\langle k \rangle}{\langle k^2 \rangle - \langle k \rangle} \tag{7.1}$$

which, for a Poisson degree distribution, is

$$\phi_c = \frac{1}{\langle k \rangle} \tag{7.2}$$

On the other hand, for a power-law degree distribution with a power between 2 and 3, the squared mean $\langle k^2 \rangle$ diverges to infinity and hence $\phi_c = 0$. This means that power-law distributions are extremely robust. Virtually all of the nodes must be removed to destroy the giant component. The size of the giant cluster is plotted in Fig. 7.1 for an exponential ($p_k \propto e^{-\lambda k}$) and for a power-law ($p_k \propto k^{-\alpha}$) degree distribution. There is a clear percolation threshold for the exponential case, but not for the power-law case.

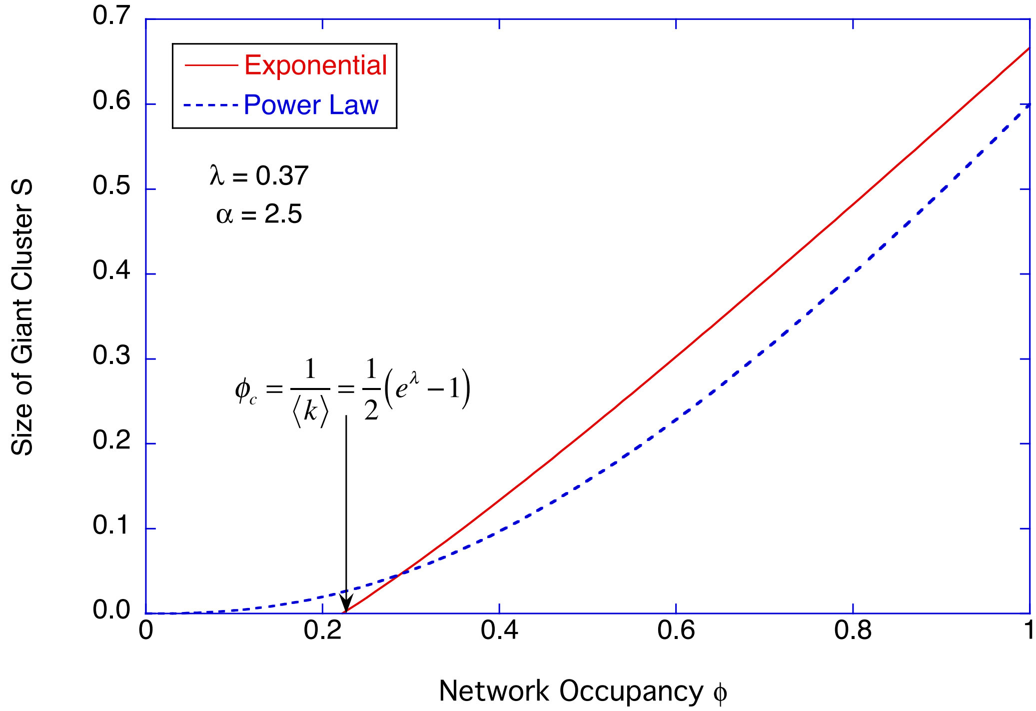

Fig. 7.1 Size of the giant component S vs. occupation probability φ□□□□□□ n exponential degree probability distribution with λ = 0.37 compared to a power-law degree distribution with α = 2.5.

There are many types of degree distributions, many types of network topologies, and many different ways nodes can be removed. Thresholds and sizes need to be calculated for each case. For instance, while being robust against *random* attacks, power-law networks can be badly vulnerable if the attack is directed preferentially at the highest-degree nodes. Conversely, epidemic spread can be effectively stopped by vaccinating these high-degree nodes. These topics are beyond the scope of this textbook. For detailed discussions, see Newman (2010).

3. Summary

Adjacency Matrix

The adjacency matrix for a graph with N nodes is an N-by-N matrix with elements

$$\begin{aligned} A_{ij} &= 1 \qquad \text{i and j connected} \\ A_{ij} &= 0 \qquad \text{i and j not connected} \\ A_{ii} &= 0 \qquad \text{zero diagonal} \end{aligned} \tag{5.4}$$

Graph Laplacian

The graph Laplacian of a network is an operator that is defined as

$$L_{ij} = \left(\sum_j A_{ij} \right) \delta_{ij} - A_{ij} = \begin{cases} k_i & i = j \\ -1 & \text{i and j connected} \\ 0 & \textit{otherwise} \end{cases} \tag{5.9}$$

Network Diameter

For a random graph, the network diameter is defined as the largest distance between two nodes. It scales with number of nodes N and average degree $\langle k \rangle$ as

$$\ell = \ell_0 + \frac{\ln N}{\ln \langle k \rangle} \tag{5.12}$$

where ℓ_0 is of order unity.

Synchronization Range

The range of coupling values for synchronization depends on the largest and smallest eigenvalues of the graph Laplacian.

$$\frac{\lambda_{\max}}{\lambda_2} < \frac{g_{\max}}{g_{\min}} \tag{5.48}$$

Kuramoto Model

The Kuramoto Model assumes a complete graph of identical coupled phase oscillators. The flow equation is

$$\frac{d\phi_k}{dt} = \omega_k + g \frac{1}{N} \sum_{j=1}^{N} \sin\left(\phi_j - \phi_k\right) \tag{5.50}$$

The Kuramoto Model has a mean field solution that shows a sharp synchronization transition.

Chapter 8 Neurodynamics and Neural Networks

1. Summary

Hodgkin and Huxley Model

A mathematical model of neuron potential V based on the multiple types of ion channels in the neuron membrane. The time derivative of membrane potential is

$$C\dot{V} = I - g_K n^4 \cdot (V - E_K) - g_{Na} m^3 h \cdot (V - E_{Na}) - g_L \cdot (V - E_L) \tag{6.1}$$

where C is the effective capacitance, V is the action potential, I is a bias current, g_K and g_{Na} and g_L are the conductances, E_K and E_{Na} and E_L are the equilibrium potentials, $n(V)$ is the voltage-dependent potassium activation variable, $m(V)$ is the voltage-dependent sodium activation variable (there are three sodium activation channels to four potassium channels, which determines the exponents) and $h(V)$ is the voltage-dependent sodium inactivation variable.

Fitzhugh-Nagumo Model

A two-dimensional simplification of neurodynamics in the space defined by V, the membrane potential and n, the number of activated membrane channels. The equations are similar to a van der Pol oscillator, and they tend to show limit cycles or stable fixed points.

$$\begin{aligned}\dot{V} &= (V+60)(a - V/75 - 0.8)(V/75 - 0.2) - 25n + I \\ \dot{n} &= 0.03(V/75 + 0.8) - 0.02n\end{aligned} \tag{6.2}$$

where I is a bias current and a is a control parameter that determines the size of the limit cycle.

NaK Model

The NaK model lies between the Fitzhugh-Nagumo and Hodgkin-Huxley models in complexity, adding voltage-dependent variables to Fitzhugh-Nagumo, but still simplifying the types of channels that are active in the neuron membrane with a two-dimensional dynamical space. The flow equations are

$$\begin{aligned}C\dot{V} &= I - g_L(V - E_L) - g_{Na} m_\infty(V)(V - E_{Na}) - g_K n(V)(V - E_K) \\ \dot{n} &= \frac{n_\infty(V) - n(V)}{\tau(V)}\end{aligned} \tag{6.5}$$

Perceptron

A perceptron is a single-layer feed forward network. The output values are a function of the input values through a synaptic weight matrix w_{kj} as

$$z_k = S\left(\sum_{j=1}^{m} w_{kj} y_j - b_k\right) \tag{6.11}$$

where the y_j are the inputs, w_{kj} is the weight for the j-th input to the *k-th* output neuron, and b_k is the threshold of the *k-th* output neuron. The transfer function $S(v_k)$ is one of the sigmoidal functions of Table 1.

Delta Rule

The Delta Rule is used to determine the synaptic weights of a feed-forward network. The value of Delta is

$$\Delta_k^\mu = \left[Z_k^\mu - \phi\left(v_k^\mu\right)\right]\phi'\left(v_k^\mu\right) \tag{6.16}$$

where the prime denotes the derivative of the transfer function. The adjustments made to the weights during training are

$$\begin{aligned} \delta w_{kj} &= \varepsilon \sum_\mu \Delta_k^\mu Y_j^\mu \\ \delta b_k &= -\varepsilon \sum_\mu \Delta_k^\mu \end{aligned} \tag{6.17}$$

where ε is a small value that prevents the adjustments from overshooting as the process is iterated. The Delta Rule is extended to multi-layer feed forward networks and is called Error Back propagation.

Hopfield Network Synaptic Weight

The synaptic weight matrix is constructed as the outer product of the fundamental memory vectors

$$\vec{\vec{w}} = \frac{1}{N}\sum_{\mu=1}^{M} \vec{\xi}_\mu \vec{\xi}_\mu^{\,T} - \frac{M}{N}\vec{\vec{I}} \tag{8.37}$$

where the synaptic weight matrix is symmetric. The outer product is a projection operator that projects onto a fundamental memory, and the synaptic weights perform the function of finding the closest fundamental memory to a partial or corrupted input.

Chapter 9 Evolutionary Dynamics

1. Fibonacci and the golden mean

The study of population dynamics has a long history. One of the famous early examples was the study of rabbit populations by Leonardo Pisano (1170-1250) more commonly known as Fibonacci. In his *Liber Abaci* "Without Abacus" (1202) he introduced Arabic numerals to Western Civilization, and he constructed a toy (and not very realistic) model for the population dynamics of rabbits with the conditions

- In the "zeroth" month, there is one pair of rabbits
- In the first month, the first pair begets another pair
- In the second month, both pairs of rabbits have another pair, and the first pair dies
- In the third month, the second pair and the new two pairs have a total of three new pairs, and the older second pair dies.
- Each pair of rabbits has 2 pairs in its lifetime, and dies.

If the population at month n is $F(n)$, then at this time, only rabbits who were alive at month n − 2 are fertile and produce offspring, so $F(n-2)$ pairs are added to the current population of $F(n-1)$. Therefore, the total is $F(n) = F(n-1) + F(n-2)$. Starting with two rabbits, the rabbit pairs for each month becomes

1, 1, 2, 3, 5, 8, 13, 21, 34, 55, 89, 144, 233, 377, 610, 987, 1597, …

This is the famous Fibonacci sequence that plays a role in many areas of mathematics related to the golden mean

$$\gamma = \lim_{n\to\infty} F(n)/F(n-1) = 1.618 \tag{9.1}$$

The golden mean also plays a role in nature, where many examples abound, such as the curve of the nautilus shell. An example of a Fibonacci spiral is shown in Fig. 4.1. The equation for this spiral (also known as the golden spiral) is

$$r = r_0 e^{b\theta} \tag{9.2}$$

for a growth rate b, where the radius of the spiral when θ is a right angle is equal to the golden mean, such that

$$e^{b\frac{\pi}{2}} = 1.618 \tag{9.3}$$

which yields the growth factor b = 0.3063. Although, this is not a very realistic example of population dynamics, it shows how venerable the field is, and it sets the stage for more realistic models.

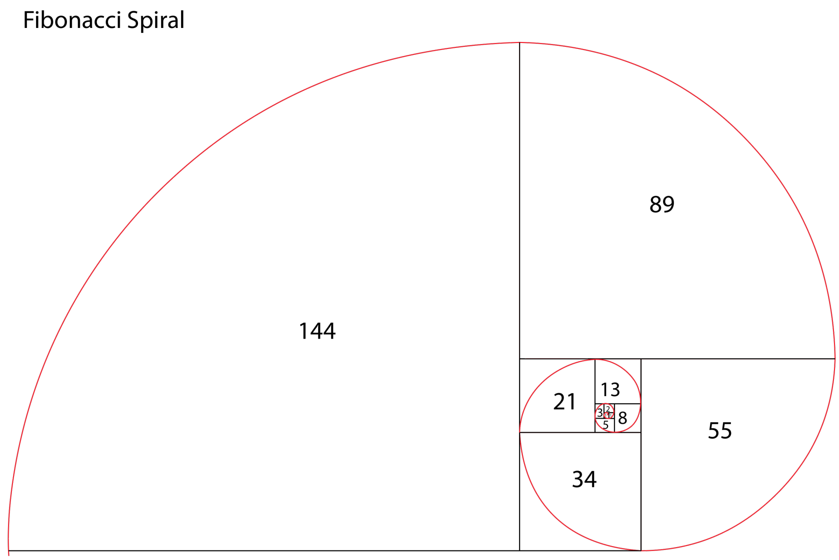

Fig. 9.1 A Fibonacci spiral enclosing areas that increase as the Fibonacci series. When θ grows by π/2, the radius grows by the golden mean.

2. Nearly Neutral Networks in Extremely High Dimensions

The theory of neutral drift occurs in landscapes with extremely high dimension, which is appropriate for biological genomes. After all, there are over a million loci in the human genome, constituting an evolutionary space of over a million dimensions. When the dimensionality is this large, there are many possible mutations that do not affect the overall fitness of the genome significantly. Furthermore, because each genome is connected to a million others by a single point mutation, the new genome can mutate again and take it a step farther in the landscape. With successive mutations, the average genome (remember that it is a diffusing population of closely related genomes spreading out in the genome space) can diffuse far from the starting genome without significant change in the fitness.

This is called neutral drift. It provides one of the central methods for timing the rate of evolution. Mutations in a genome tend to accumulate at a relatively fixed rate. By measuring the number of neutral mutations between two related genomes, the time of the divergence of the two species can be calculated using the average rate of neutral mutation. For neutral drift to be tenable, there must be far more ways to mutate neutrally than to mutate with increased fitness (or decreased fitness). With a million dimensions, this condition is satisfied. The importance of neutral drift is the tendency not to get hung up in local maxima of the fitness landscape.

Another important feature of neutral drift is the ability to cross wide valleys of low fitness to arrive at a higher fitness peak. There is far more room in sequence space to explore at altitudes around the mean fitness of the landscape than near its peak. This is illustrated in Fig. 7.8. The current population may be near a local fitness peak, but a higher fitness peak exists in the landscape. However, between the local and the global maximum is a wide valley of low fitness. If the population of species descends the local peak into the valley, the population may die out without getting to the maximum fitness peak. The theory of neutral drift, with the implicit participation of a large number of dimensions, can explain how evolution crosses such valleys. In high dimensions, there are many extra dimensions in which to move—there is literally a lot of room to move about in the extra dimensions. This feature of higher dimensions was illustrated nicely by Abbott in his famous book *Flatland* about a civilization that lives in two dimensions and observes strange phenomena, such as circles that can disappear and reappear on the far side of impenetrable barriers. From our perspective in 3D, we know that the circle was actually the cross section of a sphere, and the sphere avoids the barrier by simply moving above it, as illustrated in Fig. 7.9. Crossing the valley of low fitness, which seems impenetrable, is made possible by moving through neutral mutations in the high dimensions of sequence space.

Although the NK model is typically run with low dimensions (in the hundreds), it can be extended to include some of the effects of neutral drift. This is accomplished by making the fitness of the genomes take on discrete values. Therefore, there will be many genomes with the same fitness, representing the neutral network of neutral mutations. This simple procedure increases the distance that the genome can drift before getting frozen into a local maximum. As the discreteness is made coarser, so that a larger fraction of genomes share equal finesses, the average distance travelled through sequence space increases, until it approaches the network diameter. Therefore, neutral networks, even within the modified NK model at moderate dimensionality (this modification is called the NKP model), increase the ability of a population to sample sequence space and propagate longer distances before ultimately climbing higher peaks.

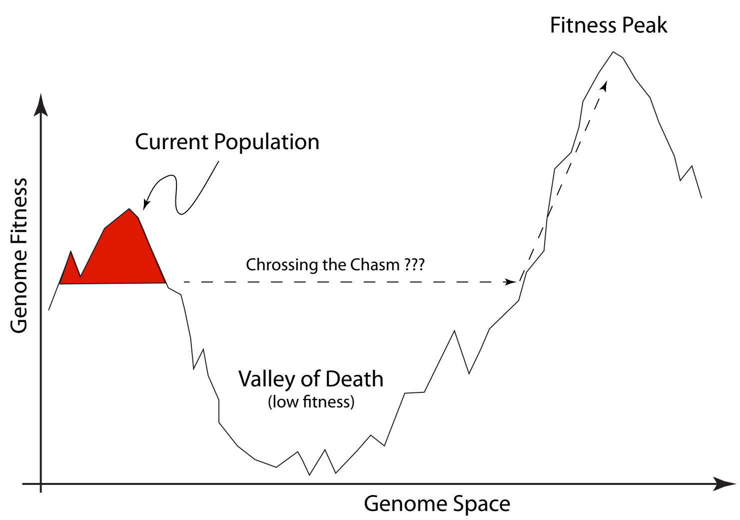

Fig. 7.8 The paradox of the valley of death (of low fitness). A population will die out if it descends into the valley and attempts to cross it to escape the local peak to get to the global fitness peak.

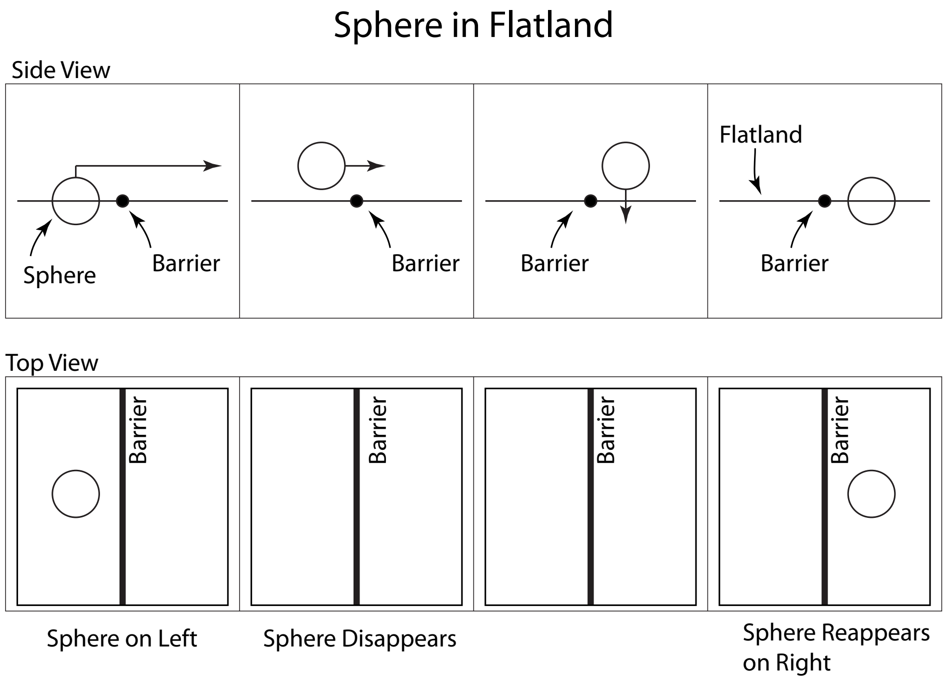

Fig. 7.9 A sphere in Flatland avoids an impenetrable barrier simply by moving above it. But to the citizens of Flatland, they see a circle disappear and reappear mysteriously on the far side of the barrier.

3. Dynamics of Finite Numbers (Optional)

The examples of evolutionary dynamics that have been presented in this chapter so far have taken a continuous approach. The replicator, mutator, quasi-species and replicator-mutator equations are all deterministic flows on continuous variables. However, there is another side to evolutionary dynamics based on the dynamics of finite numbers and stochastic processes. This is also the arena of game theory. It is beyond the scope of this book to go in this direction, but this facet of evolutionary theory is too important to omit entirely in a book on modern dynamics. The simplest consequence of having a finite population is the certainty of extinction after sufficient time. This certainty is a simple result of the finite probability for a neutral mutation to take over an entire population.

Consider a death-reproduction model in a mixed population of fixed size N that is completely neutral. Neutrality means that who dies and who reproduces is selected at random. For simplicity, assume that the mixed population consists of only two species: type A and type B individuals. There are N_A individuals of species A and $N_B = N - N_A$ individuals of species B. At every time step an individual is selected at random to reproduce, and an individual is selected at random to die. The two can be the same, when the individual first reproduces and then dies. As the model proceeds, the number of A and B individuals fluctuates randomly, but not indefinitely.

There are two fixed points in this stochastic dynamical model. They are when $N_A = N$ or $N_B = N$, that is, when every individual of one of the species has died. Once this state is reached, there is no longer any chance for the other species to reemerge (in the absence of mutation). The important point is that for a finite population size N, there is a non-zero probability that random drift eventually will bring the system to one of the fixed points.

In the field of evolutionary biology, this process of neutral drift has provided a valuable tool for measuring the rate of genetic change. Most genetic mutations are neutral. This is because the probability is very low that a mutation will improve on functions that have been optimized over millions of years of natural selection. Conversely, if a mutation is deleterious, then those individuals will not survive. Therefore, most mutations that do not kill an individual have no overt influence on the survivability of an individual—they are neutral. From the law of finite probabilities, once a mutation occurs, there is a finite chance that it eventually will spread over the entire species. The rate at which neutral genetic mutations in DNA occur has remained fairly constant throughout evolutionary history. This is the so-called theory of the "molecular clock". Therefore, by measuring the "distance" between two genomes, let's say of humans and chimpanzees, the time of divergence of the two species can be predicted with some accuracy.

The probability that a single mutation will spread over a species and become fixed in its genome is called the fixation probability. For neutral drift, the probability that a single A individual in a population of N individuals will eventually take over the species is simply

$$P = 1/N \tag{9.4}$$

When there is a reproductive advantage of A over B given by the factor $r > 1$, the fixation probability for species A becomes

$$P_A = \frac{1-\frac{1}{r}}{1-\frac{1}{r^N}} \tag{9.5}$$

and for species B becomes

$$P_B = 1 - P_A = \frac{1-r^{N-1}}{1-r^N} \tag{9.6}$$

For N_A and N_B starting individuals, the fixation probabilities are

$$P_{A,N_A} = \frac{1-\frac{1}{r^{N_A}}}{1-\frac{1}{r^N}} \qquad P_{B,N_B} = \frac{1-r^{N_B}}{1-r^N} \tag{9.7}$$

Even if A has a reproductive advantage over B, there is still a chance that B will take over the species. This is a consequence of the discrete and finite numbers, and would not be possible in a continuous system. Therefore, the dynamics of finite systems have a stochastic character with improbable outcomes still being possible. While the results presented here are based on the assumption that the total number N is constant, many of the arguments based on finite probabilities on finite numbers continue to hold even when N is not a constant, but changes slowly.

This model of neutral drift and fixation probabilities between two species is called a Moran process. As simple as this model is, the Moran process shows up in many aspects of game theory and evolutionary dynamics of finite populations. It is a winner-take-all dynamic that is common in fields as diverse as economics and language evolution. More complex finite processes continue to share many of the qualitative results of the Moran process, including natural selection that is not neutral. One of the outstanding problems in molecular evolution is the emergence of new functions with selective advantages of increased fitness. For instance, it is difficult to envision how a molecule as complicated as ATP synthase, that has multiple complex functioning parts, some of which move like mechanical gears, could have emerged from random mutations of DNA. It would seem that deep valleys in the fitness landscape would separate existing function from new advantageous functions. However, the theory of nearly neutral networks in high-dimensional spaces of DNA base-pair permutations suggests that evolution is not required to bridge deep valleys, nor take direct paths, especially when the fitness landscape has correlations. These are topics at the forefront of evolutionary biology, and they draw from the rich phenomena of evolutionary dynamics.

4. Summary

Lotka-Volterra Equations:

The simple predator-prey population dynamics equations are

$$\begin{aligned}\dot{x} &= x(\alpha - \beta y) \\ \dot{y} &= -y(\gamma - \delta x)\end{aligned} \tag{7.9}$$

where y is the number of predators, and x is the number of prey. The prey reproduce at the rate α, and are eaten with a rate β times the product of the number of prey and predators. The predator reproduces at a rate δ times the product of the number of prey and predators, and die off at a rate γ.

Replicator Equation:

The replicator equation is the growth equation for the population x_i of the i^{th} species based on its relative fitness (*with* frequency-dependent fitness through the pay-off matrix p_a^b) relative to the average fitness in the ecosystem

$$\dot{x}_a = x_a \cdot \left(f^a - \phi \right) \tag{7.20}$$

Species Fitness: $$f^a\left(\vec{x}\right) = \sum_{b=1}^{n} x_b p_a^b$$

Average Fitness: $$\phi\left(\vec{x}\right) = \sum_{a=1}^{n} f^a x_a$$

Quasi-Species Equation:

This equation describe the growth of numerous sub-species (quasi-species) under the action of a mutation matrix Q_a^b *without* frequency-dependent fitness

$$\begin{aligned} \dot{x}_a &= \sum_{b=0}^{N} x_b \left(f^b Q_a^b \right) - x_a \sum_{b=0}^{N} f^b x_b \\ &= \sum_{b=1}^{N} x_b W_a^b - \phi x_a \end{aligned} \tag{7.24}$$

Transition Matrix: $W_a^b = f^b Q_a^b$ (no implicit summation)

Replicator-Mutator Equation:

The growth equation with *both* mutation and frequency-dependent fitness is a replicator-mutator equation

$$\begin{aligned} \dot{x}_a &= \sum_{b=1}^{N} x_b f^b Q_a^b - \phi x_a \\ f^b\left(\vec{x}\right) &= \sum_{c=1}^{N} x_c p_c^b \\ \phi\left(\vec{x}\right) &= \sum_{a=1}^{n} f^a x_a \end{aligned} \tag{7.37}$$

Moran Process: A stochastic process in a finite population that exhibits neutral drift and fixation of a single subspecies, and extinction of all others, at long times.

Stochastic Matrix: A stochastic matrix is a random matrix who's columns and rows each sum to unity.

Chapter 10 Economic Dynamics

1. Robinson Crusoe and the Pareto Frontier

One of the simplest economies that captures the trade-off between labor and production on one side, and leisure and consumption on the other, is known as the Robinson Crusoe economy, named after the shipwrecked sailor who had to fend for himself on a deserted island. The Robinson Crusoe economy has a single laborer for whom there are $24*7=168$ hours in the week. Some of these hours must be spent finding food, let's say oysters, while the other hours are for leisure and rest. The production of oysters follows a production curve

$$q = F(L) \tag{10.1}$$

that is a function of labor L. There are diminishing returns in the finding of oysters for a given labor, making the production curve of oysters convex. The amount of leisure (rest) is simply

$$R = 168 - L \tag{10.2}$$

It is assumed that all oysters produced are consumed. This is known as market clearing when no surplus is built up. The production curve is a continuous trade-off between consumption and leisure, but at first look there is no obvious way to decide how much to work and how much to rest. A lazy person might be willing to go a little hungry if they can have more rest, while a busy person might want to use all waking hours to find oysters. The production curve represents something known as a Pareto frontier. It is a continuous trade-off between two qualities. Another example of a Pareto frontier is car engine efficiency versus cost. Some consumers may care more about the up-front cost of the car than the cost of gas, while other consumers may value fuel efficiency and be willing to pay higher costs to get it. What determines where to strike a balance between these two quality is the relative utility of one over the other. The utility function for Robinson Crusoe is

$$u(q,R) = u\big(F(L),168 - L\big) \tag{10.3}$$

Of course, the maximum utility would be lots of oysters without any cost of labor, even though this is not allowed by the production curve. Nonetheless, the contours of the utility function create a set of indifference curves, some of which interesect the production curve, as in Fig.

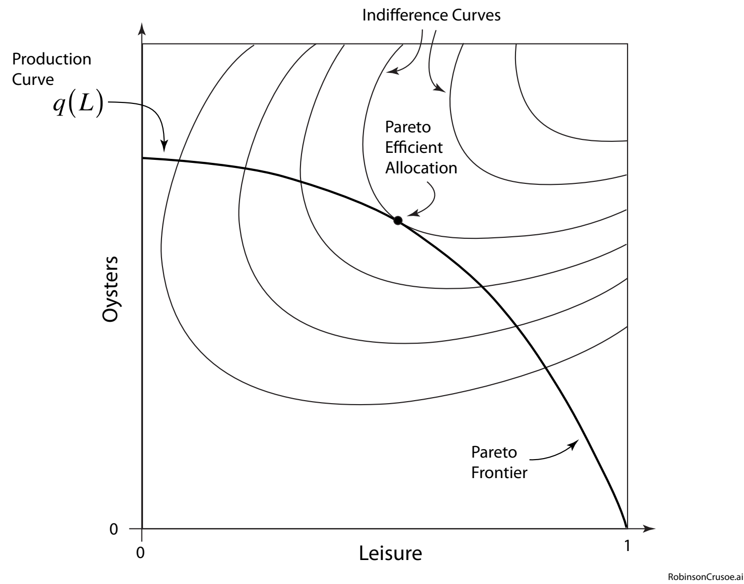

Fig. 10.1 The Robinson Crusoe economy of leisure and oysters.

2. Dynamic General Equilibrium Theory

Dynamic general equilibrium (DGE) theory attempts to model an entire macro economy from the bottom up, assuming that economies are always in a balance of economic forces. Constraints may change in time, but the economy tracks these changes in a condition of general equilibrium[8]. Equilibrium theories are a different "breed" of economic theory compared with Keynesian IS-LM models and at times make different predications about the economy.

Because DGE seeks to optimize a value function, it uses the approach of undetermined Lagrange multipliers. Therefore, the economic dynamics originate from a Lagrangian function, making a connection between economic dynamics and physics. A simple DGE model assumes that a value function takes on its optimal value under conditions of dynamic general equilibrium. This value function is based on a utility function of consumption with a discount on value in future years. The value function is[9]

$$V_t = \sum_{s=0}^{s_\infty} \beta^s U\left(c_{t+s}\right) \tag{10.4}$$

where the sum is over successive years and $0 < \beta < 1$ is the annual discount rate. This value function downweights the contribution, to the current value, by future consumption and utility in

[8] General equilibrium theory had its origin with Léon Walras in 1874, but emerged in recent years in reaction to Keynesian macroeconomics.

[9] Wickens, M. (2012). *Macroeconomic Theory: A Dynamic General Equilibrium Approach*, Princeton University Press.

future years because of economic uncertainty. The time horizon is given by s_∞, which could be taken to infinity. The utility function $U(c_{t+s})$ is assumed to have diminishing returns, meaning that it saturates at large values of consumption. The goal is to maximize the value function V_t, subject to the constraints of the economy.

A simple economic constraint is that the national output y_t in a given year t is equal to consumption plus investment (savings is set equal to investment in this simple model)

$$y_t = c_t + i_t$$

This is a discrete time model in which the time index t is taken as the year index. In addition, capital stock k_{t+1} next year is equal to the capital stock this year plus investment and minus depreciation

$$\begin{aligned} k_{t+1} &= k_t + i_t - \varepsilon k_t \\ &= k_t(1-\varepsilon) + i_t \end{aligned}$$

where the factor $0 < \varepsilon < 1$ captures depreciation of the capital stock, representing obsolescence. Finally, the national output is a nonlinear function of capital stock

$$y_t = F(k_t)$$

The output function $F(k_t)$ has diminishing returns, which means that it saturates at large values of its argument k_t. These equations combine to give the constraint equation

$$k_{t+1} = F(k_t) - c_t + (1-\varepsilon)k_t$$

To optimize the value function V_t under the economic constraints, we use the method of undetermined Lagrange multipliers. The Lagrangian function is

$$L_t = \sum_{s=0}^{s_\infty} \left[\beta^s U(c_{t+s}) + \lambda_{t+s}\left(F(k_{t+s}) - c_{t+s} - k_{t+s+1} + (1-\varepsilon)k_{t+s} \right) \right]$$

Note that this Lagrangian has no explicit velocity dependence. Therefore, the Euler-Lagrange equations are simply

$$\begin{aligned} \frac{\partial L_t}{\partial c_{t+s}} &= \beta^s \frac{\partial U}{\partial c_{t+s}} - \lambda_{t+s} = 0 \\ \frac{\partial L_t}{\partial k_{t+s}} &= \lambda_{t+s}\left[\frac{\partial F}{\partial k_{t+s}} + (1-\varepsilon) \right] - \lambda_{t+s-1} = 0 \\ \frac{\partial L_t}{\partial \lambda_{t+s}} &= F(k_{t+s}) - c_{t+s} - k_{t+s+1} + (1-\varepsilon)k_{t+s} = 0 \end{aligned}$$

The undetermined multiplier is eliminated to yield the DGE Euler equation for this optimization problem as

$$\beta \frac{U'(c_{t+1})}{U'(c_t)}\left[F'(k_{t+1})+(1-\varepsilon)\right]=1$$

expressed in terms of the annual discount rate β, the annual depreciation rate ε, the derivative of the diminishing returns utility function U' with respect to consumption and the derivative of the diminishing returns output function F' with respect to the capital stock. Collecting the Euler equation with the resource constraint defines the two-variable discrete map for the DGE model

$$k_{t+1} = F(k_t) - c_t + (1-\varepsilon)k_t \tag{10.5}$$

$$\beta \frac{U'(c_{t+1})}{U'(c_t)}\left[F'(k_{t+1})+(1-\varepsilon)\right]=1 \tag{10.6}$$

which is not expressed in the usual form. Note that the bottom equation is a nonlinear transcendental equation. The top equation is used to obtain k_{t+1}, and then the bottom equation is solved for c_{t+1}.

The fixed point of this discrete map is

$$F'(k^*) = \varepsilon + \frac{1}{\beta} - 1$$

$$c^* = F(k^*) - \varepsilon k^*$$

Linearizing around the fixed point gives

$$\frac{U''}{U'}(c_{t+1}-c^*) + \beta(k_{t+1}-k^*)F'' = \frac{U''}{U'}(c_t - c^*)$$

$$(k_{t+1}-k^*) = -(c_t - c^*) + \frac{1}{\beta}(k_t - k^*)$$

which is expressed in matrix form as

$$\begin{pmatrix} c_{t+1}-c^* \\ k_{t+1}-k^* \end{pmatrix} = \begin{pmatrix} 1+\beta\dfrac{U'F''}{U''} & -\dfrac{U'F''}{U''} \\ -1 & 1/\beta \end{pmatrix} \begin{pmatrix} c_t - c^* \\ k_t - k^* \end{pmatrix}$$

where the transformation matrix is the Floquet (Jacobian) matrix of the discrete map. The trace and determinant are

$$\tau = 1 + \beta \frac{U'F''}{U''} + 1/\beta$$
$$\Delta = 1/\beta$$

with eigenvalues

$$\lambda_{1,2} = \frac{1}{2}\left(1 + \beta \frac{U'F''}{U''} + 1/\beta\right) \pm \frac{1}{2}\sqrt{\left(1 + \beta \frac{U'F''}{U''} + 1/\beta\right)^2 - 4/\beta} \qquad (10.7)$$

Here we use the fact that U and F are diminishing return functions (saturate for large values of their arguments). These functions have $U' > 0$ and $F'' < 0$ and $U'' < 0$. This guarantees that $U'F''/U'' > 0$. Therefore, one eigenvalue has absolute value less than unity, and the other has absolute value greater than unity. This represents a saddle-point in the discrete map. To be explicit, give U and F saturating forms as

$$F(k) = \frac{1}{1+k} \qquad F'(k) = \frac{1}{(1+k)^2} \qquad F''(k) = \frac{-2}{(1+k)^3}$$
$$U(k) = \frac{1}{1+c} \qquad U'(c) = \frac{1}{(1+c)^2} \qquad U''(c) = \frac{-2}{(1+c)^3}$$

These functions are shown in the Fig.

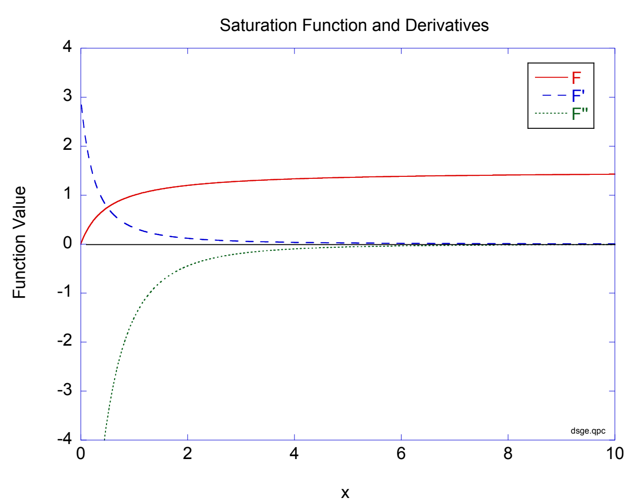

Fig. 8.1 Saturation function and its first and second derivatives. The first derivative is positive and decreasing. The second derivative is negative and decreasing in magnitude.

A discrete map that captures both the linearized as well as nonlinear behavior of the DGE model is

$$k_{n+1} = k_n + \varepsilon k_n \left(a - c_n^3\right)$$
$$c_{n+1} = c_n + \varepsilon c_n \left(b - k_n\right)$$

This has simple nullclines (a vertical line at k = b and a horizontal line at c = $a^{3/2}$). The Floquet multiplier is

$$J = \begin{pmatrix} 1 & -3a^{3/2}b^{1/2} \\ -a^{3/2} & 1 \end{pmatrix}$$

with

$$\tau = 2 \qquad\qquad \lambda = 1 \pm \varepsilon\sqrt{3a^3b^{1/2}}$$
$$\Delta = 1 - 3a^3b^{1/2}\varepsilon^2$$

whose parameters can be matched to Eq. 8.4. A related, continuous-valued flow that captures the general behavior of the dynamics is

$$\dot{k} = k\left(a - c^3\right)$$
$$\dot{c} = c\left(b - k\right)$$

These dynamics describe a saddle with stable and unstable manifolds as shown in Fig. 8.2

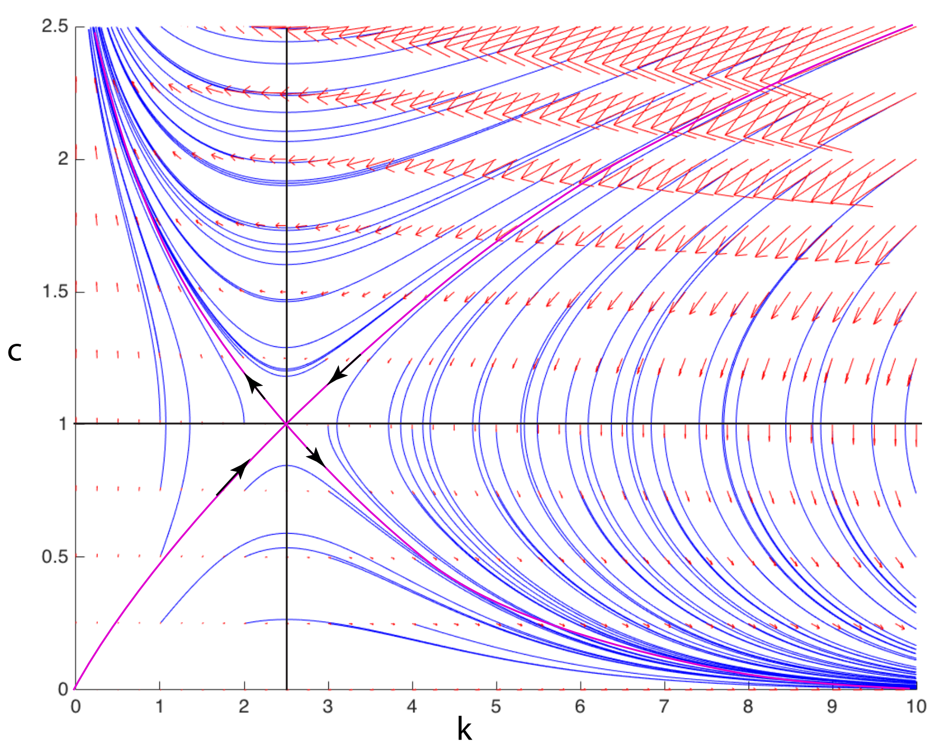

Fig. 8.2 Flow field for the discrete map (modeled as a continuous flow in capital stock (k) and consumption (c)). The equilibrium point is a saddle point. (From dsge.m dsge.ai)

A central assumption of dynamic general equilibrium theory is that the system state always resides on a stable manifold and hence approaches the equilibrium point as a stable equilibrium point. This is equivalent to having 2 degrees of freedom (capital stock and consumption) with a constraint that reduces the dynamics to 1-dimensional dynamics. The contraint is the stable manifold. This 2D approach with constraint describes the macroeconomic properties in terms of two variables (k, c), but the constraint guarantees that the system is stable (cannot fall off the stable manifold or follow the unstable manifold). This principle operates even in the presence of a shock, a sudden change in the system description, as shown in Fig. 8.3. The system moves from the original equilibrium point to the new stable manifold, which it follows to the new equilibrium point.

The constraint used by DGE theory that forces the economy always to be on a stable equilibrium is a premise rather than a physical principle. It guarantees stability to the economy, while retaining a 2-dimensional description, but it is difficult to guess the exact mechanism that allows the system to find the new stable manifold. The DGE model is interesting, because it has more structure than IS-LM models, and it is based on optimization principles (through the Lagrange multipliers). But it still must be viewed as highly idealized and hence not necessarily an accurate model of economic reality.

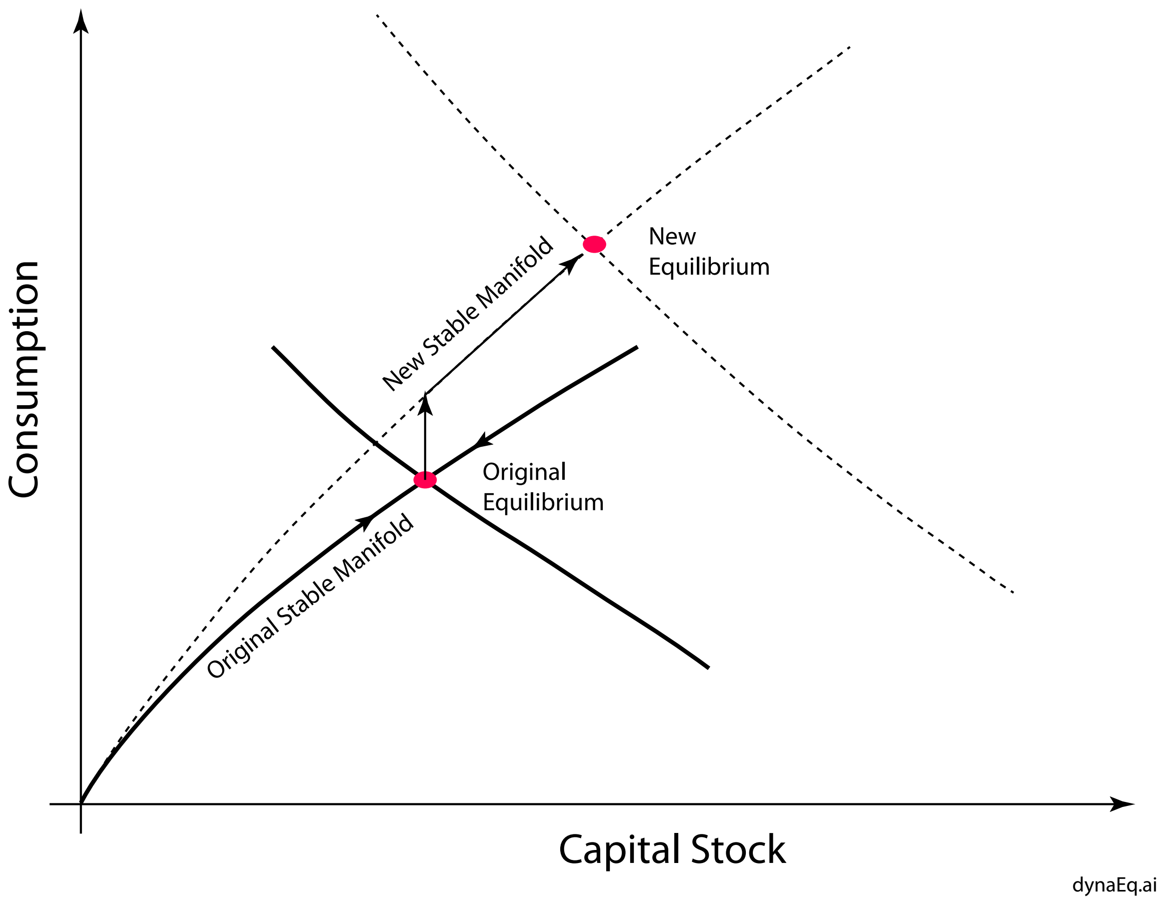

Fig. 8.3 The guiding assumption of dynamic general equilibrium theory that the system state always resides on a stable manifold of the saddle equilibrium. When the system experiences a sudden change in parameters, the system moves to the new stable manifold and then relaxes along this manifold to the new saddle equilibrium.

3. Real-World Phillip's Curve

The historical relationship between inflation and unemployment rarely obeys the Phillips curve. The historical values are plotted in Fig. 10.2 between 1941 (just after the depression) to 2013. The Phillips curve states that increasing unemployment is accompanied by lower inflation, which is not easily observed in the figure, except for fairly short periods. Larger forces on the national economy tend to overwhelm the Phillip's curve. On the other hand, for more than 70 years, both unemployment and inflation in the US has generally been below 10% without the wild increases that have been seen in some economies (such as southern Europe).

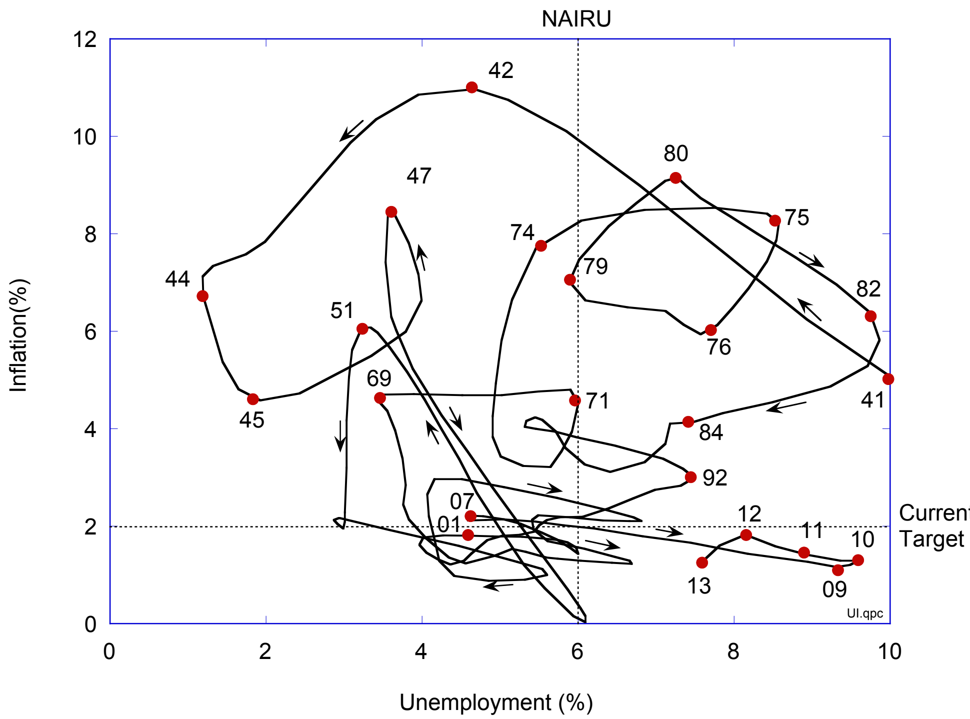

Fig. 10.2 Historical inflation and unemployment from 1941 to 2013. The current NAIRU is assumed to be around 6%, and the target inflation rate is around 2%. There is no evidence for a long-term Phillips Curve in these data.

4. Discrete Random Walks

Consider a 1-dimensional random walk in which equal steps to the right or left are possible. The probability of taking a step right or left is equal to p or q, respectively. These probabilities are independent, and $q = 1 - p$. If a total of N steps are taken, then $N = n_1 + n_2$, where n_1 is the number of steps to the right, and n_2 is the number of steps to the left. The probability after N steps to be m steps away from the starting point, for a probability of p for steps to the right and q for steps to the left is

$$P_N(m) = \frac{N!}{(N/2+m/2)!(N/2-m/2)!} p^{(N+m)/2} q^{(N+m)/2} \tag{10.8}$$

where $m = 2n_1 - N$. Note that m takes on integer values that are separated by an amount $\Delta m = 2$, where all the m are either even or odd, depending on whether N is even or odd.

The mean value of m is

$$\bar{m} = N(p-q) \tag{10.9}$$

which is zero for $p = q$. The variance of m is

$$\Delta m^2 = 4Npq \tag{10.10}$$

which, for $p = q = 0.5$, is

$$\Delta m^2 = N \tag{10.11}$$

This states the important result that the mean squared displacement of an unbiased random walk is equal to the number of steps. Equivalently, the root-mean-squared displacement grows as the square root of the number of steps.

For large N, the binomial distribution is approximated by a continuous Gaussian function

$$P(m) = \frac{1}{\sqrt{2\pi Npq}} \exp\left\{ -\frac{\left[m - N(p-q)\right]^2}{8Npq} \right\} \tag{10.12}$$

If the step size is uniform and equal to ℓ, then the distance from the origin after N steps is $x = m\ell$. The distance between possible values of x is equal to 2ℓ. Therefore, the probability density for x is

$$P(x)dx = P(m)\frac{dx}{2\ell} = \frac{1}{\sqrt{2\pi}\sigma} \exp\left\{ -\frac{\left[x-\mu\right]^2}{2\sigma^2} \right\} \tag{10.13}$$

where the mean and standard deviation are

$$\begin{aligned} \mu &= (p-q)N\ell \\ \sigma &= 2\sqrt{Npq}\,\ell \end{aligned} \tag{10.14}$$

Note that for $p = q = ½$, then

$$\begin{aligned} \mu &= 0 \\ \sigma &= \sqrt{N}\ell \\ \left\langle \Delta x^2 \right\rangle &= N\ell^2 \end{aligned} \tag{10.15}$$

Diffusion is often described in terms of random walks. The mean squared displacement for 1D diffusion is

$$\left\langle \Delta x^2 \right\rangle = N\ell^2 = 2Dt \tag{10.16}$$

and the mean-squared displacement grows linearly with time. This is an essential result of random walks and diffusion, contributing to stochastic calculus and Ito's lemma.

When the random walk is in 3D, many of these 1D results are easily extended as

$$\begin{aligned}\left\langle \Delta r^2 \right\rangle &= N_x \ell_x^2 + N_y \ell_y^2 + N_z \ell_z^2 \\ &= \frac{N}{3}\ell^2 = 6Dt\end{aligned} \tag{10.17}$$

The mean-squared displacement again grows linearly with time, but there are three independent contributions to the random walk.

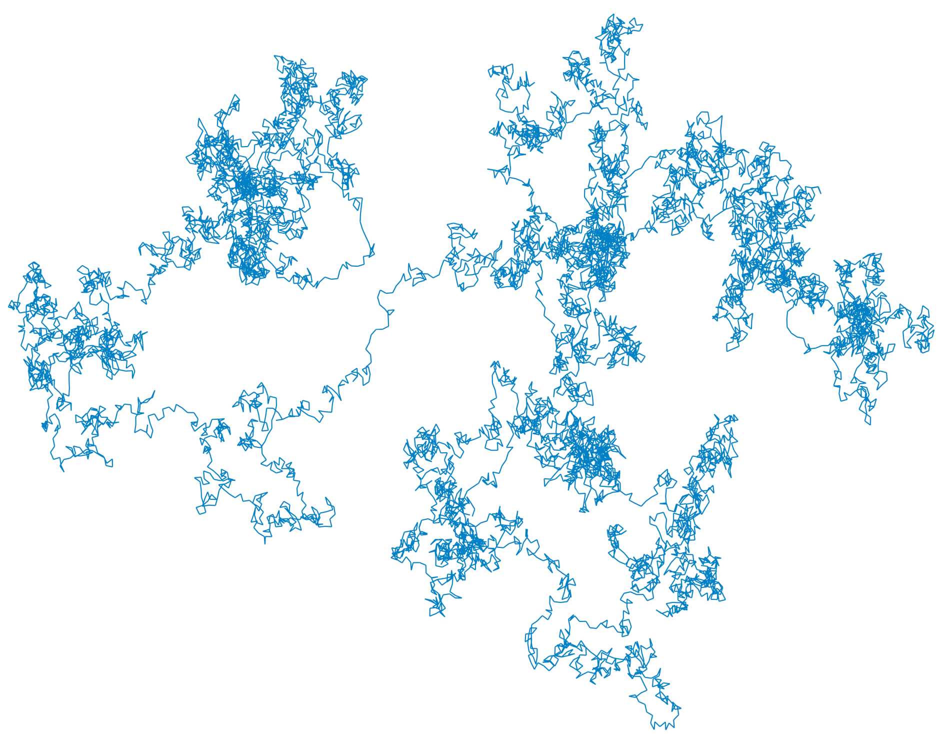

Fig. 8.4 Random Walk (From brown.m)

5. Consumer Product Coherence

Many consumer product markets are disposable markets that are not essential. Choosing an online social network is not like buying an appliance or food. Choices of consumer products like VHS over Beta, Macintosh over PCs, i-Phones over BlackBerrys are matters of taste. In such a case, the likelihood that a consumer will switch from one product to another depends on the trends which, in terms of the models we studied in Chapter 7 on evolutionary dynamics, means that there is a frequency-dependent fitness that contributes to the survival of a product in a competitive market.

As an example, consider the smart-phone consumer market. Smart phones have many features in common, but the details of operating them can be quite different. These details have to do with which buttons to push or where to find certain menu items. When two products have similar procedures, then a user can switch fairly easily from one to the other. But when two products have very different procedures, then there is a barrier for a user to switch.

Consider two specific products G_a and G_b. The probability that a user who uses product G_a uses a procedure that is compatible with the procedure of product G_b is given by the probability p_a^b. This probability defines a matrix whose values lie in the range between zero and unity with $p_a^a = 1$ (users using the same product have perfect mutual understanding). The advantage (or payoff) of a user using a procedure on G_a being able to use the same procedure on product G_b is given by the symmetric matrix

$$F_a^b = \frac{1}{2}\left(p_a^b + p_b^a\right) \tag{10.18}$$

where the matrix p_a^b is not necessarily symmetric. Among a population of users, the frequency of users who use product G_a is denoted by the variable x_a. The average payoff (loyalty) for this subpopulation of users is

$$f^a = \sum_b x_b F_b^a \tag{10.19}$$

where the payoff leads to differing levels of advantage for different subpopulations. The average fitness of the entire population is

$$\phi = \sum_a x_a f^a \tag{10.20}$$

which is called the product coherence of the population. When $\phi = 1$, then all products have converged to the same universal procedures. This is like Microsoft DOS evolving into Microsoft Windows in response to the Apple Macintosh graphical user interface.

The key element in the model is the ability of populations of users to move, meaning the ability for one set of users to change randomly (on a whim) to the competing product. This is given by the stochastic matrix Q_a^b that defines the probability that a user of product G_b converts into a user of G_a.

The dynamical equation, the flow, describing the evolution of the subpopulations of users is now

$$\dot{x}_a = \sum_b x_b \left(f^b Q_a^b \right) - \phi x_a \qquad (10.21)$$

which is the replicator-mutator Eq. (7.37) of Chapter 7. It allows instances of perfect replication (groups of friends tend to adopt the same products) as well as instances of mutation (switching). The second term, that has the minus sign, ensures that the total population size remains constant during the dynamical evolution. Depending on the procedural overlap, the fixed points can range from each individual using a different product (zero product coherence) to the situation where all users use the same product (perfect product coherence). The question is: what overlap allows the existence of product coherence? In other words, is there a threshold for a Universal Product (standardization)?

To explore this question, consider a symmetric case when all N products have the same probability of feature and procedural overlap

$$p_{aa} = 1 \qquad p_{ab} = p \qquad (10.22)$$

where p is between 0 and 1. The conversion rates are

$$Q_{aa} = q \qquad Q_{ab} = \frac{1-q}{N-1} \qquad (10.23)$$

where q is the probability of buying the same product, and

$$u = \frac{1-q}{N-1} \qquad (10.24)$$

is the probability of buying a different product. The replicator-mutator equation now is

$$\dot{x}_a = x_a \left[(q-u) f_a - \phi \right] + u\phi \qquad (10.25)$$

(no summation implied). The payoff is

$$f_a = p + (1-p) x_a \qquad (10.26)$$

and the product coherence is

$$\phi = p + (1-p) \sum_a x_a^2 \qquad (10.27)$$

One solution for this symmetric case (all $p_{ab} = p$) is when all products have an equal number of users $x_a = 1/N$, as in Fig. 7.16. *A*nother solution is when one product is dominant, while all others share equally in the remaining population

$$x_a = X \qquad x_b = \frac{1-X}{N-1} \tag{10.28}$$

for a value X that is a function of the overlap rate q. The interesting part of these conclusions is that, for a Universal Procedure Set to evolve, a finite overlap among the feature procedures is needed. Zero overlap tends to prevent the evolution of a Universal Procedure Set.

6. The Langevin Equation

This section takes a look at fundamental aspects of stochastic processes that apply to broad areas of physics. The motivation of understanding stock price fluctuations provides a convenient excuse to explore what happens when deterministic flows, that we have studied so thoroughly up to now in this textbook, acquire a stochastic element.

One of the most important conclusions of chaos theory and nonlinear dynamics is that not all random-looking processes are actually random. In deterministic chaos, one could argue that structures such as strange attractors are not random at all. But sometimes, in nature, processes really are random, or at least have to be treated as such because of their complexity. Brownian motion is a perfect example of this. At the microscopic level, the jostling of the Brownian particle can be understood in terms of deterministic momentum transfers from liquid atoms to the particle. But there are so many liquid particles, that their individual influences cannot be directly predicted. In this situation, it is more fruitful to view the atomic collisions as a stochastic process with well-defined physical parameters, and then study the problem statistically.

Stochastic processes are understood by considering a flow that includes a random function. The resulting set of equations are called the Langevin equation, namely

$$\dot{x}_a = fa_i\left(x_1, x_2, \ldots, x_N\right) + \sigma_a \xi a(t) \tag{10.29}$$

where $\xi_a(t)$ is a set of N stochastic functions, and σ_a is the standard deviation of the a-th process. The stochastic functions are in general non-differentiable, but are integrable. They have zero mean, and no temporal correlations. The solution of Eq.(10.29) is an N-dimensional trajectory that has some properties of a random walk superposed on the dynamics of the underlying flow.

As an example, take the case of a particle moving in a one-dimensional potential, subject to drag and to an additional stochastic force

$$\begin{aligned} \dot{x} &= v \\ \dot{v} &= -\gamma v - \frac{1}{m}\frac{dU}{dx} + \sqrt{2B}\,\xi(t) \end{aligned} \tag{10.30}$$

where γ is the drag coefficient, U is a potential function and B is the velocity diffusion coefficient. Take a double-well potential as an example

$$U(x) = \frac{\alpha}{2}x^2 + \frac{\beta}{4}x^4 \tag{10.31}$$

A specific stochastic trajectory is shown in Fig. 10.3 that applies discrete velocity jumps using a normal distribution of jumps of variance 2B in a mean time τ. The notable character of this trajectory, besides the random-walk character, is the ability of the particle to jump the barrier between the wells. In the deterministic system, the initial condition would dictate which stable fixed point would be approached. In the stochastic system, there are random fluctuations that take the particle from one basin of attraction to the other.

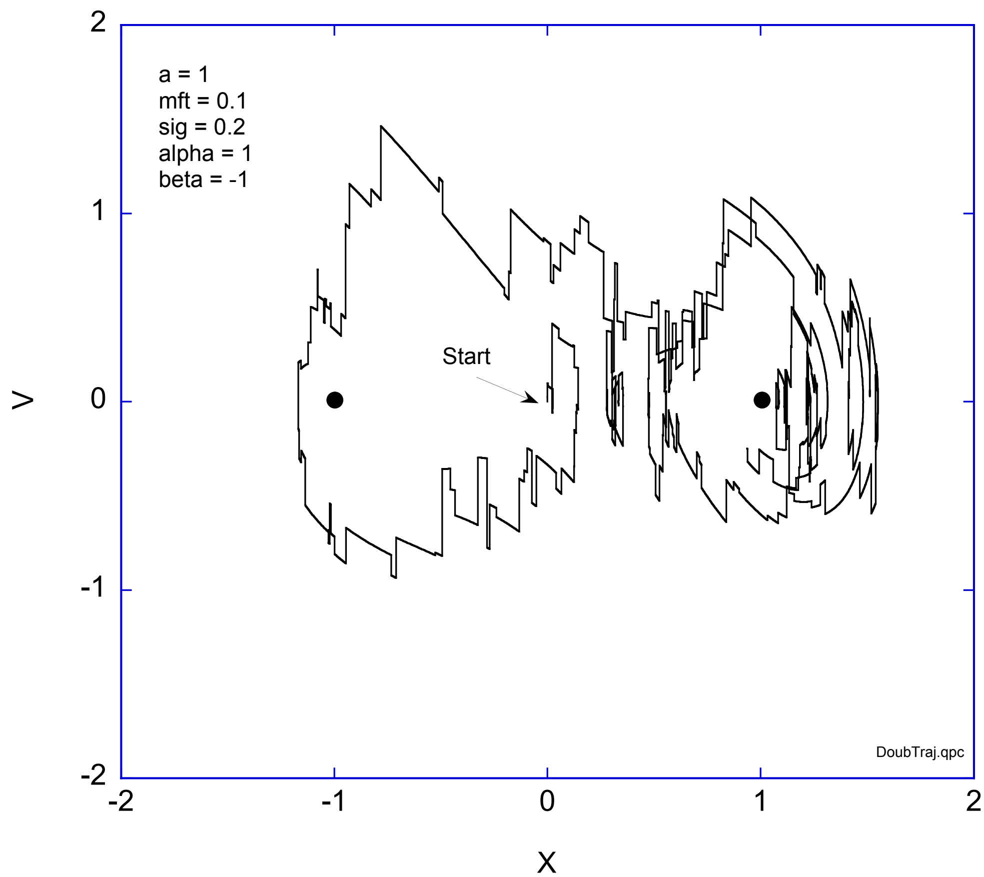

Fig. 10.3 Stochastic trajectory of a particle in a double-well potential. The start position is at the unstable fixed point between the wells, and the two stable fixed points (well centers) are the solid dots.

The density from a simulation of N = 4000 particles is shown in Fig. 10.4 for the double well potential. The probability distribution for an ensemble of particles at long times (much larger than the relaxation time) is given by

$$p(x) = \frac{e^{-2V(x)/\sigma^2}}{\int\limits_{-\infty}^{\infty} e^{-2V(x)/\sigma^2}\, dx} \tag{10.32}$$

The density in position is obtained by integrating over the velocities and is shown in Fig. 10.5 with a fit to Eq.(10.32). Larger fluctuations σ tend to smooth the probability function, while smaller σ would lead to strongly localized densities near the stable fixed points.

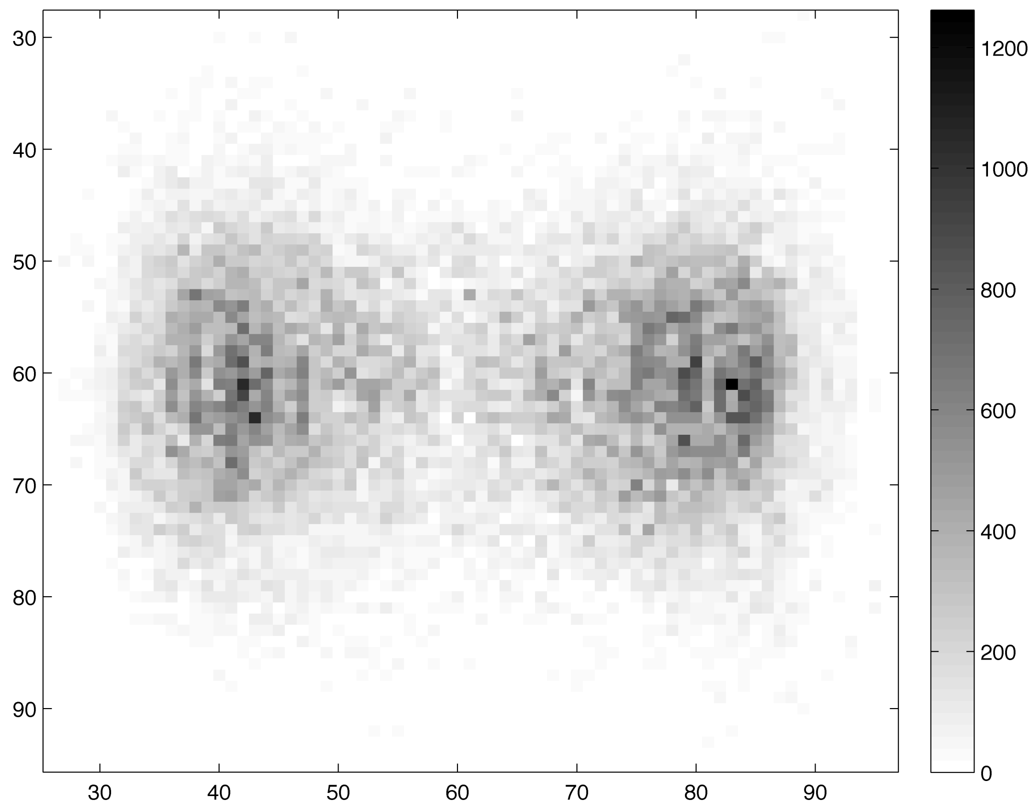

Fig. 10.4 Density of N = 4000 random-walkers in the double-well potential with σ = 1.

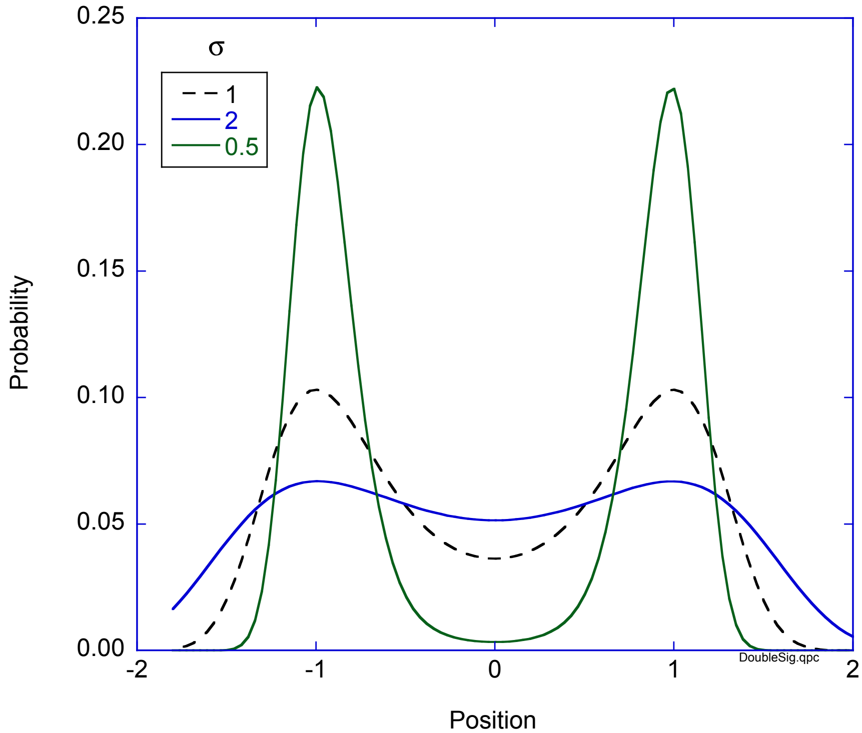

Fig. 10.5 Density of N = 4000 random walkers in the double-well potential for the same parameters as Fig. 10.4.

The stochastic long-time probability distribution p(x,v) in Fig. 10.4 introduces an interesting new view of trajectories in state space that have a different character than many of the state-space flows that we have studied in this book. If we think about starting a large number of systems with the same initial conditions, and then letting the stochastic dynamics take over, we can define a time-dependent probability distribution p(x,v,t) that describes the likely end-positions of an ensemble of trajectories on the state plane as a function of time. This introduces the idea of the trajectory of a probability cloud in state space, which has a strong analogy to time-dependent quantum mechanics. The Schrödinger equation can be viewed as a diffusion equation in complex time, which is the basis of a technique known as quantum Monte Carlo that solves for ground state wave functions using concepts of random walks. This goes beyond the topics of this textbook, but it shows how such diverse fields as econophysics, diffusion, and quantum mechanics can share common tools and language.

7. Summary

Supply and Demand

Supply of quantities and their demand have an inverse relationship on price. Supply increases with increasing price (profit), while demand falls. A simple price adjustment equation depends on excess demand $E = D - S$ as

$$\begin{aligned} \dot{p} &= kE \\ &= k\left(D - S\right) \end{aligned} \tag{8.2}$$

for positive coefficient k.

IS-LM

In macroeconomic theory, investment-savings (IS) and liquidity-money (LM) trade off against each other as a function of interest rate. As interest rates rise, there is less investment and more spending (the IS side of the economy), while the demand for money decreases (the LM side of the economy). Expenditure E and demand D adjust as

$$\begin{aligned} \dot{g} &= \alpha\left[E(t) - g(t)\right] \\ \dot{r} &= \beta\left[D(t) - m_0\right] \end{aligned} \tag{8.54}$$

for gross-domestic product g and money availability m_0.

Phillips Curve

The Phillips curve predicts a linear relationship between inflation and unemployment. In linearized form this is

$$\pi = -a\left(u - u_n\right) + \pi_e \tag{8.59}$$

where $\pi = \dot{p}$ is the current rate of inflation—the rate of change in the price p of money, u is the unemployment rate, π_e is the expected inflation rate, and u_n is the *non-accelerating inflation rate of unemployment* (NAIRU).

Adaptive Expectations

Expected prices or inflation usually do not match actual prices or inflation, and the time-rate-of-change of these quantities often adjust linearly with the difference between expected and actual values. Adaptive expectations appear in iterative cobweb models as in Eq. (8.30) in microeconomics, and in models of inflation as in

$$\dot{\pi}_e = \beta\left(\pi - \pi_e\right) \tag{8.61}$$

in macroeconomics.

Geometric Brownian Motion
The random walk in a relative property (in one dimension) is given by

$$\frac{dx}{x} = \mu dt + \sqrt{2D}dW \tag{8.68}$$

where D is a diffusion coefficient, and dW is a Wiener process with the property $dW^2 = dt$.

Ito's Formula
A very useful equation from stochastic analysis of the equation

$$dx = adt + bdW \tag{8.75}$$

is

$$df = \left[\frac{\partial f}{\partial t} + a\frac{\partial f}{\partial x} + \frac{b^2}{2}\frac{\partial^2 f}{\partial x^2}\right]dt + b\frac{\partial f}{\partial x}dW \tag{8.78}$$

which is known as Ito's Formula.

Black-Scholes Equation
A risk-free hedge has a value V determined by the Black-Scholes equation

$$\frac{\partial V}{\partial t} + \frac{1}{2}\sigma^2 S^2 \frac{\partial^2 V}{\partial S^2} + rS\frac{\partial V}{\partial S} - rV = 0 \tag{8.90}$$

where r is the guaranteed rate of return and σ is the volatility in the stock value.

Chapter 11 Metric Spaces

1. Reciprocal Spaces in Physics

Reciprocal spaces abound in math and physics with many well-known examples. Fourier space is perhaps the best known example. Any function of spatial variables can be transformed into its Fourier transform. The Fourier transform has spatial frequency, or k-vector, or wavenumber, as its coordinates. These coordinates span a space called Fourier space. Fourier space is a dual-space of the space of spatial functions and are expressed in terms of spatial frequencies k_a. The spatial frequency that is dual to a position vector $\vec{r}$ is given by the relation

$$\tilde{k} \cdot \vec{r} = k_a x^a = const. \tag{11.1}$$

Legendre transforms in Chapter 2 were dual transforms that would take a scalar function of position and velocity and transform it to a scalar function of position and momentum and then back again

$$\begin{aligned} \mathcal{L}L(x,\dot{x}) &= H(x,p) \\ \mathcal{L}H(x,p) &= L(x,\dot{x}) \end{aligned} \tag{11.2}$$

Therefore, state space and phase space are a type of reciprocal spaces.

As another example, in quantum mechanics wave functions come in two types, as functions and as Hermitian conjugates. The inner product of a wave function with its Hermitian conjugate produces a real number that is related to a probability. In the "bra – ket" notation, eigenvectors look like

$$\psi = |\psi\rangle = \psi^a \qquad \phi^\dagger = \langle\phi| = \phi_a \qquad P = \langle\phi|\psi\rangle = \phi_a \psi^a$$

In matrix notation, the eigenvectors are column matrices and the Hermitian conjugates are row vectors. The Hilbert space of Hermitian conjugates is the reciprocal space to the eigenvectors.

An important example arises in solid state physics with crystal lattices. Crystal lattices have basis vectors. Diffraction from these lattices is described as a new lattice with new basis vectors in reciprocal space which is the dual space to the original spatial lattice. The important entities known as Brillouin zones, which control many of the electronic properties of crystals, live entirely in reciprocal space. If the spatial basis vectors are $\vec{a}_1, \vec{a}_2, \vec{a}_3$ (known as primitive vectors) then the reciprocal basis vectors are

$$\begin{aligned}\vec{b}_1 &= 2\pi \frac{\vec{a}_2 \times \vec{a}_3}{\vec{a}_1 \cdot (\vec{a}_2 \times \vec{a}_3)} \\ \vec{b}_2 &= 2\pi \frac{\vec{a}_3 \times \vec{a}_1}{\vec{a}_1 \cdot (\vec{a}_2 \times \vec{a}_3)} \\ \vec{b}_3 &= 2\pi \frac{\vec{a}_1 \times \vec{a}_2}{\vec{a}_1 \cdot (\vec{a}_2 \times \vec{a}_3)}\end{aligned} \tag{11.3}$$

The primitive vectors and their reciprocals have the important property

$$e^{i\vec{K}\cdot\vec{R}} = 1 \tag{11.4}$$

where

$$\begin{aligned}\vec{R} &= n_1\vec{a}_1 + n_2\vec{a}_2 + n_3\vec{a}_3 \\ \vec{K} &= m_1\vec{b}_1 + m_2\vec{b}_2 + m_3\vec{b}_3\end{aligned} \tag{11.5}$$

are linear combinations with integer coefficients of the primitive vectors.

The feature common to all of these examples is the definition of a vector space, and the identification of an operation that converts vectors into real numbers (inner product, exponentiation of an inner product, etc.) using an entity (reciprocal vector, Hermitian conjugate, etc.) that forms its own vector space. This inverse vector space is the dual space of the original vector space.

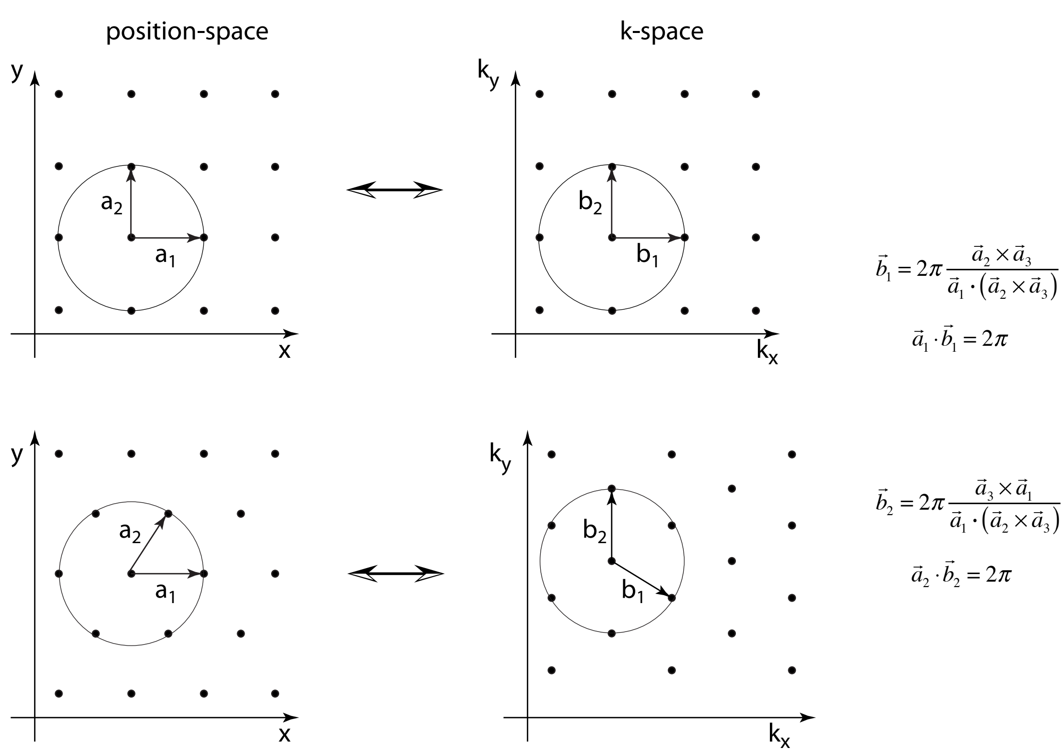

Fig. 11.1 Two-dimensional lattices and their reciprocal space. A square lattice (top) transforms to a square lattice, and a hexagonal reciprocal lattice (bottom) transforms to a hexagonal reciprocal lattice.

2. Light Orbit

Consider a radial refractive index profile

$$n(r) = 1 + n_0 r \exp\left(-r^2 / 2\sigma^2\right)$$

where the gradients are

$$\partial_a n = n_0 \exp\left(-r^2 / 2\sigma^2\right)\left(\frac{2x^a}{r} - r\frac{2x^a}{2\sigma^2}\right)$$

The refractive index for this case is shown in Fig. 11.2a. A ray path is shown in Fig. 11.2b for an initial propagation direction in the xy-plane. The ray is confined within the region of high index and orbits the low-index core.

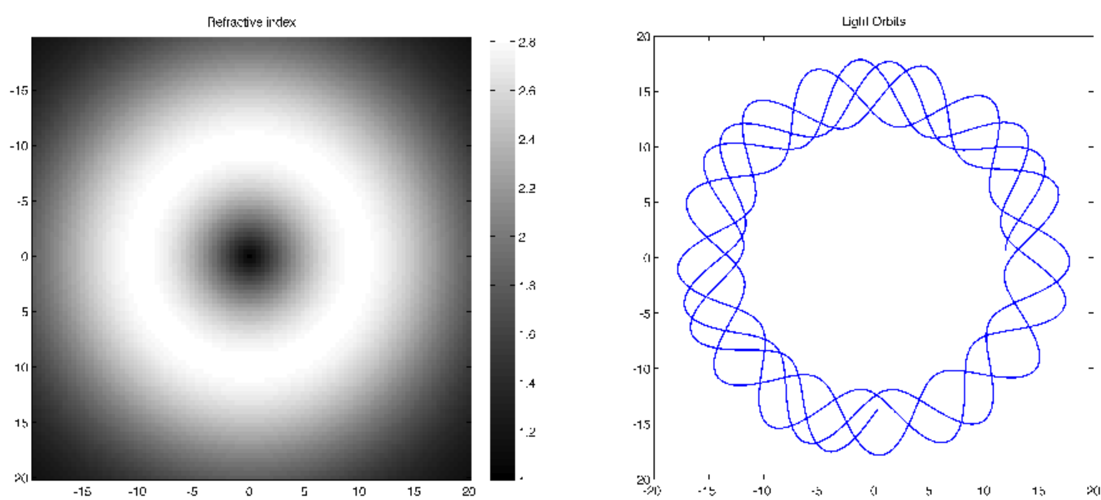

Fig. 11.2 A graded refractive index and the light orbits for n_2 = 0.3 and σ = 10. (From raysimple.m)

3. Summary

Basis Vectors
Basis vector components derive from the coordinate transformation between general coordinates and Cartesian coordinates through

$$\vec{e}_a = \left(\frac{\partial x}{\partial q^a}, \frac{\partial y}{\partial q^a}, \frac{\partial z}{\partial q^a} \right) \tag{9.22}$$

Basis vectors transform inversely to vector components.

Metric Tensor
The metric tensor determines the properties of a metric space

$$g_{ab} = \frac{\partial x}{\partial q^a}\frac{\partial x}{\partial q^b} + \frac{\partial y}{\partial q^a}\frac{\partial y}{\partial q^b} + \frac{\partial z}{\partial q^a}\frac{\partial z}{\partial q^b} \tag{9.6}$$

The metric tensor components are obtained through the inner product between basis vectors

$$g_{ab} = \vec{e}_a \cdot \vec{e}_b \tag{9.24}$$

Line Element
The line element is defined in terms of the metric tensor as

$$ds^2 = g_{ab} dx^a dx^b \tag{9.4}$$

Transformation Properties
Contravariant and covariant vectors transform inversely to each other. Covariant vectors transform as basis vectors.

$$\begin{aligned} A^{\bar{b}} &= R_a^{\bar{b}} A^a \\ A_{\bar{b}} &= R_{\bar{b}}^a A_a \\ \vec{e}_{\bar{b}} &= R_{\bar{b}}^a \vec{e}_a \end{aligned} \tag{9.31}$$

Derivative of a Vector
The derivative of a vector includes the derivative of the basis vector using the chain rule

$$\frac{\partial \vec{V}}{\partial x^\beta} = \frac{\partial V^\alpha}{\partial x^\beta}\vec{e}_\alpha + V^\alpha \frac{\partial \vec{e}_\alpha}{\partial x^\beta} \tag{9.66}$$

Christoffel Symbol

The Christoffel Symbol of the second kind arises from the covariant derivative of a basis vector

$$\frac{\partial \vec{e}_\alpha}{\partial x^\beta} = \Gamma^\mu_{\alpha\beta}\vec{e}_\mu \tag{9.67}$$

where the Christoffel symbol is related to the metric tensor through

$$\Gamma^\gamma_{\beta\mu} = \frac{1}{2} g^{\alpha\gamma}\left(\partial_\mu g_{\alpha\beta} + \partial_\beta g_{\alpha\mu} - \partial_\alpha g_{\beta\mu}\right)$$

Geodesic Equation
The geodesic equation defines a straightest path of shortest length through a metric space

$$\frac{d^2 x^a}{ds^2} + \Gamma^a_{bc}\frac{dx^b}{ds}\frac{dx^c}{ds} = 0 \tag{9.103}$$

The Ray Equation
The ray equation is an analogy to the geodesic equation. Light follows a null geodesic that is defined by the ray equation

$$\frac{d}{ds}\left(n\frac{dx^a}{ds}\right) = \frac{\partial n}{\partial x^a} \tag{9.149}$$

and in vector notation

$$\frac{d}{ds}\left(n(\vec{r})\frac{d\vec{r}}{ds}\right) = \vec{\nabla} n(\vec{r}) \tag{9.150}$$

Chapter 12 Special Relativity

1. Angular Doppler

The Doppler effect varies between blue shifts in the forward direction to red shifts in the backward direction, with a smooth variation in Doppler shift as a function of the emission angle.

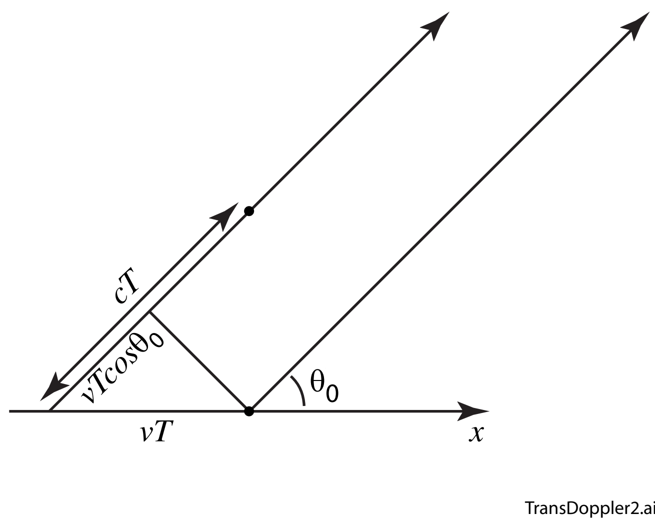

Fig. 12.1 Configuration for detection of Doppler shifts for emission angle θ_0. The light source travels a distance *vT* during the time of a single cycle, while the wavefront travels a distance *cT* towards the detector.

The observed wavelength is given by

$$\lambda = cT - vT\cos\theta \tag{12.1}$$

where T is the emission period of the moving source. The emission period is time dilated relative to the proper emission time of the source

$$T = \gamma T_0 \tag{12.2}$$

This gives

$$\begin{aligned}\lambda &= \gamma T_0\left(c - v\cos\theta\right)\\ &= \gamma\lambda_0\left(1 - \beta\cos\theta\right)\end{aligned} \tag{12.3}$$

which leads to the Angular Doppler Effect

Angular Doppler	$\lambda = \lambda_0 \dfrac{(1-\beta\cos\theta)}{\sqrt{1-\beta^2}}$	(12.4)

This expression has the expected limits:

$\theta = 0$

$$
\begin{aligned}
\lambda &= \lambda_0 \frac{(1-\beta\cos\theta)}{\sqrt{1-\beta^2}} \\
&= \lambda_0 \frac{(1-\beta)}{\sqrt{1-\beta^2}} = \lambda_0 \sqrt{\frac{1-\beta}{1+\beta}}
\end{aligned}
\tag{12.5}
$$

$\theta = \pi$

$$
\begin{aligned}
\lambda &= \lambda_0 \frac{(1-\beta\cos\theta)}{\sqrt{1-\beta^2}} \\
&= \lambda_0 \frac{(1+\beta)}{\sqrt{1-\beta^2}} = \lambda_0 \sqrt{\frac{1+\beta}{1-\beta}}
\end{aligned}
\tag{12.6}
$$

$\theta = \pi/2$

$$
\begin{aligned}
\lambda &= \lambda_0 \frac{(1-\beta\cos\theta)}{\sqrt{1-\beta^2}} \\
&= \lambda_0 \frac{1}{\sqrt{1-\beta^2}} = \gamma\lambda_0
\end{aligned}
\tag{12.7}
$$

Note that this last Doppler effect for emission at right angles is a red shift, caused only by the time dilation of the moving light source. This result is not corrected for the changing angle to the detection point as the light source moves. For the corrected "transverse Doppler effect" see problem 10.6 of the Introduction to Modern Dynamics.

The emission angle for which there is no Doppler effect can be obtained by setting

$$
\begin{aligned}
&\lambda = \lambda_0 \frac{(1-\beta\cos\theta)}{\sqrt{1-\beta^2}} = \lambda_0 \\
&\frac{(1-\beta\cos\theta)}{\sqrt{1-\beta^2}} = 1
\end{aligned}
\tag{12.8}
$$

The solution for the emission angle for which there is no observed Doppler effect is

$$\cos\theta = \frac{\gamma - 1}{\beta\gamma} \tag{12.9}$$

2. Classic Paradoxes

Because of the nonintuitive nature of Relativity, there are many physical phenomena that appear at first to lead to contradictions and hence are paradoxes that defy "common sense". However, none of these apparent paradoxes are true paradoxes, because each can be explained fully within the framework of the Theory of Relativity. The process of explaining why these are *not* paradoxes gives deep insight into the physics of relativity and can help build intuition in this unintuitive science. There are many classic paradoxes, of which three are described here. These are the *muon paradox*, the *twin paradox* and the *pole and barn paradox*.

Muon paradox:

A muon is a fundamental particle (a lepton) that has some of the properties of an electron, but it is much heavier, with a rest mass that is about 200 times heavier than the electron. In its rest frame, a muon decays into an electron (plus a neutrino) with a mean decay time of $\tau = 2.2$ microseconds. Muons are common constituents of the flux of cosmic rays that bombard the Earth's surface. They travel close to the speed of light, and hence the mean decay length of the muon would be $c\tau = 660$ meters. The muon flux can be measured at the peak of a mountain 660 meters high, and measured also at sea level. The flux ratio in this case might be expected to be $\exp(-660/c\tau) = 0.37$. However, in actual experiments, the flux ratio is about 82%. In this paradox, the resolution is obvious—the muon's lifetime is time dilated. Muons traveling at 0.98 times the speed of light, with $\gamma = 5$, have a lifetime that is about 5 times longer than the rest decay time, and the flux reaching sea level is $\exp(-660/c5\tau) = 0.82$. An alternative way to look at this problem is from the point of view of the muon. In its frame, it decays in 2.2 microseconds, but the height of the mountain is length-contracted to 660/5 = 132 meters and hence fewer muons decay between the measurement at the top of the mountain and sea level.

Twin Paradox:

This is perhaps the most famous of the relativity paradoxes and requires considerable more effort to explain compared to the muon paradox. Consider a pair of twins of exactly the same age: Bob and Alice. Alice is on Earth, while Bob is on a space ship traveling at $\beta = 0.8$ with a Lorentz factor $\gamma = 5/3$. From Alice's viewpoint, Bob travels for 5 years and then turns around and returns to Earth after a total trip time of 10 years. Because she sees Bob traveling near the speed of light, she sees his clock running slowly and hence she believes he has not aged as much as she has. Conversely, from Bob's frame, it is Alice who is moving at relativistic speeds. He sees her clock running slowly and hence he believes that she has not aged as much as he has. In other words, each sees the other's clock running slowly and each thinks the other has not aged as much. The question is, when they get back together, who has actually aged the least?

To settle this question, let's put some numbers to the problem. First, it is clear that Alice ages 10 years. Hence

$$\Delta t_A = 10\,yrs$$

Alice sees Bob's clock running slowly by a factor of 5/3, and hence she thinks

$$\Delta t_B = \frac{3}{5}10\,yrs = 6\,yrs$$

In Alice's frame, Bob travels a distance of $0.8c \cdot 5yr = 4lyrs$ outward bound for a total distance of 8 light years round-trip. From his point of view, this distance is length-contracted by a factor of 3/5, so he only measures a total round-trip distance of 4.8 light years, which takes him 6 years to cover. Therefore, Bob's elapsed time is

$$\Delta t'_B = \frac{\frac{3}{5}8lyrs}{0.8c} = 6\,yrs$$

But he sees Alice's clock running slowly by the factor of 5/3, so he thinks her clock has elapsed

$$\Delta t'_A = \frac{3}{5}6\,yrs = 3.6\,yrs\,.$$

This is then the paradox. Alice has aged 10 years but thinks Bob has aged 6 years. Bob has aged 6 years, but thinks Alice has aged 3.6 years. Each thinks the other is younger, although they both agree on Bob's age. As we put numbers to this paradox, we were careful to include both time dilation and length contraction effects, yet we are still stuck with the paradox.

To resolve the paradox, we need to do better "book keeping" on the elapsed times. To accomplish this, let both Bob and Alice emit light pulses once per year during the trip, and each measures how many times they receive light flashes from the other. By counting light flashes, they know for certain how much time has elapsed on each other's clocks. Counting light pulses emitted by a clock is equivalent to measuring a Doppler frequency shift. The situation is calculated in two parts—one for the outbound journey and one for the inbound journey. In both cases, Alice's and Bob's frequencies in their rest frames are

$$\begin{aligned} f_A &= 1/yr \\ f'_B &= 1/yr \end{aligned}$$

For the outbound journey, the frequency ratios are

$$\frac{f_B}{f'_B} = \sqrt{\frac{1-\beta}{1+\beta}} = \frac{1}{3}$$
$$\frac{f'_A}{f_A} = \sqrt{\frac{1-\beta}{1+\beta}} = \frac{1}{3}$$

from which

$$f_B = \frac{1}{3} yr^{-1}$$
$$f'_A = \frac{1}{3} yr^{-1}$$

These are the Doppler-shifted frequencies that Alice sees for Bob, and Bob sees for Alice. Each sees the same slow rate of pulse arrival, but each sees this rate for different amounts of time. The durations of the outward trip are

$$\Delta t_{out} = 5yrs + 0.8 \cdot 5yrs = 9yrs$$
$$\Delta t'_{out} = 3yrs$$

for Alice and Bob, respectively. Therefore, Alice receives 3 flashes from Bob's outward journey, and Bob receives only 1 flash from Alice during his outbound journey.

For in the inbound journey, the frequency ratios are

$$\frac{f_B}{f'_B} = \sqrt{\frac{1+\beta}{1-\beta}} = 3$$
$$\frac{f'_A}{f_A} = \sqrt{\frac{1+\beta}{1-\beta}} = 3$$

from which

$$f_B = 3yr^{-1}$$
$$f'_A = 3yr^{-1}$$

But the durations of the inward journey are

$$\Delta t_{in} = 1yr$$
$$\Delta t'_{in} = 3yrs$$

Therefore, Alice receives 3 flashes from Bob, but Bob receives 9 flashes from Alice.

In total, for the round-trip, Alice receives 3 + 3 = 6 flashes from Bob. Bob receives 1 + 9 = 10 flashes from Alice. Therefore, Alice is 10 years older after the trip, but Bob is only 6 years older, so Bob is younger than Alice, and each now agrees on the correctness of the calculations. The space-time diagram from Alice's frame is shown in Fig. 12.2. The diagonal lines are light pulses emitted by Alice (emitted from the ct axis) and the other diagonal lines are the light pulses emitted by Bob. Bob emits 6 pulses in total (the final pulse is emitted just as he arrives back at Earth), and Alice emits 10 pulses. Hence, Alice has aged 10 years to Bob's 6 years.

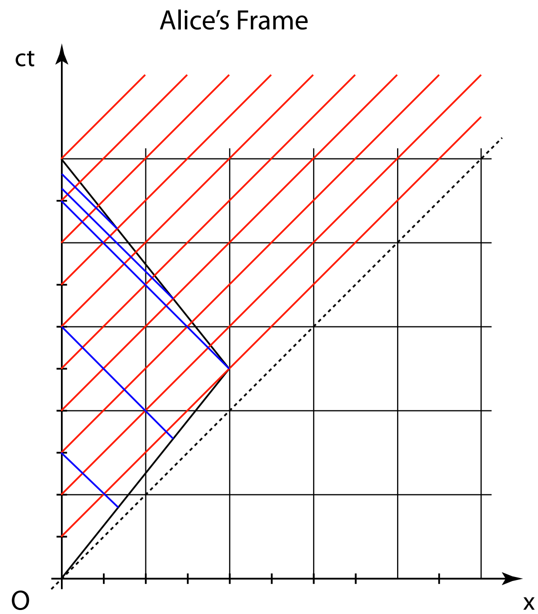

Fig. 12.2 Space-time diagram of the twin paradox from Alice's frame. The diagonal lines emerging from the *ct* axis are the photon trajectories of each of her pulses. The other diagonal lines are the photon trajectories of each of Bob's pulses. Alice emits 10 light pulses in ten years, while Bob emits only 6. Therefore, when he returns, Bob is younger than Alice.

This explanation of the Twin Paradox relies on accurate book-keeping—in other words, just arithmetic. But a qualitative explanation is still needed. The original paradox was expressed as each seeing the other's clock running slowly during the travel. This put a false emphasis on an apparent symmetry between Bob and Alice. However, this paradox has a fundamental asymmetry—because Bob must turn around. During his turn around, he would experience deceleration and then acceleration forces that Alice would never experience. Therefore, Bob must know that he had altered his motion during the trip, while Alice did not. In fact, when Bob decelerates and then reaccelerates to return home, he is no longer in an inertial reference frame. This puts the problem into the realm of the theory of General Relativity, which treats noninertial frames and the physics of gravity, which is beyond the topics of this textbook. Nonetheless, this Doppler approach does give the correct resolution to the Twin Paradox if Bob's turn-around is instantaneous.

Pole and Barn Paradox:

In this paradox, Alice is a pole vaulter carrying a pole that she measures to be 22 meters long in her rest frame. She runs at a relativistic speed of $\beta = 0.99$ ($\gamma = 7$) at a barn that is 20 meters long (in its rest frame) with a front and back door. In the Barn rest frame, the pole is length-contracted to 22/7 = 3.14 meters. Hence the pole can be completely inside the barn—in fact, both the barn doors can be closed while the pole is inside. But from Alice's point of view, the barn is length-contracted to a length 20/7 = 2.86 meters, so in fact the pole sticks out of both the front and back doors as she passes through. The paradox is: How can the barn doors be closed in the barn frame (completely enclosing the pole), when from Alice's frame the barn is so short that the pole can never fit inside and the doors cannot be closed?

The resolution of this paradox is in simultaneity (or the lack of it). In the barn frame the front and back doors close simultaneously, completely enclosing the pole. But in Alice's frame, the doors do not close simultaneously. In fact, the back door opens to allow the front of Alice's pole to enter, then the front door opens to allow the front of Alice's pole to leave the barn, but the back of her pole has yet to enter. Once the back of the pole enters the barn, the back door closes. Finally, as the back of the pole leaves the front of the barn, the front door closes. At no time were both the front and back door closed, so the pole never smashes into a door. The pole was never entirely inside the barn in Alice's frame.

3. Summary

Lorentz Transformations

Lorentz transformations are affine transformations that transform positions and time between relative frames

$$\begin{aligned} t' &= \gamma\left(t - \frac{v}{c^2}x\right) & \qquad t &= \gamma\left(t' + \frac{v}{c^2}x'\right) \\ x' &= \gamma(x - vt) & x &= \gamma(x' + vt') \\ y' &= y & y &= y' \\ z' &= z & z &= z' \end{aligned} \tag{10.3}$$

The 4-vector is transformed by the Lorentz transformation (Einstein summation convention assumed) as

$$x^{\bar{b}} = \Lambda^{\bar{b}}_{a} x^{a} \tag{10.7}$$

where the transformation matrix is

$$\Lambda_a^{\bar{b}} = \begin{pmatrix} \gamma & -\beta\gamma & 0 & 0 \\ -\beta\gamma & \gamma & 0 & 0 \\ 0 & 0 & 1 & 0 \\ 0 & 0 & 0 & 1 \end{pmatrix} \tag{10.8}$$

Velocity Addition

Velocity components observed between two frames moving along the x-axis at a relative speed v are

$$\begin{aligned} u'_x &= \frac{u_x - v}{1 - \frac{u_x v}{c^2}} \\ u'_y &= \frac{u_y}{\gamma\left(1 - \frac{u_x v}{c^2}\right)} \\ u'_z &= \frac{u_z}{\gamma\left(1 - \frac{u_x v}{c^2}\right)} \end{aligned} \tag{10.25}$$

where u_a are the velocity components in the unprimed frame.

Invariant Interval

The invariant interval is a differential line element in Minkowski space that has the same value in all frames. It is defined as

$$\begin{aligned} ds^2 &= -c^2 dt^2 + dx^2 + dy^2 + dz^2 \\ &= g_{ab} dx^a dx^b \end{aligned} \tag{10.39}$$

where the Minkowski metric tensor expressed as a matrix is

$$g_{ab} = \begin{pmatrix} -1 & 0 & 0 & 0 \\ 0 & 1 & 0 & 0 \\ 0 & 0 & 1 & 0 \\ 0 & 0 & 0 & 1 \end{pmatrix} \tag{10.40}$$

4-momentum

The 4-momentum is

$$\begin{aligned} p^a &= mv^a \\ &= \gamma m \begin{pmatrix} c \\ u^x \\ u^y \\ u^z \end{pmatrix} \end{aligned} \tag{10.48}$$

and the inner product with itself is

$$\begin{aligned} g_{ab} p^a p^b &= -\gamma^2 m^2 c^2 + \gamma^2 m^2 u^2 \\ &= -m^2 c^2 \end{aligned} \tag{10.49}$$

which is an invariant.

Energy-Momentum

The contributions of momentum and mass to total energy is

$$E^2 = \left(mc^2\right)^2 + p^2 c^2 \tag{10.60}$$

where the total energy is

$$E = \gamma mc^2 \tag{10.55}$$

and the rest energy of the particle is

$$E_0 = mc^2 \tag{10.56}$$

The kinetic energy is therefore

$$T = \left(\gamma - 1\right) mc^2 \tag{10.57}$$

Force Transformation

Forces transform between frames moving relatively along the x-axis as

$$\begin{aligned} f_x &= f'_x \\ f_y &= f'_y / \gamma \\ f_z &= f'_z / \gamma \end{aligned} \tag{10.68}$$

where the longitudinal component of the force is the same in both frames.

Chapter 13 General Relativity and Gravitation

1. Newtonian Dynamics

Trajectories in general relativity derive from the geodesic equation subject to the metric tensor. Because 4-momentum is related (by an affine transformation) to the tangent vector of a curve through the particle location, it also satisfies the geodesic equation for parallel transport

$$\nabla_{\vec{p}}\vec{p} = 0 \tag{13.1}$$

Examining the zero-th term

$$p^a \partial_a p^0 + \Gamma^0_{ab} p^a p^b = 0 \tag{13.2}$$

and using the identity

$$p^a \partial_a = mU^a \partial_a = m\frac{d}{d\tau} \tag{13.3}$$

gives

$$m\frac{dp^0}{dt} + \Gamma^0_{00}\left(p^0\right)^2 = 0 \tag{13.4}$$

because $p^0 >> p^a$ for a slow (non-relativistic $\gamma \approx 1$) particle. The connection to the metric is

$$\Gamma^0_{00} = \frac{1}{2} g^{0b}\left(\partial_0 g_{b0} + \partial_0 g_{b0} - \partial_b g_{00}\right) \tag{13.5}$$

and only the □ = 0 components are nonzero, where

$$\begin{aligned} \Gamma^0_{00} &= \frac{1}{2} g^{00}\,\partial_0 g_{00} = \frac{1}{2}\left[\frac{1}{-(1+2\phi)}\right]\partial_0(-2\phi) \\ &\approx \frac{\partial}{\partial x^0}\phi \end{aligned} \tag{13.6}$$

In the slow-particle limit, the approximate expression $\left(p^0\right)^2 \approx (mc)^2$ holds, which gives

$$\frac{d}{dt}p^0 = -mc\frac{\partial\phi}{\partial t} \tag{13.7}$$

and recognizing p^0 as the energy component of the 4-momentum, this is finally

$$\frac{dE}{dt} = -m\frac{\partial \Phi}{\partial t} \tag{13.8}$$

This is the statement of energy conservation if the gravitational potential has no explicit time dependence.

The space components obey a similar condition

$$p^a \partial_a p^c + \Gamma^c_{ab} p^a p^b = 0 \tag{13.9}$$

with explicit equations

$$\begin{aligned} m\frac{dp^a}{dt} + \Gamma^a_{00}\left(p^0\right)^2 &= 0 \\ \frac{dp^a}{dt} &= -mc^2\Gamma^a_{00} \end{aligned} \tag{13.10}$$

The metric component

$$g^{ca} = \frac{1}{1-2\phi}\delta^{ca} \tag{13.11}$$

gives

$$\begin{aligned} \Gamma^a_{00} &= \frac{1}{2}\frac{1}{1-2\phi}\delta^{ab}\left(2\frac{\partial}{\partial x^o}g_{b0} - \frac{\partial}{\partial x^b}g_{00}\right) \\ &\approx -\frac{1}{2}\frac{\partial}{\partial x^b}g_{00}\delta^{ab} \\ &\approx -\frac{1}{2}\frac{\partial}{\partial x^b}(-2\phi)\delta^{ab} \end{aligned} \tag{13.12}$$

which converts Eq.(13.10) into Newton's Second Law as

$$\frac{dp^a}{dt} = -m\frac{\partial \Phi}{\partial x^b}\delta^{ab} \tag{13.13}$$

which is just the expression from Newtonian gravity (expressed in tensor notation). Therefore in the slow-particle weak-field limit, Newton's equations and gravity emerge from the Einstein Field Equations.

2. Planetary Orbits

The second notable prediction that Einstein made concerning his new theory of General Relativity was an explanation of the precession of the perihelion of the planet Mercury. In a perfect 1/r potential, the major axis of the elliptical orbit is constant and does not precess. However, if there are radius-dependent corrections to the potential, then the axis of the ellipse precesses, which is observed for the orbit of Mercury.

The equation of a planetary orbit in the Schwarzschild geometry begins with the invariant 4-velocity

$$g_{ab}\dot{x}^a\dot{x}^b = -c^2 \tag{13.14}$$

where the dot is with respect to the proper time $\dot{x}^a = dx^a / d\tau$. In the Schwarzschild geometry this is

$$-\left(1-\frac{R_S}{r}\right)c^2\dot{t}^2 + \left(1-\frac{R_S}{r}\right)^{-1}\dot{r}^2 + r^2\left(\dot{\theta}^2 + \sin^2\theta\dot{\phi}^2\right) = -c^2 \tag{13.15}$$

Planetary motion in this metric is planar, just as in the case of Newtonian gravity, and it is convenient to choose $\theta = \pi/2$ to give

$$-\left(1-\frac{R_S}{r}\right)c^2\dot{t}^2 + \left(1-\frac{R_S}{r}\right)^{-1}\dot{r}^2 + r^2\dot{\phi}^2 = -c^2 \tag{13.16}$$

The Lagrangian $L\left(x^a, \dot{x}^a; \tau\right) = \frac{1}{2}g_{ab}\dot{x}^a\dot{x}^b$ has no explicit time dependence nor ϕ-dependence, leading to two conserved quantities through

$$\begin{aligned}\frac{\partial L}{\partial \dot{x}^0} &= g_{ab}\dot{x}^a\delta_0^b \\ \frac{\partial L}{\partial \dot{x}^3} &= g_{ab}\dot{x}^a\delta_3^b\end{aligned} \tag{13.17}$$

that are related to the constants *E* and *l* (energy and angular momentum). In the presence of a metric that differs from the Minkowski metric, relativistic energy and angular momentum are expressed as

$$\begin{aligned}E/mc &= -g_{00}c\dot{t} \\ l &= mg_{\phi\phi}\dot{\phi} = mr^2\dot{\phi}\end{aligned} \tag{13.18}$$

Both of these quantities are conserved. Using these constants in Eq.(13.16) gives

$$-\left(1-\frac{R_S}{r}\right)^{-1}\frac{E^2}{m^2c^2}+\left(1-\frac{R_S}{r}\right)^{-1}\dot{r}^2+\frac{l^2}{m^2r^2}=-c^2 \tag{13.19}$$

and after some re-arrangement

$$\frac{1}{2}m\dot{r}^2+\frac{1}{2}\frac{l^2}{mr^2}\left(1-\frac{R_S}{r}\right)-\frac{GmM}{r}=\frac{1}{2}\frac{E^2}{mc^2}-\frac{1}{2}mc^2 \tag{13.20}$$

The right-hand side is a constant of the motion with units of energy[10], which will be denoted by the expression T_∞, and the equation is finally

$$\frac{1}{2}m\dot{r}^2+\frac{1}{2}\frac{l^2}{mr^2}\left(1-\frac{R_S}{r}\right)-\frac{GmM}{r}=T_\infty \tag{13.21}$$

This is recognized as the equation for the non-relativistic central force problem, but with an extra factor of $\left(1-\frac{R_S}{r}\right)$ in the angular momentum term. This extra factor is the General Relativistic correction that leads to a deviation from the perfect 1/r potential, and hence leads to precession of the orbit.

The differential equation in Eq.(13.21) is commonly expressed in terms of derivatives of the angle ϕ by using Eq.(13.18) to yield

$$\left(\frac{1}{r^2}\frac{dr}{d\phi}\right)^2+\frac{1}{r^2}\left(1-\frac{R_S}{r}\right)-\frac{2GMm^2}{rl^2}=\frac{2m}{l^2}T_\infty \tag{13.22}$$

The substitution $u = 1/r$ makes this

$$\left(\frac{du}{d\phi}\right)^2+u^2=\frac{2m}{l^2}T_\infty+\frac{2GMm^2}{l^2}u+R_Su^3 \tag{13.23}$$

Differentiating with respect to u leads to a simple form

---

[10] By using the result from special relativity $E^2=p^2c^2+m^2c^4$, the constant can be expressed as

$$T_\infty=\frac{1}{2}\left(\frac{E^2}{mc^2}-mc^2\right)=\frac{p^2}{2m}$$

which is the non-relativistic particle kinetic energy far from the gravitating body.

$$\frac{d^2u}{d\phi^2}+u=\frac{GMm^2}{l^2}+\frac{3GM}{c^2}u^2 \tag{13.24}$$

which is valid for particle (or planet) speeds much less than *c*.

In the absence of the last term of Eq.(13.24), this is the classical orbital result for an inverse square law

$$\frac{d^2u}{d\phi^2}+u=\frac{GMm^2}{l^2} \tag{13.25}$$

which has the elliptical solution

$$\frac{1}{r}=\frac{GMm^2}{l^2}\left(1+\varepsilon\cos\phi\right)=u_0 \tag{13.26}$$

where ε is the ellipticity. When this ideal solution is substituted into Eq. (13.24), the result is

$$\frac{d^2u_0}{d\phi^2}+u_0=\frac{GMm^2}{l^2}+\frac{3G^3M^3m^4}{l^4c^2}\left[1+2\varepsilon\cos\phi+\frac{\varepsilon^2}{2}\left(1+\cos 2\phi\right)\right] \tag{13.27}$$

Only the second term in the brackets leads to first-order effects, giving the approximation to the solution as[11]

$$u_1=u_0+\frac{3G^3M^3m^4}{l^4c^2}\varepsilon\phi\sin\phi \tag{13.28}$$

which can be rewritten

$$u_1=\frac{GMm^2}{l^2}\left[1+\varepsilon\cos\left(\phi\left[1-3\left(\frac{GMm}{\ell c}\right)^2\right]\right)\right] \tag{13.29}$$

When ϕ equals 2π then the angle at the maximum radius has shifted (precessed) by the angle

GR Precession Angle

$$\Delta\phi=6\pi\left(\frac{GMm}{lc}\right)^2 \tag{13.30}$$

[11] Details of the secular solution can be found in Section 8.9 of Thornton and Marion, *Classical Dynamics of Particles and Systems*, 5th Ed. (Thomson, 2004)

In the case of the orbit of Mercury, this is 43 seconds of arc per century. This was what was derived by Einstein in 1915 during a particularly productive two weeks that also included his prediction of the deflection of light by the Sun.

3. Eddington -Finkelstein Coordinates

To get a feel for the light curves begin by finding the null geodesics. The null geodesic has $ds^2 = 0$ and gives

$$dr = \pm\left(1 - 2GM / c^2 r\right) d\tau \qquad (13.31)$$

This integrates to

$$\tau = \pm\left(r - \frac{2GM}{c^2} \ln\left| r - \frac{2GM}{c^2} \right| \right) + const. \qquad (13.32)$$

This result can be used to make a coordinate transformation to a new time parameter

$$\tau^* = \tau + \frac{2GM}{c^2} \ln\left| r - \frac{2GM}{c^2} \right| \qquad (13.33)$$

with the differential

$$d\tau = d\tau^* - \frac{2GM}{c^2} \frac{dr}{r - \frac{2GM}{c^2}} \qquad (13.34)$$

When this is put into the Schwarzschild metric, it becomes

$$ds^2 = \left(1 + \frac{2GM}{c^2 r}\right) dr^2 + \frac{4GM}{c^2 r} dr d\tau^* - \left(1 - \frac{2GM}{c^2 r}\right)\left(d\tau^*\right)^2 \qquad (13.35)$$

This is called the Eddington-Finkelstein metric, and there is no longer a divergent term at the Schwarzschild radius.

The null geodesics in the Eddington-Finkelstein metric are described by $ds^2 = 0$, which gives the differential equation

$$\left(1 + \frac{2GM}{c^2 r}\right)\left(\frac{dr}{d\tau^*}\right)^2 + \frac{4GM}{c^2 r}\frac{dr}{d\tau^*} - \left(1 - \frac{2GM}{c^2 r}\right) = 0 \qquad (13.36)$$

This simplifies to

$$\frac{dr}{d\tau^*} = \left(\begin{array}{ccc} -1 & , & \dfrac{1-\dfrac{2GM}{c^2 r}}{1+\dfrac{2GM}{c^2 r}} \end{array} \right) \tag{13.37}$$

for the two sets of null geodesics (analogous to the slopes of +1 and -1 in Minkowski space). Note that the -1 slope solution remains as for Schwarzschild space, but the + null-geodesic solution does not. The + null geodesics are

$$\begin{aligned} \tau^* &= \int \frac{\left(r + \dfrac{2GM}{c^2}\right)}{\left(r - \dfrac{2GM}{c^2}\right)} dr \\ &= r + \frac{4GM}{c^2} \ln\left|1 - \frac{2GM}{c^2 r}\right| \end{aligned} \tag{13.38}$$

which still show something important happening at the Schwarzschild radius.

The null geodesics are shown in the Eddington-Finkelstein metric in Fig. 11.1 for a spherically symmetric black hole. These coordinates are what an inertial observer sees who is far from the black hole. For large radii, the light cone has its usual 45° angles. However, as the event horizon nears, the light cone tilts towards the origin. At the event horizon, the light cone is tilted sufficiently that a photon emitted in the radial direction remains stationary (as observed by the distant observer). Locally, an astronaut emitting the photon sees the photon recede from her at the speed of light. If the astronaut is even a little inside the event horizon, the radially emitted photon is dragged inward and asymptotically approaches the true singularity at r = 0. So too for the astronaut. There is no amount of rocket thrust that will keep her from the singularity.

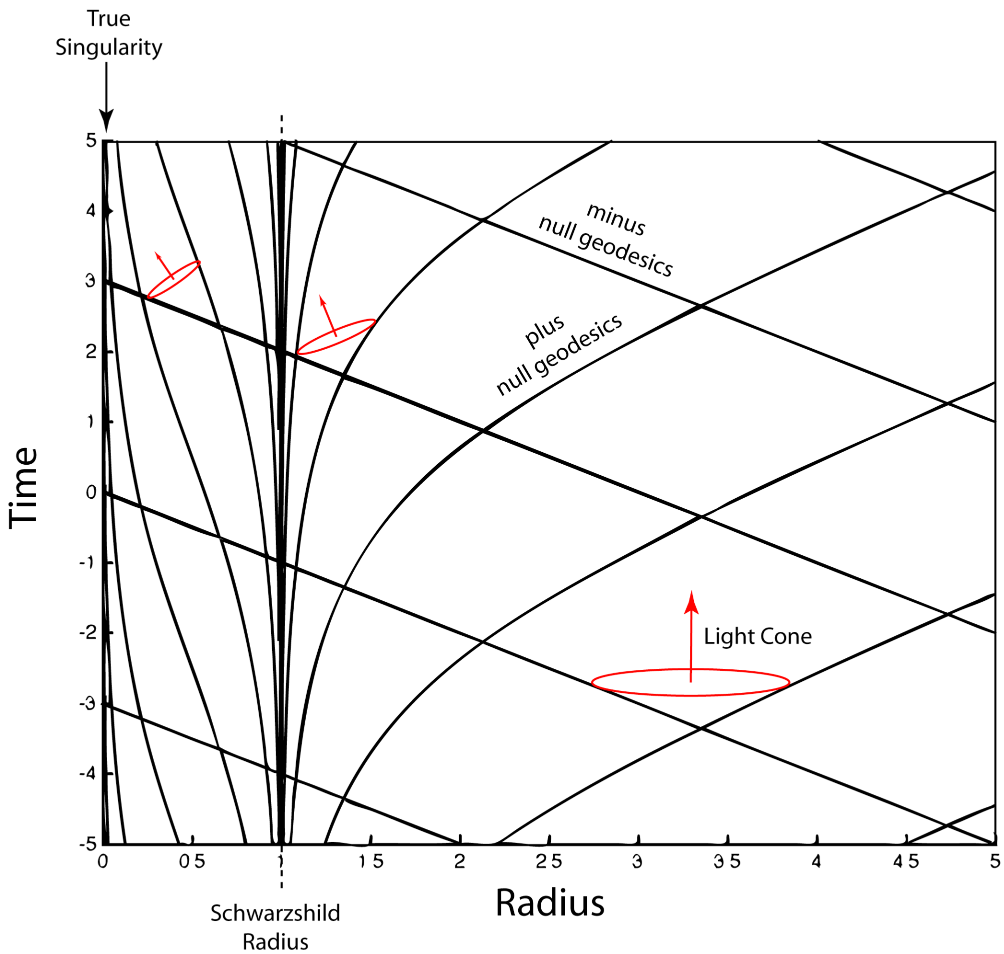

Fig. 13.1 Null geodesics in the Eddington-Finkelstein metric of a black hole. The minus geodesics remain the same as for Minkowski space, even through the event horizon. The plus geodesics have infinite slope at the event horizon, but the invariant interval remains finite. Note that the light cones at large radius have the normal 45° angles, but tip left for smaller radii. A photon emitted in the radial direction at the even horizon remains stationary (as observed by an inertial observer far from the black hole).

4. Summary

Riemann Curvature Tensor and Ricci Tensor and Scalar

The curvature of a metric space is captured by the Riemann curvature tensor and its contractions into the Ricci tensor and scalar

$$R^a_{bcd} = \partial_c \Gamma^a_{bd} - \partial_d \Gamma^a_{bc} + \Gamma^e_{bd}\Gamma^a_{ec} - \Gamma^e_{bc}\Gamma^a_{ed} \tag{11.5}$$

$$R_{ab} = R^c_{acb} = g^{cd} R_{dacb} \tag{11.7}$$

$$R = g^{ab} R_{ab} \tag{11.8}$$

Einstein Field Equations

The Field Equations of general relativity relate the curvature of space-time, captured in the Einstein tensor

$$G^{ab} = R^{ab} - \frac{1}{2} g^{ab} R \tag{11.24}$$

to the mass-energy density T^{ab} through

$$G^{ab} + \Lambda g^{ab} = \frac{8\pi G}{c^4} T^{ab} \tag{11.25}$$

where Λ is the "cosmological constant", which is an on-going topic of astrophysical research through its connection to *Dark Energy* and the expansion of the Universe.

Spherically-Symmetric Metrics

For spherical symmetry, the weak-field metric in Cartesian coordinates is

$$ds^2 = -\left(1 - \frac{2GM}{c^2 r}\right) c^2 dt^2 + \left(1 + \frac{2GM}{c^2 r}\right)\left(dx^2 + dy^2 + dz^2\right) \tag{11.45}$$

The Schwarzschild metric (for arbitrary field strength) in spherical polar coordinates is

$$ds^2 = -\left(1 - \frac{2GM}{c^2 r}\right) c^2 dt^2 + \frac{dr^2}{\left(1 - \frac{2GM}{c^2 r}\right)} + r^2\left(d\theta^2 + \sin^2\theta d\phi^2\right) \tag{11.46}$$

Gravitational Time Dilation and Length Contraction

Clocks higher in a gravitational potential tick faster than those lower in the potential. (Clocks in satellites tick faster than clocks on Earth.) Clocks at the Schwarzschild radius of a black hole stop ticking altogether (when considered from a position far away). Yardsticks parallel to the radius vector of a gravitating body compress as they approach the body, and compress to zero length at the Schwarzschild radius.

Angular Deflection of Light by the Sun

Light passing by a spherically gravitating body with impact parameter b is deflected by an angle

$$\Delta\phi = \frac{4GM}{c^2 b} \tag{11.66}$$

which, for the Sun, is 1.7 arcseconds.

Orbital Precession Angle

The general relativistic contributions to orbital mechanics produces a deviation from the perfect inverse square law of Newtonian orbits. Elliptical orbits with an orbital angular momentum l precess by an angle

$$\Delta\phi = 6\pi\left(\frac{GMm}{lc}\right)^2 \tag{11.84}$$

which, in the case of the orbit of Mercury, is 43 arcseconds per century.

Chapter 14 Appendix

1. Elliptic Integrals

Elliptic integrals are encountered routinely in the study of periodic systems such as gravitational orbits and pendula.

The *incomplete* elliptic integral of the second kind is expressed as

$$E(\alpha,k)=\int_0^\alpha \sqrt{1-k^2\sin^2\theta}\,d\theta$$

The *complete* elliptic integral of the second kind is expressed as

$$E(k)=\int_0^{\pi/2} \sqrt{1-k^2\sin^2\theta}\,d\theta$$

The circumference of an ellipse with semimajor axis a is expressed in terms of the complete integral as

$$C=4aE(e)$$

where the excentricity *e* of the ellipse is given by

$$e=\sqrt{1-b^2/a^2}$$

E(k) is a weakly varying function of its argument, varying from π/2 at k = 0 to 1 at k = 1.

The *incomplete* elliptic integral of the first kind is expressed as

$$K(\alpha,k)=\int_0^\alpha \frac{d\theta}{\sqrt{1-k^2\sin^2\theta}}$$

and the incomplete integral has as its limit the complete integral when α = π/2

$$K(k)=\int_0^{\pi/2} \frac{d\theta}{\sqrt{1-k^2\sin^2\theta}}$$

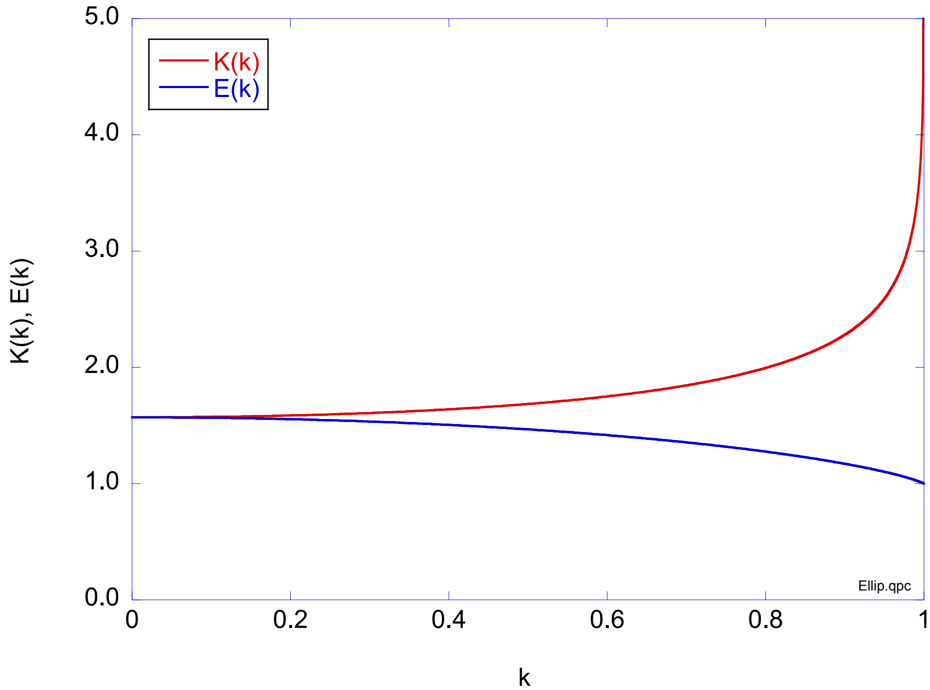

Fig. Complete elliptic integrals of the first kind K(k) and second kind E(k).

The period of a pendulum is expressed in terms of the incomplete elliptic integral of the first kind. Beginning with the Hamiltonian

$$H = \frac{p_\phi^2}{2I} + mgd\left(1 - \cos\phi\right) = E$$

the momentum is

$$md^2\frac{d\phi}{dt} = \sqrt{2md^2E}\sqrt{1 - \frac{2mgd}{E}\sin^2\frac{\phi}{2}}$$

which can be rexpressed as

$$dt = \frac{md^2 d\phi}{\sqrt{2md^2E}\sqrt{1 - \frac{2mgd}{E}\sin^2\frac{\phi}{2}}}$$

This is integrated to give the quarter period of the pendulum

$$\frac{T}{4} = \frac{md^2}{\sqrt{2md^2E}} \int_0^{\phi_{\max}} \frac{d\phi}{\sqrt{1 - \frac{2mgd}{E}\sin^2\frac{\phi}{2}}}$$

where

$$\sin\left(\frac{\phi_{\max}}{2}\right) = \sqrt{\frac{E}{2mgd}}$$

Hence the period is given by

$$\begin{aligned} T &= \frac{4md^2}{\sqrt{2md^2E}} \int_0^{\phi_{\max}} \frac{d\phi}{\sqrt{1 - \frac{2mgd}{E}\sin^2\frac{\phi}{2}}} \\ &= \frac{8d}{\sqrt{\frac{2E}{m}}} K\left(\frac{\phi_{\max}}{2}, \sqrt{\frac{2mgd}{E}}\right) \end{aligned}$$

2. Misc.

A helpful integral:

$$\int_0^T t\sin(\omega t)\cos(\omega t)\,dt = -4\pi^2$$